

Copyright©

by

Sergio E. Rodriguez

2018

The Dissertation Supervisory Committee for *Sergio Enrique Rodriguez*
Certifies that this is the approved version of the following dissertation:

**Studying the Biology of, and Developing Countermeasures to, a Tick-
transmitted Hemorrhagic Fever Virus**

Thomas W. Geisbert, M.Sci., Ph.D.,
Supervisor (Chair)

Dennis A. Bente, D.V.M., Ph.D.,
Co-Supervisor (Mentor)

Chad E. Mire, Ph.D.
Member

Tetsuro Ikegami, D.V.M., Ph.D.
Member

Éric Bergeron, M.Sci., Ph.D.
External Member, CDC-Atlanta, GA

Committee:

David W. Niesel, M.Sci., Ph.D.
Dean, Graduate School

**Studying the Biology of, and Developing Countermeasures to, a Tick-
transmitted Hemorrhagic Fever Virus**

by

Sergio Enrique Rodriguez, *B.Sci., M.Sci.*

Dissertation

Presented to the Faculty of the Graduate School of

The University of Texas Medical Branch

in Partial Fulfillment

of the Requirements

for the Degree of

Doctor of Philosophy

The University of Texas Medical Branch

November, 2018

Benediction & Dedication

"May there never develop in me the notion that my

education is complete but give me the strength

and leisure and zeal continually to

enlarge my knowledge."

- Maimonides -

This is dedicated to Britt, Sarah, Henry, Watson, and Crick.

*As well as the many family and friends that tolerated my forfeiture
from family and collegial life, whilst I completed the studies for this degree.*

Acknowledgements

I could fill an equal number of pages, comparable to the rest of this dissertation, which would still be inadequate in conveying the acknowledgements and the thanks I have for so many that have aided and guided me these many years. However, as is overstated in many methods sections...

Briefly, I acknowledge and give many thanks for the guidance and support of my two co-mentors, Tom Geisbert and Dennis Bente. Tom, you took a chance on me, before I even started graduate school and you saw a drive and motivation in me and decided to fan these flames—knowing full well I could have burned down your lab. You provided me the resources, tools, personnel, and learning opportunities that so few in graduate school are privy to. I count myself among the most fortunate of students to have had these opportunities you worked so hard to provide us. We had our share of learning experiences, and I am grateful that you continued providing chances for me to learn from. You have instilled your motto, passed on from COL Kelly Davis, of “*Do What’s Right.*” A simple, but true phrase to live by—especially in science. For this, and everything else, thank you. As for Dennis, I wouldn’t have made it to the finish line without you and your continued mentorship and support. Co-existing in two parent labs can be difficult, but you always went out of your way (often at detriment to you) to smooth things over, put out fires I started, deflect various academic/bureaucratic excrement that was flung my way, and empower me in networking, teaching/mentorship, and in critical thinking. I will always look up to you as my older brother in science. Thank you, Dennis, for making this journey possible, bearable, and even—fun!

To the members of my graduate committee, I give thanks for your stewardships of my doctoral education. Chad Mire, there’s so much to say—much of which I would likely get emotional about. Both of us taught and learned from one another in unique ways. You taught me how to think like a molecular scientist. How to visualize phenomena that

couldn't be. Your philosophies and love of the processes that occur which permit life and enable disease, are schools of thought I will carry with me for the rest of my life—and which are ones I will pass on to the next generation. Thank you for always being honest, thank you for hard love, but most of all thank you for believing in me. To Tetsuro Ikegami I offer my thanks for the feedback of my dissertation and its progression. Your insights were not only immeasurably useful for this dissertation, but necessary for its completion. To Éric Bergeron, thank you for challenging me to stay grounded in what is published, but inspiring me to dream about things that could be. I will forever appreciate your patience, your penchant for having a humorous and unshakeable scientific insight, and for your willingness to freely share knowledge in both the material and immaterial senses.

Both Geisbert and Bente labs have become my family, full of downs and ups, drama and love, but each family has been there for me—for this I cannot express how thankful I have been to know and learn from these groups. This dissertation was green-lit because of a co-first authored publication that Alex McAuley generously shared with me. Alex taught me many things in lab, but above all—I will remember his final lesson of humility, so thank you Alex—I am in your debt. As for Bob Cross, you taught me how to be a classically trained virologist and the power of old methods in influencing the new. Thank you for imparting both wisdom and hard-knocks, which will be immeasurably influential in my career moving forward. I thank Krystle Agans for her technical wisdom and patience. When I started, I had a steep learning curve in molecular biology, Krystle played a large role along with Chad and Bob, in forging me into a competent technical scientist who can design appropriate methodology to answer a scientific query. There are many other members of these labs, my graduate student cohort, and UTMB faculty and staff, both past and present, which have all contributed to my project through human power, mentorship, and/or collegiality. I give many thanks to Katie Schmitz, David Briley, Ben Satterfield, Joel Berends, Krista Versteeg, Courtney Williams, Gordon Wong, Angel Padilla, Maria Cajimat, Tera Sorvillo, Nathan Bopp, Stephanie Foster, Corey Fulton, Shannon Ronca,

Charles Umbaugh, Karla Fenton, Auja Smith, Isolde Schuster, Preethi Gampala, Megan Mears, Aysen Gargili, Siri Karr, Jim LeDuc, Mary Lou Millazzo, Patrick Newman, Connie Holubar, Joan Geisbert, Daniel Deer, Kevin Melody, Vika Borisevich, Corri Levine, Trevor Gale, Han Xia, Paymon Mosavi, Tais Saito, Joon Moon, Victoria Petruzzi, and Tim Wanninger.

Administratively, the GSBS and Dept. of Microbiology & Immunology have not only supported me but have funded portions of this dissertation. The people leading these two entities, are true gems that have gone out of their way to ensure student success. I am sincerely grateful to Dave Niesel for this once in a life-time opportunity to undertake this type of work outlined in this dissertation. It was the dream of my adult life to study ecology and develop countermeasures for BSL-4 viruses, so thank you Dave Niesel, for enabling this. Lynn Soong, Aneth Zertuche, and Laura Teed are others that I owe a great deal to. You all expertly facilitated classes and the administrative process, which finally allowed me to reach the end. I am grateful to each of you for your care and support of my education.

Lastly, but certainly not least, I express the deepest of thanks to my family. My mother and father, Sarah and Henry Rodriguez, have spent the better part of fourteen years, waiting for me to finish my university education and to see where life will take me. At times, I'm sure they didn't understand the 'why,' but their unyielding love and support transcended this, where they only ever asked the 'how,' *'how can I help?'* I could not ask for better people in this world to call Mom and Dad—this is both for you, and only possible because of you. To my wife and best friend, Brittany Ross, I am so grateful that you came into my life. You have supported me with love and laughter through some of the toughest challenges I've faced. You have shown me the fun and wealth of finally growing up and in starting a family. I sincerely look forward to the many adventures we will share together and am eternally grateful to evolution for yielding the dynamic pattern—that is you.

Studying the Biology of, and Developing Countermeasures to, a Tick-transmitted Hemorrhagic Fever Virus

Publication No. _____

Sergio Enrique Rodriguez, Doctor of Philosophy

The University of Texas Medical Branch, 2018

Supervisors: Drs. Thomas William Geisbert & Dennis Axel Bente

Crimean-Congo hemorrhagic fever (CCHF) is one of the world's most medically relevant tick-borne viral diseases. The CCHF virus (CCHFV) is transmitted in seasonal cycles among ticks and animals and is endemic to the Eastern hemisphere. Severe disease may develop with outbreak case fatality rates up to 30%. Pathogenesis studies have focused on the later stages of disease, whereas little is known about the influence of the tick-vector in disease outcome. Herein, the role of tick-transmission of CCHFV was investigated to examine the biology and early pathogenesis of CCHF. Concurrently, there are no licensed prevention or treatment options for CCHF and work with live CCHFV is restricted to biosafety level 4 (BSL-4) laboratories. This measure, while preserving biosafety, has hampered progress towards developing medical countermeasures. Recombinant vesicular stomatitis viruses (rVSV) expressing foreign glycoproteins have shown promise as both experimental vaccines and as a surrogate model at a lower biosafety level (BSL-2), called pseudotypes, for several viral pathogens. Herein, rVSV pseudotypes expressing the CCHFV glycoprotein precursor (GPC) were developed, which encodes CCHFV structural glycoproteins (GP). Two distinct recombinant viruses were generated: one infectious but replication deficient, and the other replication competent. Both constructs drive strong expression of CCHFV-GP in tissue cultures, with the replication

competent vector possessing CCHFV-GP on the virion surface of rVSV. This permitted studies for the biology of the CCHFV-GPC and the application to a serological detection and characterization means for CCHFV antibodies. The replication-competent pseudotype also demonstrated its use in a screening of antiviral compounds targeting the GPC. Both rVSV constructs were further evaluated as vaccines for CCHF. Varying degrees of efficacy were observed depending on the construct and experimental conditions, with up to a 100% efficacy observed using the replication-competent pseudotype for the vaccination in a lethal CCHFV animal model. This dissertation offers insight into the biology of CCHFV and its tick vector and highlights the utility of pseudotyped rVSV as a tool to further medical countermeasure developments for this deadly human pathogen and global public health concern.

TABLE OF CONTENTS

List of Tables	xii
List of Figures	xiii
List of Illustrations	xvi
i	
List of Abbreviations	xix
Chapter 1: Introductions	22
Crimean-Congo Hemorrhagic Fever Virus.....	22
Re-emerging Threats.....	29
Tamping Gaps of Knowledge	32
CHAPTER 2: Early Pathogenesis of Crimean-Congo Hemorrhagic Fever Virus ...	35
Influences of the Tick Vector on Disease Transmission	35
Studying the Effects of Tick-saliva on Crimean-Congo Hemorrhagic Fever Virus Replication and Cell Response in Antigen Presenting Cells	36
CHAPTER 3: Selecting Crimean-Congo Hemorrhagic Fever Virus Countermeasure Targets	46
Examining Targets at the Viral Order, Family, and Genus Levels.....	46
Selecting the Crimean-Congo Hemorrhagic Fever Virus Glycoprotein Precursor as a Target for Viral Countermeasure Developments.....	53
CHAPTER 4: Developing Tools to Study the Crimean-Congo Hemorrhagic Fever Virus Glycoprotein Precursor	56
Available Tools to Study the Crimean-Congo Hemorrhagic Fever virus Glycoprotein Precursor	56
Developing Recombinant Vesicular Stomatitis Viruses Expressing the Crimean- Congo Hemorrhagic Fever Virus Glycoprotein Precursor	57
Characterizing the Recombinant Vesicular Stomatitis Viruses Pseudotype	59
Genomic and <i>In Trans</i> Studies Into Replication Competence of the Δ GrVSV- Δ CCHFV-GPC Pseudotype.....	67
Using the Recombinant Vesicular Stomatitis Virus Pseudotype for Antibody Testing	74

CHAPTER 5: Screening Crimean-Congo Hemorrhagic Fever Virus Entry Inhibitors	78
Viral Entry: Role of the Fusion Peptide.....	78
Small Peptides Used as Broad-Spectrum Virus Attachment and Viral-Fusion Inhibitors	80
Designing <i>Nairoviridae</i> Entry Inhibitor Peptides: Selecting Residues in the G _C as Primary Targets	81
Screening Peptides on Pseudotyped Recombinant Vesicular Stomatitis Virus	85
Evaluating Selected Peptides on Crimean-Congo Hemorrhagic Fever Virus ..	87
Developing and Evaluating a <i>Nairoviridae</i> Fusion Assay.....	89
CHAPTER 6: Screening Crimean-Congo Hemorrhagic Fever Virus Glycoprotein Precursor Processing Inhibitors	99
Pathogen Box	99
Screening Pathogen Box Compounds on Pseudotyped Recombinant and Wild-Type Vesicular Stomatitis Viruses	100
Evaluating Selected Compounds on Wild-Type Crimean-Congo Hemorrhagic Fever Virus	104
CHAPTER 7: Experimental Vaccine Development for Crimean-Congo Hemorrhagic Fever Virus	108
Current Approaches in Experimental Vaccine Development for Crimean-Congo Hemorrhagic Fever Virus	108
Evaluating Pseudotyped Recombinant Vesicular Stomatitis Viruses as Experimental Vaccines for Crimean-Congo Hemorrhagic Fever Virus..	109
CHAPTER 8: Methodology.....	124
Cell culture, challenge virus, and antibodies	124
Generation of ΔGrVSV-CCHFV-GPC vectors	125
Infections, enumeration, growth kinetics, and preparation of viral material	125
CCHFV-G _C protein analysis	126
RNA purification, cDNA creation, and Sanger sequencing analysis	127
Deep sequence analysis of viral RNA genomes	128
Ultrastructural analysis	129
Ethics of care, vaccination, and animal challenge	129
Anti-CCHFV-GPC IgG ELISA development	130

Plaque reduction neutralization assay	131
Immunohistochemistry of tissues	132
Generation of Human Dermal Dendritic Cells and Langerhans Cells.....	132
Tick Salivary Gland Extract Preparation	133
LC and dDC Studies	134
Gene Array Assay	134
Cytokine Detection	135
Migration Assay.....	135
Fusion assay	137
<i>In Silico</i> Sequence Analysis.....	137
Statistical analysis.....	137
CHAPTER 9: All Things Considered.....	139
Understanding the Ecology of Crimean-Congo.....	139
Lessons Learned: From Pseudotyped Vesicular Stomatitis Virus, with Love .	141
The Moral of the Story: Preventing and Treating Crimean-Congo	143
References	145
Vita	161

List of Tables

Table 1: Review of experimental countermeasures for members of <i>Bunyavirales</i> ...	47
Table 2: Predicted characteristics and host cell processing of the genus members within the family <i>Nairoviridae</i> ²³	51
Table 3: Identities and similarities of residues among all GenBank published CCHFV-GPC	53
Table 4: Synonymous and non-synonymous mutations within the genomes of the replication-deficient and replication-competent pseudotypes	67
Table 5: Details of selected inhibitory Pathogen Box compounds on Δ GrVSV- Δ CCHFV-GPC pseudotype	104
Table 6: Published and unpublished CCHFV experimental vaccines and animal models	109

List of Figures

Figure 1: CCHFV titers from infected and tick salivary gland extract (SGE) treated skin antigen presenting cells (APC) ⁹²	40
Figure 2: Expression of antigen presentation genes following CCHFV infection or <i>Hyalomma</i> tick salivary gland extract (SGE) ⁹²	41
Figure 3: Cytokine and chemokine responses of mock, virus, and <i>Hyalomma</i> tick SGE treated human skin APC ⁹²	43
Figure 4: Salivary gland extract (SGE) from <i>Hyalomma</i> ticks inhibits migration of human monocyte-derived dendritic cells (moDC) ⁹²	44
Figure 5: Cell surface expression of CCHFV-G _C from codon optimized CCHFV-GPC	60
Figure 6: Characterization of the rVSV-CCHFV-GPC vectors.....	63
Figure 7: Immunofluorescence microscopy of G _N and G _C antigens expressed by plasmids encoding the N-terminal and C-terminal CCHFV-GPC truncations.....	70
Figure 8: Titers from <i>in trans</i> complemented cells using a single-round replicative reporter VSV	72
Figure 9: Coomassie and western blot of <i>in trans</i> -expressed, semi-purified	73
Figure 10: Neutralization of ΔGrVSV-ΔCCHFV-GPC by CCHFV monoclonal antibodies (MAb)	75

Figure 11: Validating enzyme linked immunosorbent assay coated with CCHFV-GPC pseudotyped or wild-type VSV, against multiple CCHFV antibody reagents	76
Figure 12: Percent plaque reduction neutralization test of 10 μ M of inhibitory peptides on pseudotyped Δ GrVSV- Δ CCHFV-GPC.....	86
Figure 13: Specificity of inhibitory peptides on wild-type vesicular stomatitis virus (VSV).....	87
Figure 14: Percent plaque reduction neutralization test of selected inhibitory compounds on wild-type CCHFV	88
Figure 15: Nairovirus fusion assay using pCAGG-CCHFV-GPC	91
Figure 16: Nairovirus fusion assay using Hazara virus	92
Figure 17: Nairovirus fusion assay using Δ GrVSV- Δ CCHFV-GPC	93
Figure 18: Nairovirus fusion assay using Dugbe virus	94
Figure 19: Nairovirus fusion assay using CCHFV virus	95
Figure 20: Role of inhibitory peptides on nairovirus fusion using pseudotyped Δ GrVSV- Δ CCHFV-GPC	96
Figure 21: Role of inhibitory peptides on nairovirus fusion using CCHFV	97
Figure 22: Screening of Pathogen Box, plate 'A' compounds using Δ GrVSV- Δ CCHFV-GPC pseudotype	101

Figure 23: Screening of Pathogen Box, plate ‘B’ compounds using Δ GrVSV- Δ CCHFV-GPC pseudotype	101
Figure 24: Screening of Pathogen Box, plate ‘C’ compounds using Δ GrVSV- Δ CCHFV-GPC pseudotype	102
Figure 25: Screening of Pathogen Box, plate ‘D’ compounds using Δ GrVSV- Δ CCHFV-GPC pseudotype	102
Figure 26: Screening of Pathogen Box, plate ‘E’ compounds using Δ GrVSV- Δ CCHFV-GPC pseudotype	103
Figure 27: Difference in inhibition between wild-type VSV and Δ GrVSV- Δ CCHFV- GPC pseudotype	104
Figure 28: Time course experiment using selected inhibitory Pathogen Box compounds from Δ GrVSV- Δ CCHFV-GPC pseudotype screening.....	105
Figure 29: Comparison of wild-type VSV, Δ GrVSV- Δ CCHFV-GPC pseudotype, and wild-type CCHFV on selected inhibitory Pathogen Box compounds ..	106
Figure 30: Mean weights and temperatures from pilot study mice	111
Figure 31: Pilot study mice survival following CCHFV challenge	112
Figure 32: Follow up <i>in vivo</i> CCHFV experimental vaccine study data: animal survival, average weights, average temperatures, and maximum clinical scoring.....	117
Figure 33: Follow up <i>in vivo</i> CCHFV experimental vaccine study humoral immune responses	118

Figure 34: Immunohistochemistry of murine tissues.....119

List of Illustrations

Illustration 1: Distribution of CCHFV ⁹	23
Illustration 2: Ecology of CCHFV and <i>Hyalomma</i> ticks ⁷	24
Illustration 3: CCHFV genome products	26
Illustration 4: Viral ‘life’ cycle of CCHFV ⁷	28
Illustration 5: Map of Spanish tick collection areas, identifications, and PCR results ⁵⁹	31
Illustration 6: Inhibition of skin innate immune responses by tick saliva ⁶⁸	36
Illustration 7: Experimental design for generating human dermal antigen presenting cells and <i>Hyalomma</i> tick salivary gland extract ⁹²	38
Illustration 8: Amino acid residue conservations among Nairoviruses	50
Illustration 9: Areas pertinent to the viral life cycle encoded within the genome of CCHFV	54
Illustration 10: rVSV-CCHFV-GPC vectors design and creation	61
Illustration 11: Sanger and next generation sequencing of the CCHFV-GPC.....	68
Illustration 12: Selecting CCHFV regions of interest from successful RVFV inhibitory peptide regions and from Nairovirus conserved regions within the G _C	82

Illustration 13: CCHFV inhibitory peptide selection and linker group descriptions .	84
Illustration 14: Pilot <i>in vivo</i> CCHFV experimental vaccine study	111
Illustration 15: Follow up <i>in vivo</i> CCHFV experimental vaccine study.....	114
Illustration 16: Similarities map of amino acid residues for CCHFV-GPC comparisons between all complete/GenBank-published strains and IbAr10200 versus Turkey2004	115

List of Abbreviations

UTMB	The University of Texas Medical Branch at Galveston
GSBS	Graduate School of Biomedical Sciences
USA	United States of America
USSR	Union of Soviet Socialist Republics
WHO	World Health Organization
NIH	National Institutes of Health
CDC	Centers for Disease Control and Prevention
BSL	Biosafety level
MAb	Monoclonal antibodies
HMAF	Hyper-immune mouse ascitic fluid
nm	nanometers
μm or λ	micrometers
kDa	Molecular weight of 1,000 Daltons
CCHF	Crimean-Congo hemorrhagic fever
CCHFV	Crimean-Congo hemorrhagic fever virus
rCCHFV	Recombinant Crimean-Congo hemorrhagic fever virus
DUGV	Dugbe virus
HAZV	Hazara virus
VLP	Virus-like particle(s)
tcVLP	Transcriptionally-competent virus-like particle(s)
VSV	Vesicular Stomatitis Virus
rVSV	Recombinant vesicular stomatitis virus
DNA/RNA	Deoxyribonucleic acid/Ribonucleic acid
S-segment	Small segment
M-segment	Medium segment
L-segment	Large segment
NP	Nucleoprotein
GPC	Glycoprotein precursor
ΔGPC	Altered glycoprotein precursor
GPC*	Glycoprotein precursor complementation
GP	Glycoprotein
Pre-G _N	Precursor molecule of N-terminus glycoprotein
Pre-G _C	Precursor molecule of C-terminus glycoprotein
GP160	Glycoprotein of 160 kilodaltons in size
GP85	Glycoprotein of 85 kilodaltons in size
MLD	Mucin-like domain
GP38	Glycoprotein of 38 kilodaltons in size
G _N	Mature form of N-terminal glycoprotein
NS _M	Non-structural M-segment protein
G _C	Mature form of C-terminal glycoprotein
TMD	Transmembrane domain
RdRp	RNA-dependent RNA-polymerase
RNP	Ribonuclearprotein complex

VSV-G	Vesicular stomatitis virus glycoprotein
VSV-G*	Vesicular stomatitis virus glycoprotein complementation
Δ G	Without (encoded) vesicular stomatitis virus glycoprotein
<i>spp.</i>	Species
<i>H.</i>	<i>Hyalomma</i> (genus)
STAT-1 ^(-/-)	Signal transducer and activator of transcription 1 knock-out mice
IFNAR	Interferon α/β receptor knock-out mice
IS	Interferon (transiently) suppressed mice
ORF	Open reading frame
CDS	Coding sequence
UTR	Untranslated region
MVA	Modified (recombinant) Vaccinia virus
ADV	Adenovirus
HF	Hemorrhagic fever
HFV	Hemorrhagic fever virus(es)
EBOV	Ebola virus
EVD	Ebola virus disease
MARV	Marburg virus
HNTV	Hantaan virus
SFTSV	Severe fever with thrombocytopenia syndrome virus
RVFV	Rift Valley fever virus
ANDV	Andes virus
SEOV	Seoul virus
PUUV	Puumala virus
SNV	Sin Nombre virus
siRNA	Small interfering RNA
shRNA	Small hairpin RNA
CD	Cluster of differentiation
APC	Antigen presenting cells
DC	Dendritic cells
dDC	Dermal dendritic cells
LC	Langerhans cells
moDC	Monocyte (CD14 ⁺) derived dendritic cells
SGE	Tick salivary gland extract
HSC	Hematopoietic stem cells
IL	Interleukin
TNF	Tumor necrosis factor
TGF	Tumor growth factor
GM-CSF	Granulocyte-macrophage colony stimulating factor
FLT3	FMS(gene)-like tyrosine kinase 3
SCF	Stem cell factor
MO	Monocyte(s)
M Φ	Macrophage(s)
IFN	Interferon
MxA	Human myxovirus resistance protein 1
WRCEVA	World Reference Center for Emerging Viruses and Arboviruses

NGS	Next generation sequencing
NSDV	Nairobi sheep disease virus
KETV	Ketarah virus
TBEV	Tick-borne encephalitis virus
ZEBOV	Zaire Ebolavirus
SARS-CoV	Severe-acute respiratory syndrome corona virus
PEG	Polyethylene glycol
RSV	Respiratory syncytial virus
HCV	Hepatitis C virus
PRNT	Plaque reduction neutralization test
AA	Amino acid
HR	Heptad-repeat region
HIV	Human immunodeficiency virus
HPI	Hour(s) post infection
IRF	Interferon regulatory factor
TAPBP	Tapasin binding protein
TAP	Antigenic Peptide Transporter
BHK	Baby hamster kidney cell line
Huh-7	Human hepatocarcinoma cell line
SW-13-CDC	Human adrenal carcinoma cell line (CDC clone)
Wt or wt	Wild-type

Chapter 1: Introductions

CRIMEAN-CONGO HEMORRHAGIC FEVER VIRUS

History

An outbreak occurred at the close of World War II (1944-1945) in the Crimean Peninsula of the former Ukrainian Soviet Socialist Republic. This disease struck about 200 Soviet military personnel who presented with varying degrees of febrile illness and hemorrhagic syndromes ¹⁻⁴. Given the geographic location of this outbreak, the disease was termed Crimean hemorrhagic fever and was propagated through suckling mice and human ‘volunteers’ for identification via Koch’s postulates and further study ^{1,2}. For two decades, similar disease outbreaks sprang up in Central Asia, the Balkans and elsewhere in the Union of Soviet Socialist Republics (USSR) that were tick-borne in nature ¹. A hemorrhagic fever outbreak over 3,600 miles away from the Crimean Peninsula—in what is now the Democratic Republic of Congo occurred where tick-transmission was implicated ^{1,5,6}. This outbreak occurred during 1956 and the illness was termed ‘Congo hemorrhagic fever’ ^{1,5,6}. In a coordinated international study centered at the Yale Arbovirus Research Unit at New Haven, Connecticut, United States of America (USA), Soviet and American scientists discovered that the agents of both Crimean and Congo hemorrhagic fevers, along with numerous tick-transmitted human hemorrhagic disease samples from across the world, were indistinguishable based on physiochemical, serological, and structural characterization ¹. The name of these various isolates was then consolidated to Crimean-Congo hemorrhagic fever virus (CCHFV), the causative agent of Crimean-Congo hemorrhagic fever (CCHF). This single breakthrough demonstrated the significance in archiving and maintaining reagents for arthropod-borne viruses for future scientific endeavors. Since its designation, CCHFV has continued to expand in both geographic range and in the number of human lives taken due to CCHF.

Ecology

CCFHV has the largest geographic distribution of any known medically relevant tick-borne virus. Serological evidence and/or symptomatic disease occurs throughout 30 countries spanning across Asia, southeastern Europe, Africa, and the Middle East (Illustration 1) ^{1,7,8}.

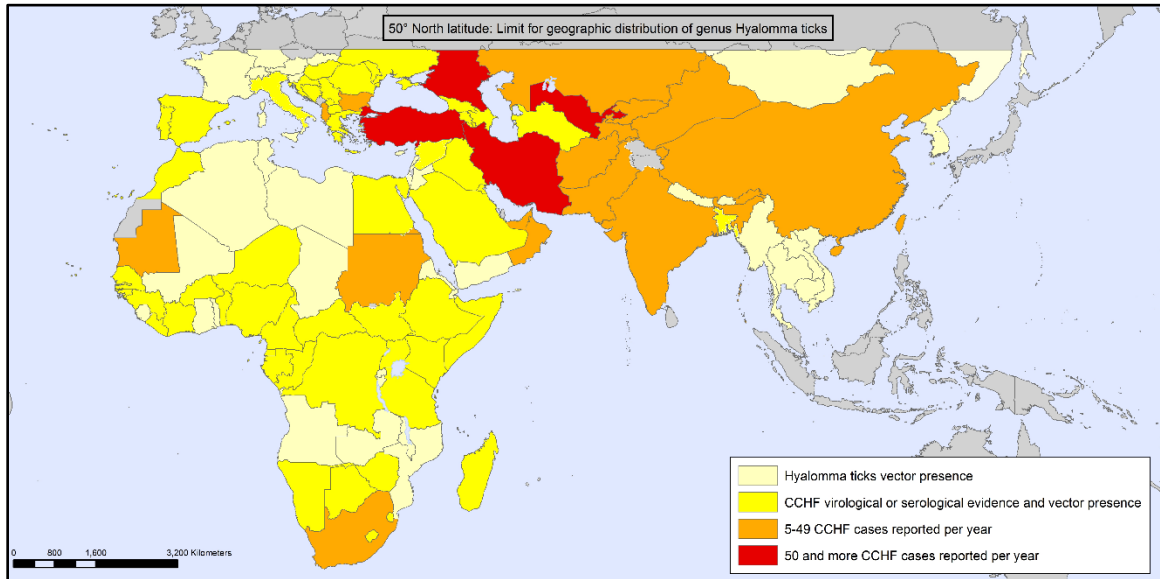


Illustration 1: Distribution of CCHFV ⁹

The geographic distribution of Crimean-Congo hemorrhagic fever virus (CCHFV), modified from a 2017 World Health Organization (WHO) CCHFV distribution map. Tick vector presence is indicated by any coloring aside from grey. CCHFV serological or virological presence is indicated by yellow coloring. Clinical cases are demarked by orange and red for 5-49 cases and >50 cases per year, respectively. Used and modified under the Creative Commons Attribution 4.0 International License ¹⁰.

It is maintained in endemic areas via vertical and horizontal transmission cycles of its reservoir host, ixodid hard hunting ticks belonging to the genus *Hyalomma* ^{1,7,11,12}. *Hyalomma* remain infected throughout their various life stages (Illustration 2) and several-year lifespan ^{1,11,13,14}. This can result in asymptomatic infection of small mammals, ungulates, and birds that are fed on by CCHFV infected ticks (Illustration 2). Interactions with infected arthropods, viremic animals, and human-to-human transmission during nosocomial infections, are the principal sources of human CCHF (Illustration 2) ^{1,7,11–13,15}.

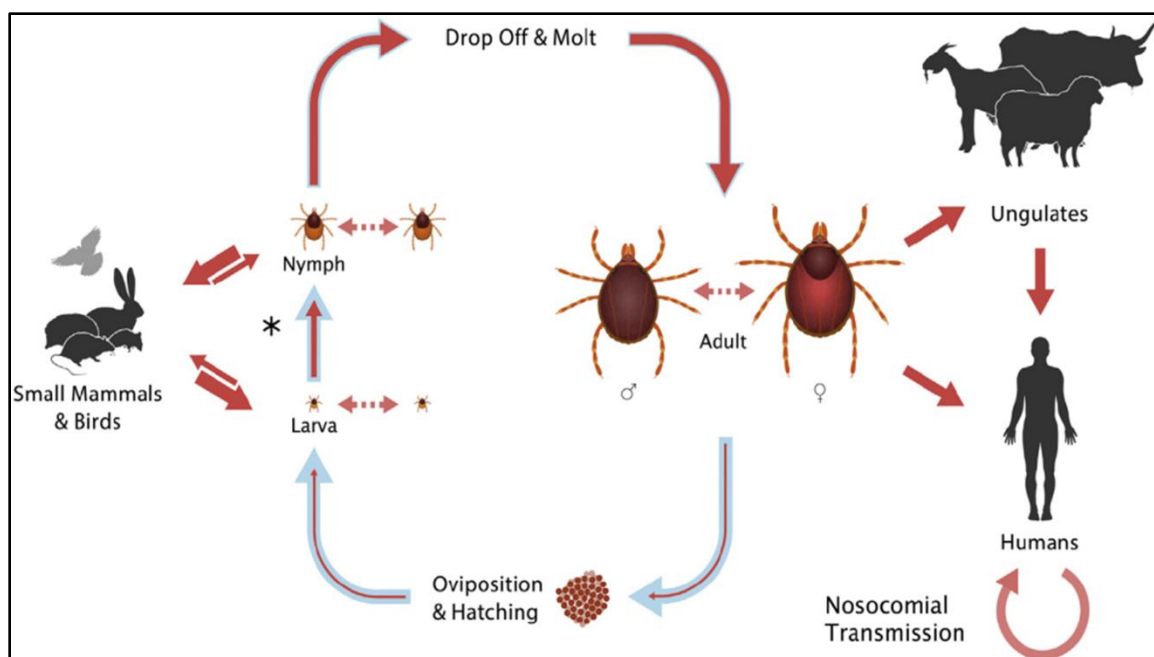


Illustration 2: Ecology of CCHFV and *Hyalomma* ticks ⁷

Life cycle of the Hyalomma tick genus. Arrows indicate either blood meal taking from various animals, or developmental stages. Red arrows of varying thickness within the blue arrows, indicates the efficiency of virus transmission or propagation. Infection of humans involves either direct tick bite, contact with infected bodily fluids from infected animals, or via nosocomial transmission. Asterisk () designates the differentiation between two- and three-host tick feeding patterns. Used with permission from Elsevier Publishing Group, 2018; License: 4400960047404.*

Clinical Perspectives

CCHFV can cause symptoms initially akin to mild, nonspecific febrile illness. In severe cases, a hemorrhagic condition can develop with vivid ecchymoses across patient extremities. Mucosal, venipuncture site, gastrointestinal, cerebral, urogenital tract, and abdominal musculature bleeding can occur in severe instances ⁸. In fatal cases, death occurs between the fifth and fourteenth day from initial onset of symptoms as a result of multi-organ failure, hemorrhage, and shock ^{7,8}. Case fatality rates of hospitalized patients vary widely depending on CCHFV isolate type, geographic region, and availability of supportive care. The Centers for Disease Control and Prevention (CDC) estimates mortality to range from 9% - 50%, though outbreak fatality rates as high as 80% have been documented ^{2,7,8}. For CCHF survivors, a full recovery may take up to a year and sequelae

such as hair loss, chronic fatigue, hepato/renal loss-of-function, polyneuritis, hearing loss, vision loss, and impaired memory can diminish the overall quality of life ⁸.

Currently, no licensed treatment is available; though ribavirin, a guanosine analogue licensed for both hepatitis C virus (HCV) and respiratory syncytial virus (RSV), has been used compassionately with mixed results to treat CCHF ^{8,16,17}. Conflicting reports exist as to its efficacy in humans, though *in vitro* and *in vivo* studies have shown inhibition of CCHFV replication in cell culture and animal models ¹⁸. There are also no licensed vaccines, outside the country of Bulgaria, for prevention of CCHFV.

A vaccine was developed in Bulgaria in 1970 following nearly two decades of active CCHFV outbreaks. The preparation consists of a suckling mouse brains infected with wild-type (wt) CCHFV inactivated by both heat and chloroform ¹⁹. This crude vaccine was primarily provided to medical and military personnel, along with farmers living in endemic regions ²⁰. A four-fold decrease in the total incidence of CCHF cases has been detected since the vaccine's implementation ^{20,21}. Individuals vaccinated with this suckling mouse brain derived vaccine, do develop anti-CCHFV responses for both antibodies and T-cell activity ²⁰. While there appears to be a trend in vaccinated individuals that have received a three dose regimen the first year, and a booster given every 5th year, this particular vaccine preparation is unlikely to be further licensed in World Health Organization (WHO) member countries ¹⁹. This due to biosafety concerns regarding manufacturing, safety issues surrounding administering mouse brain and chloroform, and the number of doses required to generate and maintain an immune response.

Molecular Biology

CCHFV is taxonomically classified as a Baltimore Class 'V' virus, due to its negative sense RNA genome and belongs to the viral order *Bunyavirales*, family *Orthonairoviridae* ^{7,22–26}. Most nairoviruses have their negative sense RNA genomes divided into three parts, enclosed by a host-cell derived lipid envelope approximately 80-

100 nanometers (nm) in diameter^{24–27}. Mature CCHFV particles contain tri-partite viral genomes of single stranded, negative sense RNA, called small (S), medium (M), and large (L) segments (Illustration 3).

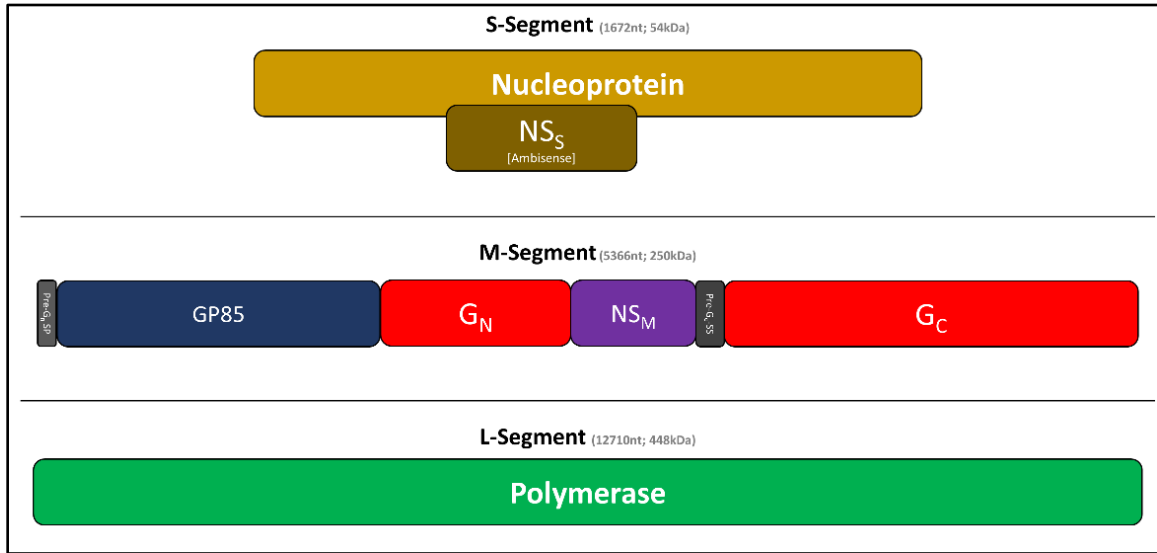


Illustration 3: CCHFV genome products

The CCHFV genome organization and resulting products from various open reading frames (ORFs). S-segment encodes two products: NP and NS_S in two separate ambisense ORFs. M-segment encodes one ORF of a polyprotein glycoprotein precursor molecule (GPC) that is proteolytically processed in host cells to yield mucin-like domain (MLD), and a secreted glycoprotein of 38 kDa in size (GP38). These two proteins can also be left as a single peptide to form a secreted glycoprotein of 85 kDa in size (GP85) which can dimerize with itself to form the dimeric secreted glycoprotein of 160 kDa in size (GP160). Structural glycoprotein on the N-terminus (G_N), along with a nonstructural protein (NS_M) and the final structural glycoprotein on the C-terminus (G_C), are also encoded within the ORF of the polyprotein GPC. There are also two signal peptides present at the leads of the precursor molecules Pre-G_N and Pre-G_C. Lastly, the L-segment encodes the whole polymerase module which is predicted to be ~450 kDa in size.

The S-segment contains two ambisense open reading frames (ORFs). The positive sense S-segment ORF encodes a non-structural protein (NS_S) (Illustration 3)²⁸. On the negative sense ORF of the S-segment, a structural nucleoprotein (NP) is encoded. NP forms a complex²⁹ with each genomic segment along with the 450 kDa viral RNA-dependent RNA-polymerase (RdRp), which is encoded on the L-segment (Illustration 3)^{7,24,25}. The M-segment contains a 5.1 kilobase ORF which codes for a polypeptide called the glycoprotein precursor (GPC), the largest and most complex of all studied members belonging to the order *Bunyavirales* (Illustration 3)³⁰. Host cell processing, cleavage

events, and post-translational modifications of this GPC yield two ‘mature’ structural glycoproteins (GP) called G_N and G_C, along with several non-structural glycoproteins which aid in structural G_N and G_C maturation (Illustration 3) ^{30–34}.

CCHFV genomic segments of RNA are bound by NP and the RdRp, which forms a complex called the ribonucleoprotein complex (RNP). The RNP of each segment (S-, M-, and L-segments), enclosed by a lipid envelope with membrane studded heterodimeric G_N and G_C, make up the components of a mature virion ³³. This mature virion can bind to cell surface receptor proteins to initiate the infection cycle of CCHFV. Although the receptor or entry mechanism(s) for arthropod and mammalian tissues are unknown. Cell surface nucleolin has been shown in precipitation assays to bind with components the G_C monomer ³⁵, whereas no follow-up studies have validated the biological use of this receptor by CCHFV. Once bound to their respective mammalian cell receptor(s), CCHF virions are internalized via receptor-mediated endocytosis that is both clathrin- and cholesterol-dependent ^{36,37}. Endocytic trafficking requires multivesicular bodies, ESCRT regulators, and vesicular acidification predicted to be pH-dependent around early endosomal compartmentalization ^{36,37}. A putative fusion domain has been demonstrated *in silico* within the G_C which is thought to mediate the fusion of virion and vesicular membrane in endosomes ^{38,39}. Once fused, the RNPs are released into the host cytosol, which can be transcribed by the virion-associated RdRp into complementary positive strand intermediates (cNA) for replication as well as messenger RNA (mRNA) for transcription ^{7,24}. The positive strand intermediates can be used as templates for the synthesis of negative strand viral RNA (vRNA) ²⁴. From the mRNA, viral proteins can be translated by host ribosomes within the cytoplasm ^{7,24}.

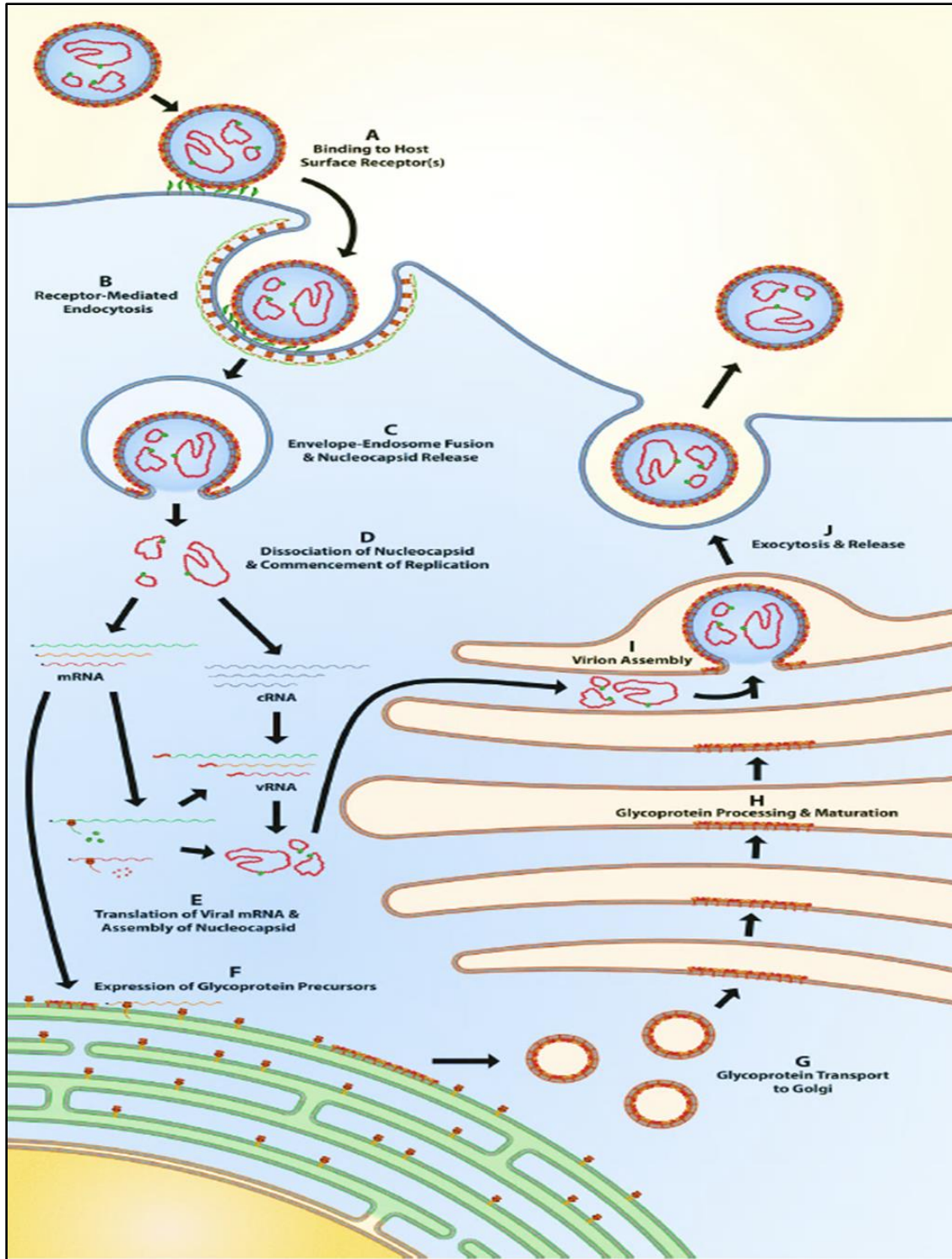


Illustration 4: Viral 'life' cycle of CCHFV ⁷

As summarized by Bente et al., 2013. The viral life cycle of attachment, endocytosis, genome release, replication, translation and assembly of structural proteins, virion assembly, Golgi mediated exocytosis and mature virion egress of CCHFV, described throughout steps A through J within the illustration. Used with permission from Elsevier Publishing Group, 2018; License: 4400960047404.

Each Bunyavirus genomic segment encodes partly complementary 5' and 3' termini of untranslated regions (UTRs) which forms a pan-handle structure of each RNA segment, and serves as *cis*-acting elements necessary for the encapsidation with NP, transcription, replication, and packaging ^{40,41}. These UTR sequences within the 'panhandle' regions are highly conserved among all Nairoviruses (3'-AGAGUUUCU... and 5'-AGAAACUCU...) ^{40,41}.

The coding sequence (CDS) of the M-segment encodes a signal peptide at the N-terminus, which likely initiate several host factors that prevent further translation from the GPC mRNA, and target the ribosome with nascent proteins to the endoplasmic reticulum (ER) ^{30,42}. The GPC is then further translated into the secretory pathway via ribosomes present on the surfaces of the ER. The residues are then woven into an out of the lumen to form various GPC products: *i.e.*, precursor G_N (Pre-G_N) and precursor G_C (Pre-G_C). Pre-G_N and Pre-G_C are processed by proprotein convertases and N-linked glycosylated in the lumen of the ER ³¹. Complexes form between the various products and enable trafficking to the trans Golgi network (TGN) ^{30,31,33}. There, secretion, further O-linked glycosylation, and cleavage events occur on various products of the GPC ³⁰. Ultimately, matured G_N and G_C form heterodimers within the lumen of the Golgi ^{24,43}. The tails of both G_N and G_C are thought to mediate the assembly of RNP into the G_NG_C heterodimer complex, and invagination of immature particles into the lumen of the Golgi ^{41,44,45}. From the Golgi, vesicles are thought to be transport matured CCHFV particles to the plasma membrane and release particles into the surrounding milieu for the viral 'life' cycle to start anew ^{7,24,40}.

RE-EMERGING THREATS

Since the 1990s, an increase of both disease and serological evidence of CCHFV infections in humans and animals, have been reported in previously CCHF-free areas, such as: Turkey, Pakistan, India, Greece, Iran, Republic of Georgia, and other Balkan countries ⁷. In the last decade, nearly 10,000 cases have been diagnosed in Turkey alone ^{7,46–48} and

an increase in seroprevalence has been observed in Greece ⁴⁹. Interestingly, the epidemiological surveys in Turkey ⁴⁷, Bulgaria ⁵⁰, Albania ⁵¹, and Greece ⁴⁹ have indicated that there is strong serological evidence of a CCHFV in both ungulates and humans, yet the actual infection rates remain quite low. This has been hypothesized to be due to the presence of sub-clinical CCHFV infections in human populations—though the reason for this remains to be determined.

Under the warmer conditions predicted by future climate scenarios, these models suggest continued tick expansion into previously *Hyalomma*-free areas ^{52–55}. Provided these ticks maintain their ability to serve as the main reservoir and transmission vector for CCHFV, incidence of human cases within these areas are expected to increase. Within the past decade, *Hyalomma spp.* have been detected in non-endemic areas such as Norway⁵³ as well as southern Germany ⁵⁶. Both tick-vectors and CCHFV genomic RNA have additionally been detected in Italy and other countries with proximity to the Iberian Peninsula, such as Portugal and Spain ^{15,57–59}. The first autochthonous case in Spain occurred in 2016, and resulted in the index case succumbing to CCHFV and nosocomial transmission from this primary case ⁵⁸. These autochthonous cases represent a grave milestone for the spread of the disease. It further highlights the need for increased surveillance of both the *Hyalomma* tick vector and CCHFV detection.

Spain, *Hyalomma* Ticks, and Crimean-Congo Hemorrhagic Fever Virus¹

To address this specific need of *Hyalomma* tick and CCHFV surveillance in Spain, our group participated in detecting and isolating CCHFV from tick pools obtained from the Extremadura region within the municipality of Cáceres, Spain. Forty-five tick pools, consisting of 210 ticks total, were isolated between the years 2014-2015 (Illustration 4).

¹ This section within Chapter 1 was previously published as a portion of: Cajimat M.N.B., **Rodriguez S.E.**, Schuster I.U.E., Swetnam D.M., Ksiazek T.G., Habela M.A., Negredo A.I., Estrada-Peña A., Barret A.D.T., and Bente D.A. Genomic characterization of Crimean-Congo hemorrhagic fever virus in *Hyalomma* tick from Spain, 2014. *Vector-Borne and Zoonotic Diseases*. 2017 Aug 24;17(10) PMID: 28836897

These ticks were identified as *Hyalomma lusitanicum* (*H. lusitanicum*), *Dermacentor spp.*, and *Rhipicephalus spp.* The tick pools were homogenized and tested by nested PCR for the presence of CCHFV using conserved primers for the genomic S-segment (Illustration 4). A tick pool consisting of *Hyalomma lusitanicum*, tested positive by PCR for CCHFV from the Cáceres locality of Herrera de Alcántara (Illustration 4). The virus was sequenced via overlapping primers for the S-, M-, and L-segments using forward and reverse walking primers previously published ^{14,60}. These contiguous sequences were assembled using ClustalW and full length S-, M-, and L-segment ORFs were submitted to GenBank under the accession numbers MF547415, MF547416, and MF547417, respectively. These sequences collectively were referred to the CCHFV isolate with the GenBank designation Cáceres2014.

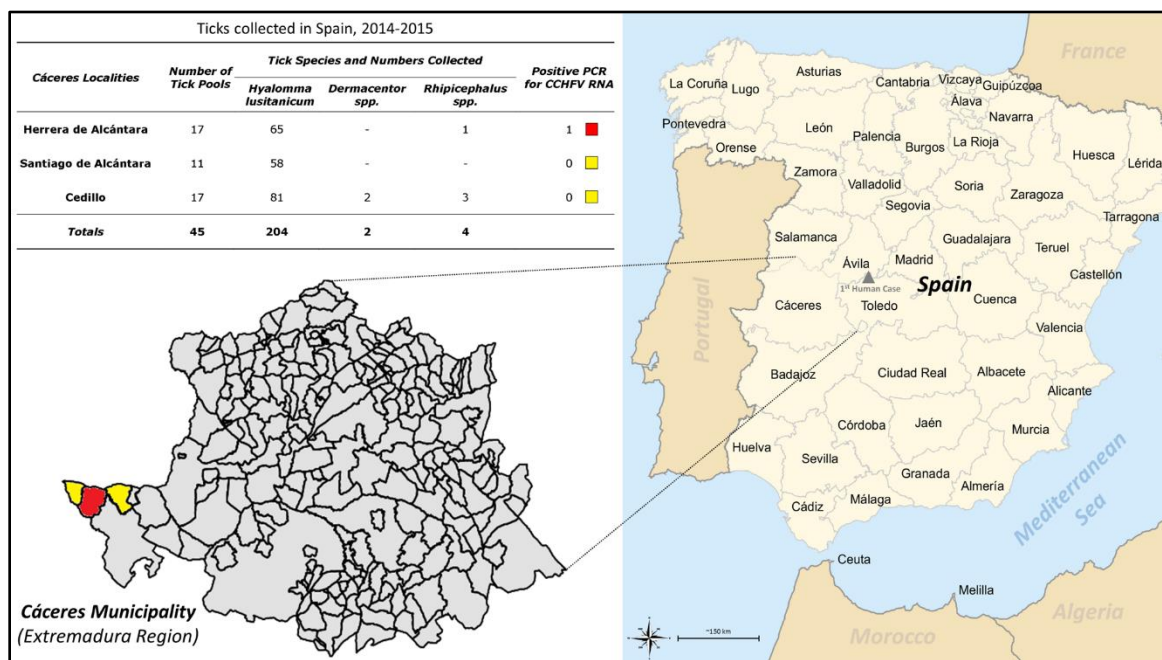


Illustration 5: Map of Spanish tick collection areas, identifications, and PCR results ⁵⁹

A map of Spain's provinces with the outset of Cáceres province, Extremadura region. The colored (yellow and red) municipalities of Herrera de Alcántara, Santiago de Alcántara, and Cedillo, had respective tick pools outlines in the table within the illustration. Used with permission from Mary Ann Liebert, Inc Publishing, 2018, via personal communications with Ms. Karen Ballen, Permissions Manager, Mary Ann Liebert, Inc.

Sequence comparisons of Cáceres2014 showed 99.4% nucleotide identity with a CCHFV S-segment fragment obtained from a *H. lusitanicum* during 2010 ¹⁵ and 99.0% identity with S-segment fragments obtained from both the fatal and nosocomial cases in the 2016 autochthonous outbreak in Avila, Spain ⁵⁸. A *H. marginatum* tick obtained from Iberian Peninsula migratory birds isolated within Morocco in 2011, tested positive for a CCHFV S-segment fragment, and our Cáceres2014 sequence matched it to 98.8% identity ⁶¹. Additionally, sequences from human cases from Mauritania and Daral, isolated during 2012, showed the highest identity with more than 99.7% nucleotide identity ⁶². Unfortunately, these comparison studies were limited to only S-segment fragments as none of the European or African isolates sequences had sequenced M- or L-segments.

These comparisons studies support the hypothesis that CCHFV spread into Spain, and probably Portugal, is driven by vector spread from West Africa—likely from migratory bird populations during northward migration events ⁶¹. As mentioned earlier, the detection of CCHFV genome/genomic-segments from *Hyalomma* ticks and the emergence of two autochthonous CCHF cases, highlight the need for active surveillance and further ecological studies in not only Spain, but for all Western Europe.

TAMPING GAPS OF KNOWLEDGE

CCHFV is a major public health threat due to its debilitating hemorrhagic disease, associated high mortality, continual spread into previously non-endemic regions, widespread availability, and potential for human misuse. As such, the USA has designated it as a federal select agent and as a ‘Category A Priority Pathogen of Biodefense and Emerging Infectious Disease’ ⁶³. This designation prioritizes research in the USA on CCHFV, due to a threat assessment of it possessing the highest risk to national security and public health ⁶³. Additionally, the WHO has categorized it as a ‘priority pathogen’ for research and development ⁶⁴. This designation highlights the need for research and

development worldwide in a public health emergency context due to the public health risk, epidemic potential, and lack of medical countermeasures for said pathogen ⁶⁴.

Part of developing scientific resources that can yield tangible medical benefits in assuaging CCHF, first starts with understanding basic concepts of how the disease establishes itself in human populations. A major gap of knowledge within the CCHFV field is in understanding why some individuals get full blown hemorrhagic fever (HF), and why some populations or regions appear to have evidence of CCHFV but lack clinical cases of CCHF. There are several hypotheses in the field that center around socioeconomics, strain-to-strain differences, routes/type of exposure, or epigenetic differences among those populations. Additionally, the major medical gap for the field is also finding ways to best prevent or treat CCHF—especially at various stages of the disease course (*i.e.*, exposure/incubation, febrile, hemorrhagic). Discovering what targets could be inhibited or exploited for medical countermeasure developments, are vital to being able to advance a preventative measure of therapeutic intervention for clinical trials in humans.

I had two unique avenues of research during my dissertation studies where I examined the influences of the *Hyalomma* tick vector on the initial transmission and pathogenesis of CCHFV. I also sought to develop a tool to study the biology of the CCHFV-GPC, which I will detail as a prime target for countermeasure developments against CCHFV. The latter project, in developing such a tool, a viral vector for CCHFV known as a pseudotype, enabled applied research in questing for countermeasure developments in a three-pronged approach at lower containment settings (BSL-2). The first approach centered on taking the pseudotype and using it as a screening tool for USA Food and Drug Administration (FDA) approved drugs, or analogous compounds of approved drugs, for inhibition of CCHFV. The second approach involved developing peptide inhibitors that can target and inhibit CCHFV from gaining access to permissive tissues, and again using the pseudotype to screen the most promising of these inhibitors. The last approach focused on using this pseudotype as a means of generating an immune

response to the CCHFV-GPC in an animal model, *i.e.* an experimental vaccine for CCHF. Each of these three applied research efforts into countermeasure developments for CCHF have bridging potential or precedence in being used clinically in humans, as detailed in the respective chapters that follow. This body of work serves to add understanding regarding the early disease course of CCHF. This dissertation also highlights the abilities of pseudotyped viruses in furthering biomedical research at low containment settings for high containment viruses and demonstrates the potential of CCHFV-GPC as a target for research and development in combating this threat to global human health.

CHAPTER 2: Early Pathogenesis of Crimean-Congo Hemorrhagic Fever Virus ²

INFLUENCES OF THE TICK VECTOR ON DISEASE TRANSMISSION

Evidence exists indicating that vectors, such as ticks, play a major role in the overall disease outcome of vector-borne pathogens ^{47,65,66}. Ticks are obligate blood-feeding ectoparasites. They use specialized mouthpieces called hypostomes to cut into the host's skin and anchor at feeding sites. While cutting into the skin, the tick secretes a glycoprotein rich 'cement' to further anchor their hypostome for prolonged blood-meals lasting up to several days ⁶⁵. Once the hypostome is cemented in place, ticks transform the site into a feeding lesion by injecting their saliva to mediate host factors regulating pain, coagulation, and immune response (Illustration 5) ^{65,67,68}. This host alteration is critical to the tick's overall success as an ectoparasite. Vector-borne pathogens utilize the ticks mediating factors as a means of initial entry into susceptible hosts and often as a 'cloak-and-dagger' approach for systemic spread ^{69,70}.

This evidence suggests that tick-borne viruses have co-evolved with their arthropod vector to utilize the ticks' subversion tactics to gain a foothold in systemically spreading. The primary transmission route of CCHFV infection is through an infected tick-bite. Antigen-presenting cells (APC) present at the tick-feeding site and orchestrate innate and adaptive immune responses, and are also likely the initial targets of CCHFV infection ⁷¹⁻⁷³. Once activated, APCs migrate to the lymph nodes to interact with effector cells, eliciting an immune response ⁷¹. Based upon studies with other tick-borne pathogens, it is likely that the tick plays a role in altering APC activation or migration in CCHFV infections ^{68,74,75}. Gaining insight into the initial steps of CCHFV pathogenesis is critical to understanding how the disease course progresses in a pathological sense and may lead to

² Portions of this chapter have been previously published as:

Rodriguez S.E.*, McAuley A.J.*, Gargili A., and Bente D.A. Interactions of Human Dermal Dendritic Cells and Langerhans Cells Treated with Hyalomma Tick Saliva with Crimean-Congo Hemorrhagic Fever Virus. *Viruses*. 2018 July 20;10(7) PMID: 3003690 (* Co-first authors)

unraveling the differences in disease outcomes and in finding mechanisms to antagonize the infection. The tick-bite therefore, plays an important role in the early pathogenesis of CCHFV, with *Hyalomma* tick saliva likely influencing both transmission and host immunoregulation.

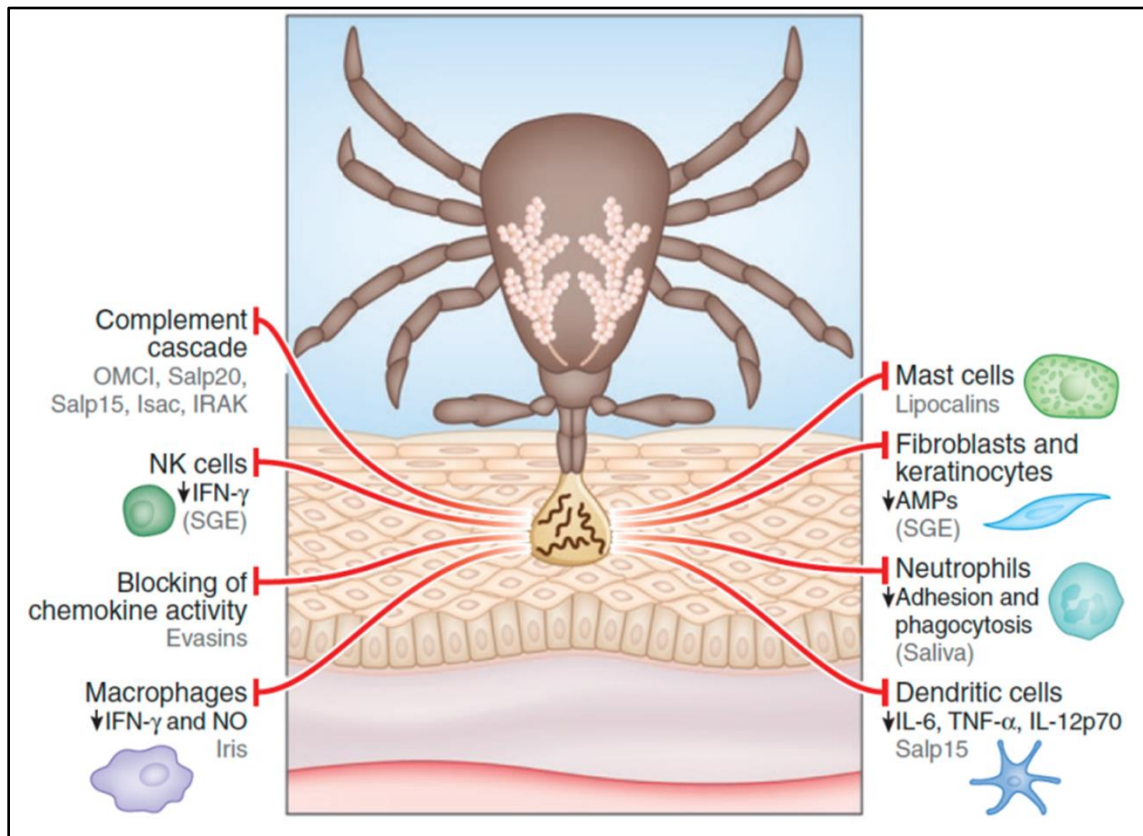


Illustration 6: Inhibition of skin innate immune responses by tick saliva ⁶⁸

During feeding, the tick introduces cement and saliva into host skin. This saliva contains numerous compounds/proteins that affect the innate immunity of the host cells. Depicted are several known salivary proteins with identified functions as reviewed in Hovius, 2009. Used with permission from Elsevier Publishing Group, 2018; License: 4414401044338.

STUDYING THE EFFECTS OF TICK-SALIVA ON CRIMEAN-CONGO HEMORRHAGIC FEVER VIRUS REPLICATION AND CELL RESPONSE IN ANTIGEN PRESENTING CELLS

Little is known about the tick–virus–host interface and the early aspects of pathogenesis for CCHF ^{7,13,46,76,77}. To elucidate this mechanism, experiments to examine which initial cells are permissive to infection, was undertaken. Previous studies have

shown that dendritic cells (DC) and macrophages are the main cells in circulation susceptible to CCHFV infection ^{72,73} and can serve as target cells for other hemorrhagic fever viruses ⁷⁸. Infection with CCHFV results in two likely immediate effects. The virus must enter and begin replication in permissive host tissues, and there will likely be modulation of cellular immune functions to establish further replication. There are two distinct immune cell populations that principally modulate immune activity within the skin; Langerhans cells (LC) and dermal dendritic cells (dDC) ⁷¹. LC reside within the epidermis and sample antigens occurring within this region of tissue. The LC are heavily involved in regulating immune activation, specifically tolerance, and local T-cell effector functions. They also participate as antigen-presenting cells (APCs) in local draining lymph nodes ⁷⁹. dDCs reside within the dermis, engage in migratory immune surveillance, draining lymph node antigen cross-presentation, and local T-cell subtype polarization ^{80,81}. Both LC and dDC, oversee the immune status and cellular response across the entirety of the skin. Studies have demonstrated that viruses employ different ways to target and immunomodulate this subset of dermal APCs ⁸²⁻⁸⁴.

As mentioned, tick saliva is a complex mixture of effector proteins, serving a variety of functions including cytolytic, vasodilator, anticoagulant, anti-inflammatory, and immunosuppressive activity ⁸⁵. Co-evolution of ticks, vertebrate hosts and tick-borne pathogens has led to a phenomenon called saliva-assisted transmission (SAT) in which enhancement of transmission of tick-borne pathogens occurs by tick saliva, with the effect documented for several tick-borne pathogens ⁸⁶. However, few studies have looked at the functions of saliva from the genus *Hyalomma* ⁸⁷⁻⁸⁹ and there is only limited information that suggest SAT occurs during CCHFV transmission ⁹⁰. Here, human dermal antigen presenting cells (dDCs and LCs) were generated from umbilical cord CD34⁺ progenitor stem cells. Using positive selections, various cytokines, incubations, and flow cytometry for confirmation and purity assessments, dDC and LC were generated according to methods outlined in Rozis *et al.* 2008 (Illustration 6) ⁹¹. *H. marginatum* tick salivary gland

extract (SGE) was obtained from various tick pools from both male and female *H. marginatum* ticks that had fed on rabbits for at least three days (Illustration 6). Ticks were dissected and the salivary glands (acinus and salivary ducts) were removed and pooled according to sex and engorgement status. The salivary glands were lysed and homogenized. Clarified supernatants were quantified, filtered, and designated tick SGE. Our overall goal was to expose skin APC to both *H. marginatum* SGE and CCHFV and survey outcomes that can affect host response(s) as shown in Illustration 6.

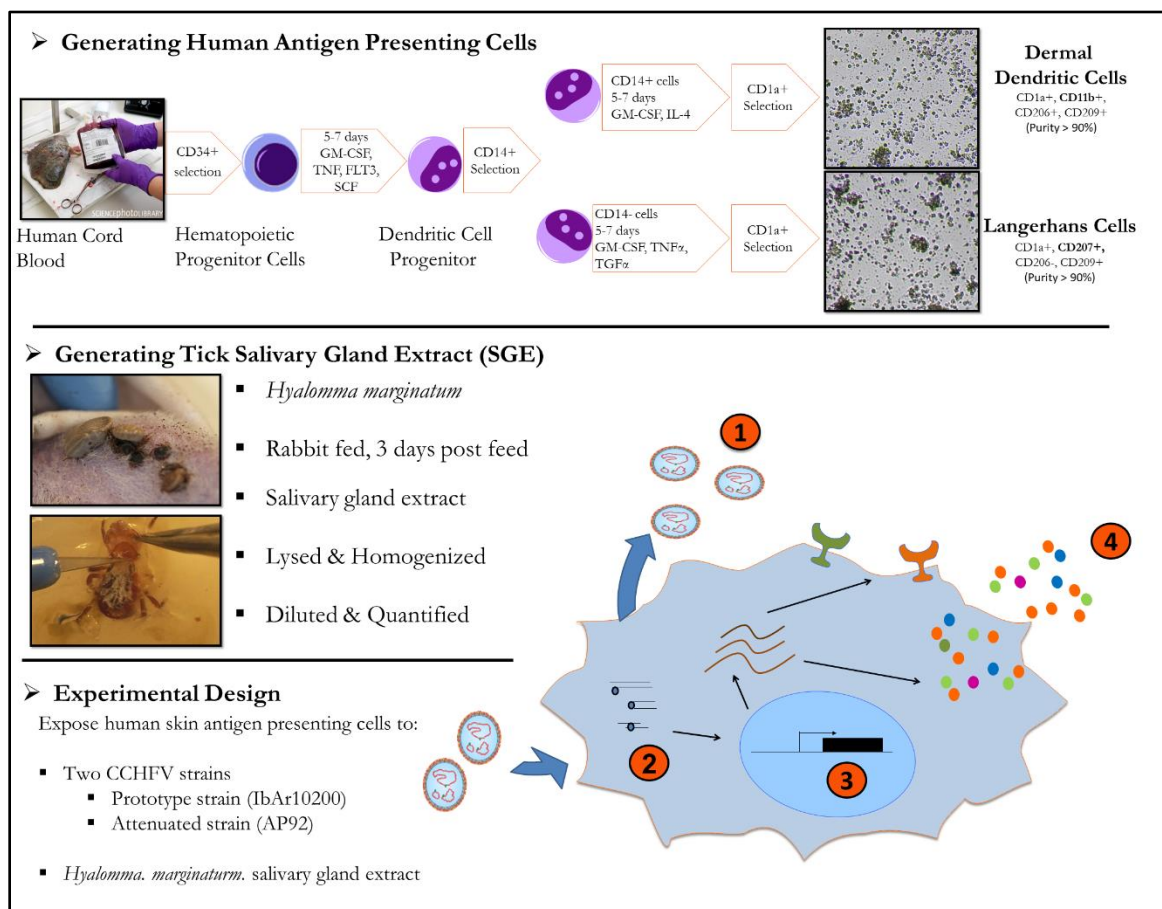


Illustration 7: Experimental design for generating human dermal antigen presenting cells and *Hyalomma* tick salivary gland extract⁹²

As described in Rodriguez et al., 2018, human dermal antigen presenting cells (APC) were generated by isolating hematopoietic stem cells (HSC) from placental cord blood from various donors. HSC were positively selected for cells bearing the human clusters of differentiation (CD) markers CD34⁺, CD14⁺, and CD1a⁺ on their exterior surfaces following various cytokine treatments and incubations as described in Rozis et al., 2008. Skin APC were confirmed by flow cytometry for CD markers for human dermal dendritic cells (dDC) and Langerhans cells (LC). *Hyalomma* tick salivary gland extract (SGE) was prepared by feeding *H.*

marginatum adult male and female ticks on rabbits for several days as described in Gargili et al., 2013. Various pools of female and male fed ticks were euthanized and necropsied for salivary gland acinus organ removal at various days post tick-attachment. Acinus were washed, sanitized, lysed, and homogenized by methods described in Rodriguez et al., 2018. Homogenate was termed SGE and was quantified and sterile filtered before use. Skin APC were exposed to 10 ug/mL of SGE and to the prototype or attenuated strains of CCHFV, IbAr10200 and AP92, respectively. Supernatants and cell lysates were collected and measured for various cytokines and transcriptional profiling. Used and modified under the Creative Commons Attribution 4.0 International License ¹⁰.

Given that both dendritic cells and macrophages are susceptible to CCHFV, we hypothesized that dDC and LC would also be permissive to infection. Both dDC and LC were infected and were 25% and 3%, respectively, permissive to CCHFV (strain: IbAr10200) infection at a MOI of 0.1 using flow cytometry using immunofluorescence against the NP (data not shown). Both dDC and LC were then exposed to CCHFV alone, and in the presence of *H. marginatum* SGE (Figure 1).

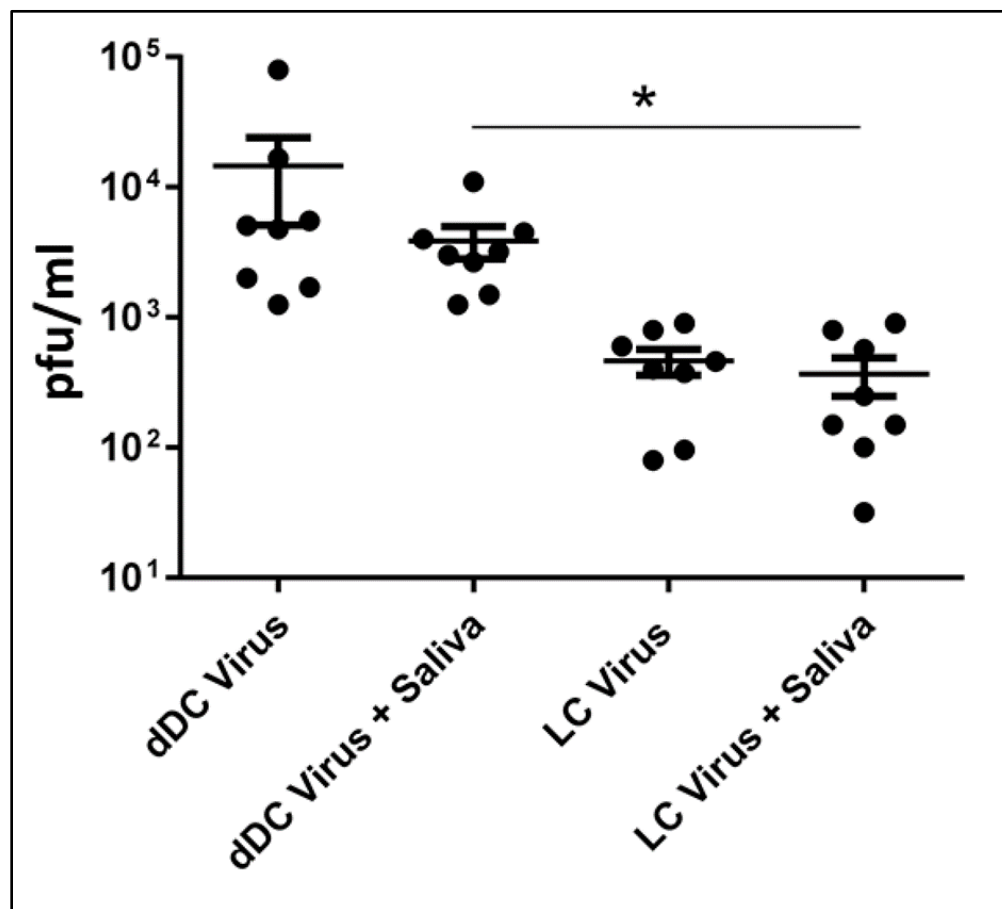


Figure 1: CCHFV titers from infected and tick salivary gland extract (SGE) treated skin antigen presenting cells (APC) ⁹²

Human skin APC were generated from eight different donors and were infected with CCHFV strain IbAr10200 at a MOI of 0.1 and treated with 10 ug of SGE. Supernatants were harvested 48 hours post infection, and CCHFV titers were determined by plaque assay on SW-13 cells. Significance between mock and treatment groups at $p < 0.05$ is designated with an asterisk (). Used and modified under the Creative Commons Attribution 4.0 International License ¹⁰.*

Our results indicate that dDC are both more permissive to infection and replicate the CCHFV to higher titers. There was notable donor-to-donor variability in viral output with titers ranging from 40 pfu/mL to 8×10^4 pfu/mL (Figure 1). A significant difference was observed between the viral titers between dDC and LC, although *Hyalomma* tick SGE did not significantly influence titers from either skin APC type (Figure 1).

In a similar manner, dDC and LC were also infected with CCHFV (strain: IbAr10200) and exposed to *Hyalomma* tick SGE, and transcriptomic profiles were assayed for each cell type and condition following 12 hours of either exposure or infection. A considerable degree of variability in gene expression was observed between the two cell types with gene fold-changes greater in LC than dDC (Figure 2A). The three more markedly altered genes for each cell type were analyzed using Ingenuity Pathway Analysis. High levels of expression of Tapasin Binding Protein (TAPBP) and Antigenic Peptide Transporter 2 (TAP2) was observed in infected alone, and infected/SGE-exposed LC (Figure 2B). A decreased express of other factors suggested a strong interferon regulatory factor (IRF)-1 activation. High levels of expression of cluster of differentiation (CD)40 were also observed in infected cells and infected/SGE-exposed dDC. Similarly, to LC, the dDC also had lower expression of other factors suggesting an IFR-7 activation (Figure 2B).

When skin APC were exposed to SGE, this did not seem to impact transcriptional profiles in either infected or naïve cells. To a small extent, SGE exposure alone on dDC and LC did display general downregulation (approximately two-fold)—though in dDC, SGE led to a small increase in CCL3 expression of mock cells (Figure 2A). Gene expression of skin APC after CCHFV infection and infection/SGE exposure were similar.

The only exceptions noted were CD4 and CCL3 expression within dDC, where SGE seemed to enhance virus-associated gene expression (Figure 2A).

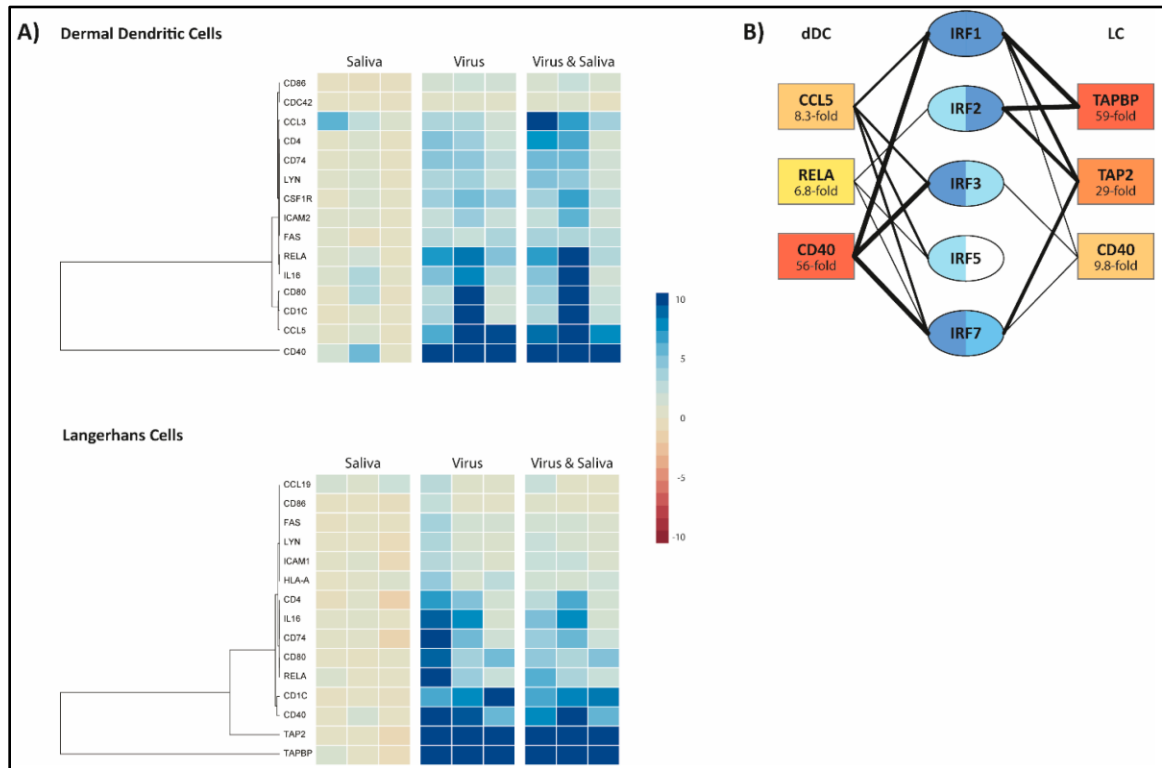


Figure 2: Expression of antigen presentation genes following CCHFV infection or *Hyalomma* tick salivary gland extract (SGE) ⁹²

Human skin APC were infected to CCHFV (strain: IbAr10200) and/or exposed Hyalomma tick (SGE). Twelve hours after exposure or infection, APC were lysed, and cell RNA was prepared for qRT-PCR. (A) Genes with a significant (fold-change) in expression was determined by hierarchical clustering. (B) Ingenuity Pathway Analysis for the three most altered genes for upstream transcription factor activation prediction. Used under the Creative Commons Attribution 4.0 International License ¹⁰.

A multiplexed detection assay for detection of various chemokines and cytokines was performed on clarified dDC and LC supernatants. Supernatants were harvested at 24 hours post infection (hpi) from cells infected with CCHFV (strain: IbAr10200) or those additionally treated with SGE. Thirteen total cytokines/chemokines were assayed and displayed in Figure 3 are the four which demonstrated substantial changes compared to baseline (mock) or amongst respective treatment groups. As expected, the profiles of

cytokines and chemokines secreted, was different between the types of skin APC ⁹³. A statistically significant increase in the detection of the chemokine MCP-1 and cytokine IL-6 from dDC supernatants that were infected with CCHFV and treated with *Hyalomma marginatum* SGE was observed (Figure 3A,C). Supernatants from LC also showed significant increases in SGE-treated LC compared to mock with regards to the cytokine TNF- α (Figure 3D). Increased levels of both chemokines IL-8 and MCP-1 were also found among all treatment groups of dDC compared to LC (Figure 3B,C).

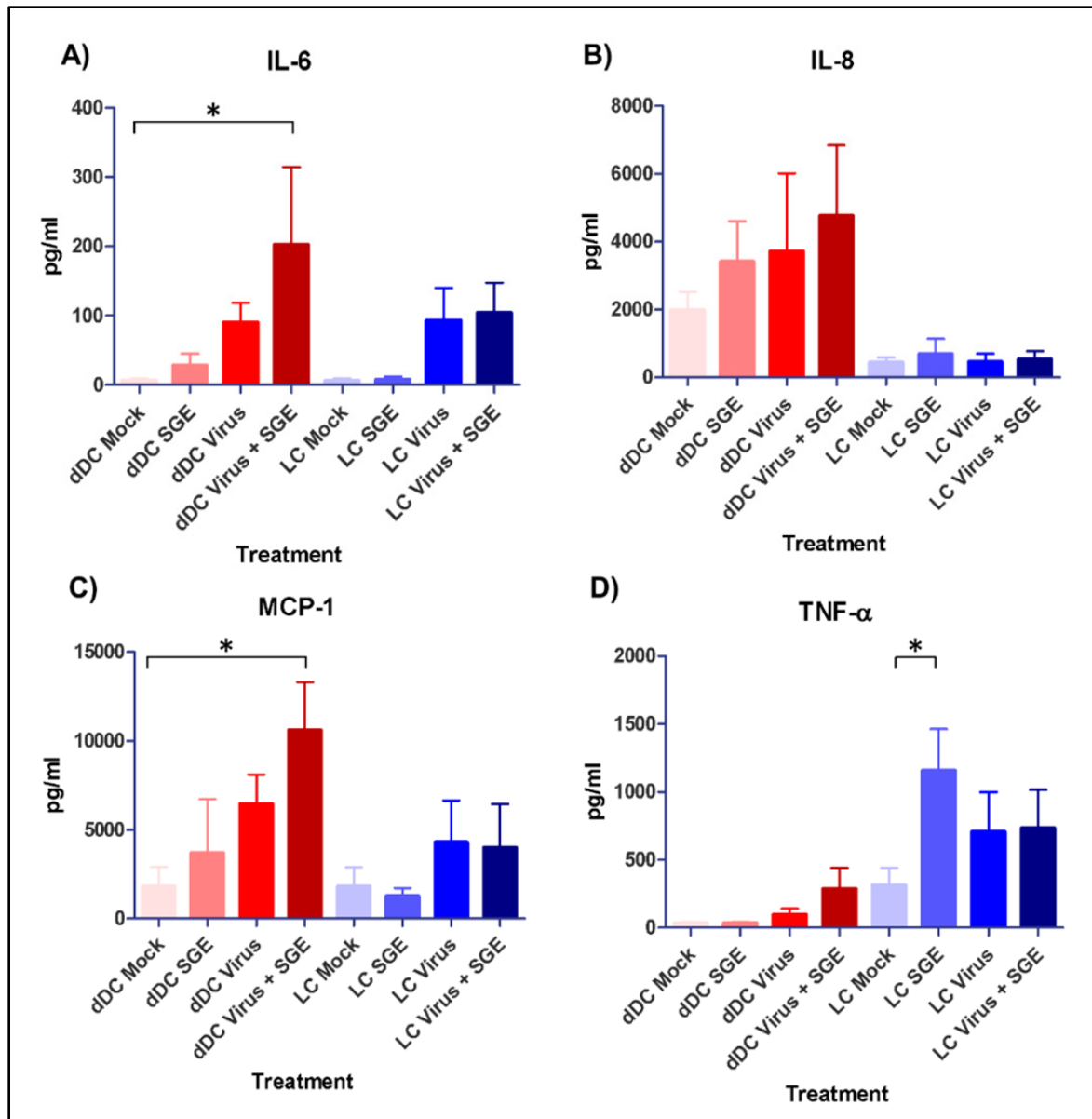


Figure 3: Cytokine and chemokine responses of mock, virus, and *Hyalomma* tick SGE treated human skin APC⁹²

Human dDC and LC were studied using a multiplexed antibody and analyte detection assay. Cytokines (A, D) and chemokines (B, C) were detected by harvesting mock and treatment cell clarified supernatants at 24 hours post infection (hpi) after infection with CCHFV (strain: IbAr10200) and treatment with or without *Hyalomma* tick SGE. These samples were run in technical duplicate on a Luminex bead-based multiplex system with kit provided control standards for pg/mL determinations. Significance between mock and indicated treatment groups at $p < 0.05$ is designated with an asterisk (*) symbol. Used under the Creative Commons Attribution 4.0 International License¹⁰.

Studies have shown that tick saliva can also inhibit not only the activation and maturation of APC, but of migration capabilities as well^{67,68,74,75,94}. Once activated, cell

migration of APC is a primary function in order to initiate antigen presentation and furthering immune and inflammatory responses ⁷¹. Our group has investigated migration markers, such as CD197, and have found that this marker is expressed during monocyte derived dendritic cells (moDC) infection with CCHFV (data not shown). Currently, no published studies exist examining the effects of *Hyalomma* tick SGE on APC migration abilities. To study this, I employed a system for quantitative determination of numerous factors on cell migration using pharmacological agents, similar to a Boyden chamber migration assay (Figure 4).

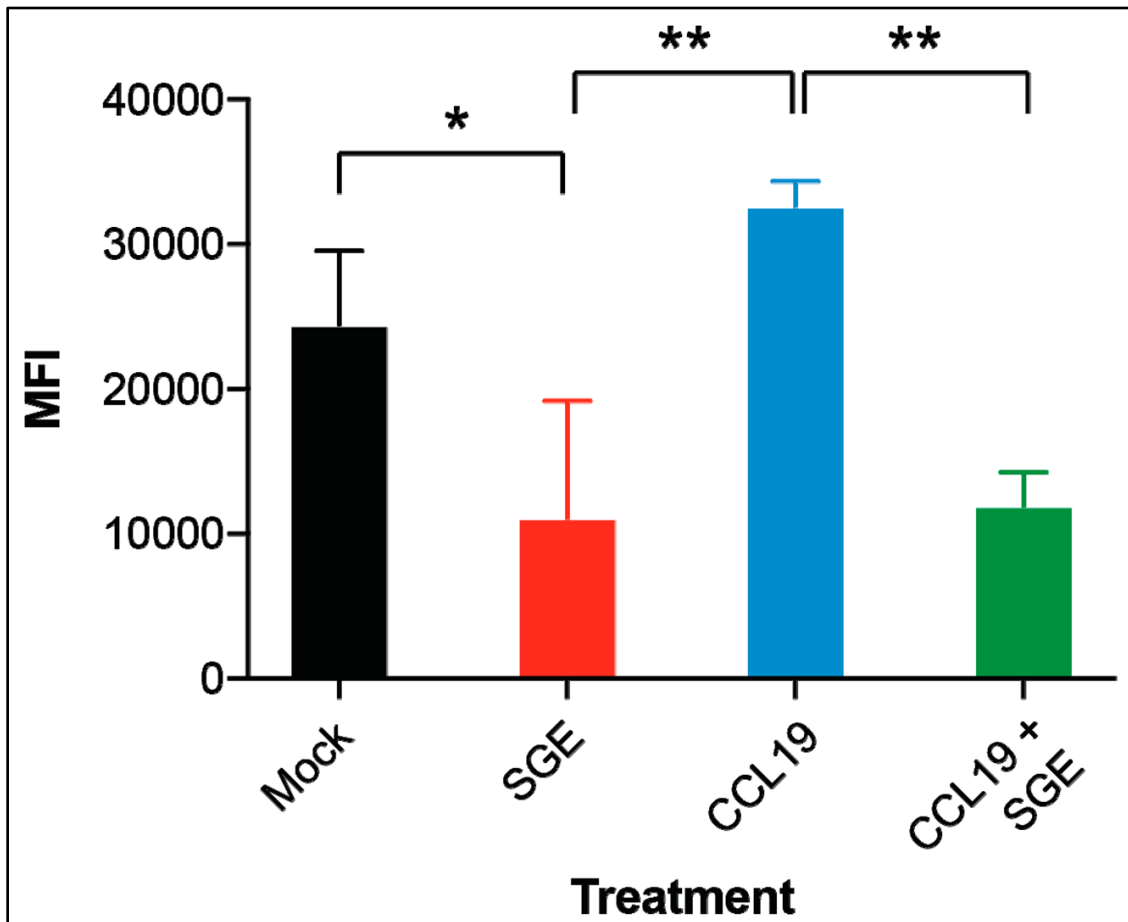


Figure 4: Salivary gland extract (SGE) from *Hyalomma* ticks inhibits migration of human monocyte-derived dendritic cells (moDC) ⁹²

moDC migration was studied in a trans-well migration assay. When *moDC* were exposed to salivary gland extract (SGE) fewer cells migrated to the other side of the trans-well (mock = RMPI only) or with chemoattractant (CCL19). The number of migrated cells was assessed by lysing cells and analyzing DNA content with an intercalating dye. Fluorescence was measured as mean fluorescence intensity (MFI).

Significance between mock and indicated treatment groups at $p < 0.05$ and $p < 0.01$ is designated with one or two asterisk (*) symbols, respectively. Used under the Creative Commons Attribution 4.0 International License¹⁰.

Under serum starved conditions, monocyte-derived dendritic cells (moDC) were exposed to *Hyalomma* tick SGE. The chemokine C-C motif ligand (CCL) 19, a chemoattractant molecule for APC to hone to lymph nodes was used either alone or combined with SGE onto SGE pre-treated cells⁹⁵. Cells treated with *Hyalomma* tick SGE were inhibited from migrating across chamber wells, with a significant decrease compared to mock (Figure 4). The chambers which contained CCL19 had an increase in the mean fluorescence intensity (MFI) indicating moDC migration into these chambers. This indicated enhanced migration due to chemotaxis (Figure 4). When CCL19 and SGE were combined as co-treatments, a statistically significant decrease in the number of cells migrating into the chemotaxis (CCL19) chamber was observed. CCL19 is known to bind to several receptors, however its principle receptor is the chemokine receptor chemokine C-C motif receptor (CCR) 7^{96,97}. Transcriptional analysis outlined in Figure 2 did not demonstrate a fold change of CCR7 or other binding co-receptors for CCL19 such as CCR5, CXCR4⁹⁷. The SGE-mediated inhibition of moDC migration is therefore likely not due to the downregulation of those CCL19 receptors. It is curious if there is an alternative mechanism inhibiting migration under the exposure of CCL19.

This is the first instance of *Hyalomma* tick saliva being tested in this manner, confirming the paradigm that tick saliva plays an overall immunomodulatory role. These findings indicate that human dDC and LC are susceptible and permissive to CCHFV infection. SGE does not necessarily have an influence on CCHFV replication in cultured dDC or LC. The result indicated that migration of dDC or LC could be affected by SGE in the initial pathogenesis, and the infection via *Hyalomma* tick likely plays an important role in the immunomodulation of host innate immune responses.

CHAPTER 3: Selecting Crimean-Congo Hemorrhagic Fever Virus

Countermeasure Targets³

EXAMINING TARGETS AT THE VIRAL ORDER, FAMILY, AND GENUS LEVELS

The viral order *Bunyavirales* contains a diverse array of virus families and genera, many of the respective viral species have broad host associations. Over 500 members of this order infect, and in some cases cause disease, in various vertebrates and invertebrates⁴⁰. Bunyaviruses are largely transmitted via mammals and arthropods. Those that are transmitted by arthropods are designated ‘arboviruses’ (arthropod-borne viruses) which can be transmitted by either ticks, mosquitos, midges, sandflies, or thrips⁹⁸. Of these arboviruses belonging to the order *Bunyavirales*, several members are also important pathogens which can inflict devastating diseases in economically and/or agriculturally important plants and animals. The most threatening members can cause severe encephalitis or hemorrhagic diseases in humans (*e.g* CCHFV) and have been responsible for large outbreaks which have resulted in the loss of human lives²⁴.

Experimental countermeasures for the viral order *Bunyaviridae*

At present, there are no broadly licensed preventative vaccines or antiviral therapies approved to treat human infections with pathogenic bunyaviruses⁹⁹. Though, advances in basic and applied virology have yielded several promising experimental countermeasures for members of *Bunyavirales*⁹⁹. Table 1 details what has been accomplished in the bunyaviruses field with respect to experimental antiviral countermeasure developments. The most promising experimental countermeasures are currently Ribavirin and Favipiravir, the latter formerly known as T-705. The reason behind these experimental success stories

³ Portions of this chapter have been previously published in: Kuhn J.H., Wiley M.R., **Rodriguez S.E.**, Bao Y., Prieto K., Travassos da Rosa A.P.A., Guzman H., Savji N., Ladner J.T., Tesh R.B., Wada J., Jahrling P.B., Bente D.A., and Palacios G. Genomic characterization of the genus *Nairovirus* (family *Bunyaviridae*). *Viruses*. 2016 Jun 10;8(6) PMID: 27294949; PMCID: PMC4926184

is due to their broad-spectrum antiviral activity across viral orders and their demonstrated *in vitro* and in most cases, *in vivo*, antagonism of several pathogenic members of *Bunyavirales*. Both Ribavirin and Favipiravir have demonstrated *in vitro* and *in vivo* antagonism of CCHFV if administered early during infection in CCHF mouse models^{100,101}. Ribavirin has been repurposed for human CCHF cases and used compassionately for decades, with mixed results when used clinically^{7,16–18,102–107}. Favipiravir is currently undergoing clinical trials and has been used experimentally in humans for influenza treatment but not yet applied to human CCHF cases¹⁰⁸.

Table 1: Review of experimental countermeasures for members of *Bunyavirales*

Bunyavirus	Target	Compound	Type	Citation
<u>CCHFV</u> , HNTV, SFTSV, RVFV	Host Response	IFN/Poly(ICLC)	IFN/Nucleicacid Mimic	Gowen et al. (2014), Peters et al. (1986), Anderson et al., (2006), Oelschlegel et al. (2007), Bordin et al. (2015), Shimajima et al., (2015)
HAZV, RVFV, ANDV	NP, GPC, RdRp	siRNA/shRNA	Nucleicacid	Flusin et al. (2011), Faburay and Richt (2016), Chiang et al. (2014), Scott et al. (2012)
ANDV, RVFV, <u>CCHFV</u> , SFTSV	RdRp	Favipiravir(T-705)	Small molecule	Safronetz et al. (2013), Scharton et al. (2014), Caroline et al. (2014), Oestereich et al. (2014), Tani et al. (2016), Gowen et al. (2016)
ANDV, RVFV, <u>CCHFV</u> , SFTSV, HNTV, SEOV	RdRp	Ribavirin	Small molecule	Kende et al. (1995), Peters et al. (1986), Scharton et al. (2014) Safronetz et al. (2011), Ogg et al. (2013), Oestereich et al. (2014) Tani et al. (2016), Huggins et al. (1986), Murphy et al. (2001)
RVFV	RdRp	BCX4430	Small molecule	Warren et al. (2014)
HNTV	RdRp	ETAR	Small molecule	Chung et al. (2008)
HNTV, RVFV, PUUV	NP	MxA	GTPase	Frese et al. (1996), Kanerva et al. (1996), Bridgen et al. (2004)
RVFV	NP	RNA Aptamer	Nucleicacid	Ellenbecker et al. (2015)
RVFV, SFTSV	NP	Suramin	Small molecule	Jiao et al. (2013), Ellenbecker et al. (2014)
ANDV, SNV	NP	K31/34/103772	Small Molecules	Salim et al. (2016)
RVFV	GPC	JL118/JL122	Small molecule	Vigant et al. (2013)
ANDV, SFTSV, PUUV	GPC	Immunoglobulins	Small molecule	Haese et al. (2015), Guo et al. (2013), DE Carvalho Nicacio et al. (2000)
SEOV	GPC	Lactoferrin	Small molecule	Murphy et al. (2001)
<u>CCHFV</u>	GPC	Chloroquine	Aminoquinoline	Ferraris et al. (2015)
RVFV	GPC	G202-0362/C795-0925	Small molecule	Mudhasani et al. (2014)
RVFV, ANDV, PUUV	GPC	Fusion Inhibitor Peptides	Conjugated Peptides	Koehler et al. (2013), Barriga et al. (2016)
SNV ANDV	GPC	Anti-Attachment Peptides	Conjugated Peptides	Hall et al. (2007, 2009)
SNV ANDV HNTV	GPC	Anti-Attachment Molecules	Small Molecules	Hall et al. (2010)
RVFV	GPC	LJ001	Small Molecules	Wolf et al. (2010)
RVFV	GPC	Sorafenib	Small Molecules	Bendict et al. (2015)

This table summarizes the findings of Gowen and Hickerson (2017) and details the antiviral types and compounds developed for human pathogenic Bunyaviruses⁹⁹. It further details the targeted protein for each compound/virus. Abbreviations are defined as the following: nucleoprotein (NP), glycoprotein precursor (GPC), RNA-dependent RNA-polymerase (RdRp), interferon (IFN), MxA (human myxovirus resistance protein 1), Crimean-Congo hemorrhagic fever virus (CCHFV), Hazara virus (HAZV), Hantaan virus (HNTV), severe fever with thrombocytopenia syndrome virus (SFTSV), Rift valley fever virus (RVFV), Andes virus (ANDV), Seoul virus (SEOV), Puumala virus (PUUV), Sin Nombre virus (SNV), small interfering RNA (siRNA), and small hairpin RNA (shRNA).

Many of the listed antiviral experimental compounds in Table 1, target host factors that antagonize viral entry, or attempt to induce antiviral states. Many of the compounds in Table 1 target conserved portions of the products encoded by the three ORFs among the bunyavirus genomes. This compiled information was useful in moving forward with honing the search for effective countermeasure targets for the *Nairoviridae* family. The initial working hypothesis for countermeasure design, was that conserved areas within the *Bunyavirales* order, where multiple existing compounds have demonstrated *in vitro* and/or *in vivo* efficacy, would be the most promising areas to construct countermeasures against viruses within the family *Nairoviridae*.

Homologies of genome encoded proteins among bunyaviruses within the family *Nairoviridae*

Based off the countermeasures that had been designed against the order level, conserved amino acid residues encoded within the genomic segments of viruses within the family *Nairoviridae*, were examined. The working hypothesis was that a genomic analysis would provide evidence of conserved residues which would imply functionally important viral components, pertinent to the Nairovirus ‘life’ cycle. A typical Nairovirus genome is around 18.8 kilobases (kb), with the S-segment approximately 1.7 kb, the M-segment approximately 4.9 kb, and the L-segment approximately 12.2 kb ²⁴. Sequenced/published and un-sequenced isolates from the World Reference Center of Emerging Viruses and Arboviruses (WRCEVA), Galveston, Texas, USA, were obtained. Viral RNA was extracted and was then converted to cDNA and sequenced via next generation sequencing (NGS) methods. All genomic sequences for S-, M-, and L-segments were assembled, translated, and residues were aligned using an alignment score matrix. Phylogenetic analysis was conducted, and twelve distinct Nairovirus species groups were identified consisting of 43 members, total. All 43 nairoviruses had their respective genomes aligned

using bioinformatics software, and a similarities index was applied to translated amino acids within each segment's ORF as outlined in Illustration 8.

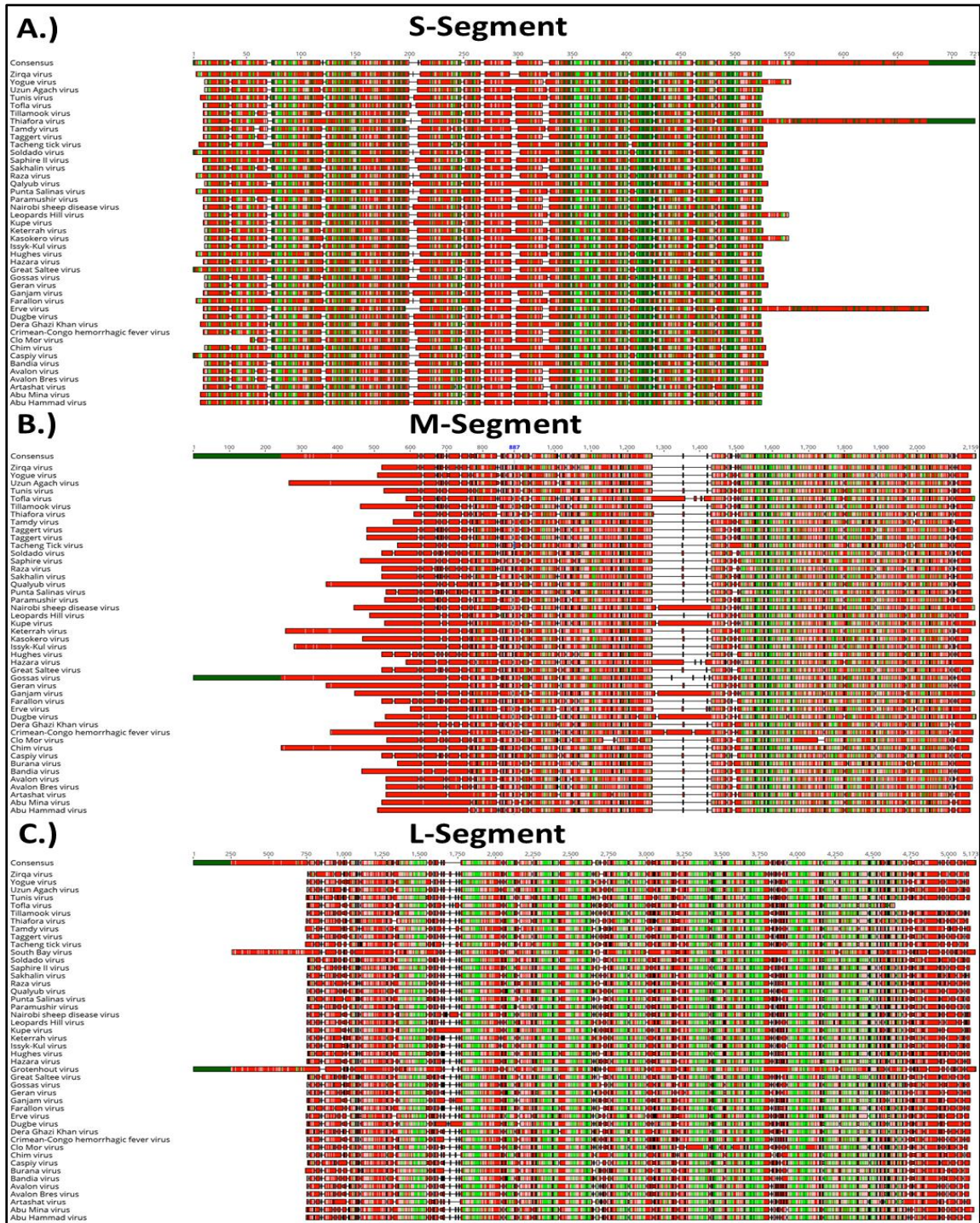


Illustration 8: Amino acid residue conservations among Nairoviruses

The predicted complete open reading frames (ORF) of each genomic segment. These analyses do not include untranslated regions (UTR). Using a Blosum62 score matrix (Geneious software), all sites were aligned using the Geneious global alignment with free end gaps (gap open penalty 12, extension penalty 3), and sites within aligned columns must have a score equal to or exceeding a specified threshold for being identical or similar (depending on score matrix for residue size, hydrophobicity, polarity, isoelectric point, etc.). The color for that column depicts the fraction of similar residues from the alignment within the full group. Legend: Dark green indicates 100% similarity among residues (higher conservation); light green indicates >80% similarity among residues; pink indicates >60% similarity among residues; red indicates <60% similarity among residues (lower conservation). The similarities map of all published (and complete) Nairovirus, NP (A), GPC (B), and RdRp (C). Some isolates, like Burana and Grotenhout Nairoviruses, were not included in specific genomic segment analysis due to incomplete ORF.

As shown in Illustrations 8, there were several areas within Nairovirus ORFs which encode the various NP, GPC, and RdRp, which are shaded light or darker green, indicating a high degree of similarity and conservation in these areas. The *Nairoviridae* NP has four regions of high similarity, three of them located on the C-terminal portion of the ORF. The Nairovirus GPC has one region of high similarity scoring between residues 1,500-1,600; where the predicted N-terminus of the Nairovirus G_C would be. This is estimated based off empirical data for CCHFV G_C and the conserved motifs RKLL or RKPL found upstream of the approximate 1,500-2,100 residues within the Nairovirus GPC. The Nairovirus RdRp has nine regions with higher similarity spaced throughout the ORF. This information indicates that the NP and RdRp appear to have more similar areas among Nairoviruses, whereas the GPCs of those Nairoviruses have only a single conserved region within the G_C. Next, I examined how Nairovirus polyproteins might be processed by host-cell factors, like proprotein convertases, glycosylation events, and the number/type of structural proteins generated.

Very little is known about the majority of Nairovirus GPC processing, and only the CCHFV-GPC has been studied and detailed^{24,27,109,110}. As discussed in previous chapters, CCHFV has one of the largest and most complex GPC among all bunyavirus GPCs. It requires numerous host factors for processing, cleavage, glycosylation, and maturation to yield the mature structural proteins required for virion assembly. I used experimentally proven processing motifs for CCHFV (RSKR, RKPL, RRLL, RKLL)^{30,33,42} and *in silico*

modeling to determine whether these motifs, or similar proprotein cleavage motifs were predicted on the other members of the family *Nairoviridae*, and if so, which might be conserved at the family level. Table 2 details the predicted Nairovirus processing events, which include conservation of protein convertase cleavage sites, glycosylation events, as well as the number of transmembrane domains. All members had signal peptides that permit a complex GPC polyprotein that is likely threaded in and out of the ER lumen given the multiple predicted transmembrane domains²³. These facets suggest the requirement of ER processing overall, for all Nairovirus GPC. The proprotein cleavage motif RKRL (SKI-1 like protease) is present throughout all family members, and RRLL (SKI-1 protease)⁴² is present in more than 90% of all *Nairoviridae* member GPC. All members have predicted N- and O-linked glycosylation sites to varying degrees²³. Of the predicted glycosylation patterns, the highest numbers of both N- and O-linked were associated with the pathogenic members such as CCHFV, Nairobi sheep disease virus (NSDV), and Ketarah virus (KETV)²³.

Table 2: Predicted characteristics and host cell processing of the genus members within the family *Nairoviridae*²³

Predicted Glycoprotein Precursor Processing	<i>Crimean-Congo hemorrhagic fever nairovirus</i>	<i>Hazara nairovirus</i>	<i>Dugbe nairovirus</i>	<i>Sakhalin nairovirus</i>	<i>Thiafora nairovirus</i>	<i>Kasokero nairovirus</i>	<i>Qalyub nairovirus</i>	<i>Keterah nairovirus</i>	<i>Dera Ghazi Khan nairovirus</i>	<i>Hughes nairovirus</i>	<i>Burana nairovirus</i>
Polyprotein Mass (deduced kDa)	187	158	173	158	144	159	164	183	157	155	150*
Glycoproteins [§]	5	3	3	3	3	2	4	4	3	2	3
Conserved Cleavage Sites	RSKR, RKPL, RRLL, RKLL	RRLL, RKLL	RKPL, RRLL, RKLL	RRLL, RKLL, RKPL	RRLL, RKLL	RRLL, RKLL	RKPL, RKLL	RKLL	RRLL, RKLL	RRLL, RKLL	RRLL, RKLL, RKPL
O-Linked Glycosylations	100	29	38	35	33	38	48	135	17	4	38
N-Linked Glycosylations	11	6	7	17	12	12	12	20	12	12	9
Transmembrane domains (TMDs)	5	5	5	3	3	4	2 ^{¶¶}	3	3	4	3
Glycosylated Regions/Mucin-like domains (MLDs)	1	1	1	1	1	1	1	2-3	1	None	1
MLD Mass (deduced kDa)	23	3-5	11	3-10	7	8-11	10-12	8-37	3-5	0	8-11

Nairovirus M-segment polyprotein descriptions. Each species column depicts averages of its members. Sample sizes are: Crimean-Congo hemorrhagic fever nairovirus n=121, “Hazara nairovirus” n=2, Dugbe nairovirus n=5 (which included Nairobi sheep disease nairovirus genus), Sakhalin nairovirus n=4, Thiafora nairovirus n=2, “Kasokero nairovirus” n=3, Qalyub nairovirus n=2, “Keterah nairovirus” n=2, Dera Ghazi Khan nairovirus n=5, Hughes nairovirus n=7, and “Burana nairovirus” n=3. Averages for predicted characteristics were rounded up. Proposed new taxa are highlighted in red and placed in quotation marks. □□□A single member of this species group (Qalyub nairovirus) is predicted to contain only a single transmembrane region. ¥ No differentiation of structural versus non-structural glycoproteins. φ Two

*members of the species Burana nairovirus are predicted to have two open reading frames on the M-segment encoding a separate stand-alone glycoprotein next to the polyprotein (GPC). Used under the Creative Commons Attribution 4.0 International License*¹⁰.

As demonstrated, at the genus level, members of *Nairoviridae* conserve several host cell processing features for GPC maturation. Based off this *in silico* data, the family *Nairoviridae* appears to contain numerous conserved factors that are likely necessary for host processing of the GPC. As demonstrated with Table 2, modulation or disruption of host cell processing machinery, could be a useful avenue in derailing the processing and maturation of Nairovirus GPCs.

Examining putative functional amino acid residues for the genus *Crimean-Congo hemorrhagic fever virus*

The GPC encodes for elements that are vital to the overall viral life cycle, but perhaps most importantly, it encodes for elements that dictate tissue tropisms, likely for both animal and arthropod cells. Given the broad geographic range of CCHFV, it was important to understand how this geographic range has influenced diversity of the various CCHFV species/isolates. Antigenic drift, or recombination events resulting in antigenic shift, can alter how effective countermeasures, especially vectored vaccines, might be in combating circulating strains of CCHFV. To examine the variability among CCHFV, I examined the translated GPC from all published and complete GenBank isolates (Table 3). Much of the variability attributed to the M-segment lies within the nonstructural proteins, with only approximately 3% of all MLD amino acid residues being conserved across all the CCHFV genus (Table 3). However, despite the broad geographic range, over 65% of residues within the ectodomain of the G_C are identical (Table 3). While there is no empirical cut off that defines conservation of antigenic targets on viruses, it is noteworthy that the highest conservation of the surface glycoproteins is on the ectodomain of the G_C among all CCHFV published strains.

Table 3: Identities and similarities of residues among all GenBank published CCHFV-GPC

Residue Comparisons		GPC	Non Structural			Structural			
			Mucin	GP38	NS _M	G _N	G _C	Ecto-G _N	Ecto-G _C
% Identical Sites	All Published Strains	44.0	2.8	39.0	40.2	55.2	60.6	53.8	65.2
% Similar Sites	All Published Strains	90.2	57.5	91.4	94.6	96.7	97.8	97.1	98.5

A total of 121 complete ORF of the CCHFV-GPC were aligned using a Blosum62 score matrix (Geneious software) with global alignment, free end gaps (gap open penalty 12, extension penalty 3), and sites within aligned columns must have a score equal to or exceeding a specified threshold for being identical or similar (depending on score matrix for residue size, hydrophobicity, polarity, isoelectric point, etc.). A consensus level map was divided into Mucin-like domain (MLD), GP38, G_N, NS_M, and G_C. Both G_N and G_C were further analyzed with respect to the ectodomains—the portions on the exterior of mature CCHFV particles.

SELECTING THE CRIMEAN-CONGO HEMORRHAGIC FEVER VIRUS GLYCOPROTEIN PRECURSOR AS A TARGET FOR VIRAL COUNTERMEASURE DEVELOPMENTS

Based on these findings outlined in Illustration 8 and Tables 2 and 3, the NP among Nairoviruses showed the strongest similarity scoring among ORFs. The RdRp had several groups of moderate similarity scoring, and the GPC had one strong area of similarity.

This area within the GPC is predicted to be the G_C glycoprotein, which for CCHFV—contains important elements regulating viral entry such as binding to the putative cell receptor nucleolin ³⁵, possessing a putative class II fusion domain ³⁹, and contains areas which antibodies can bind ^{111,112} (Illustration 9).

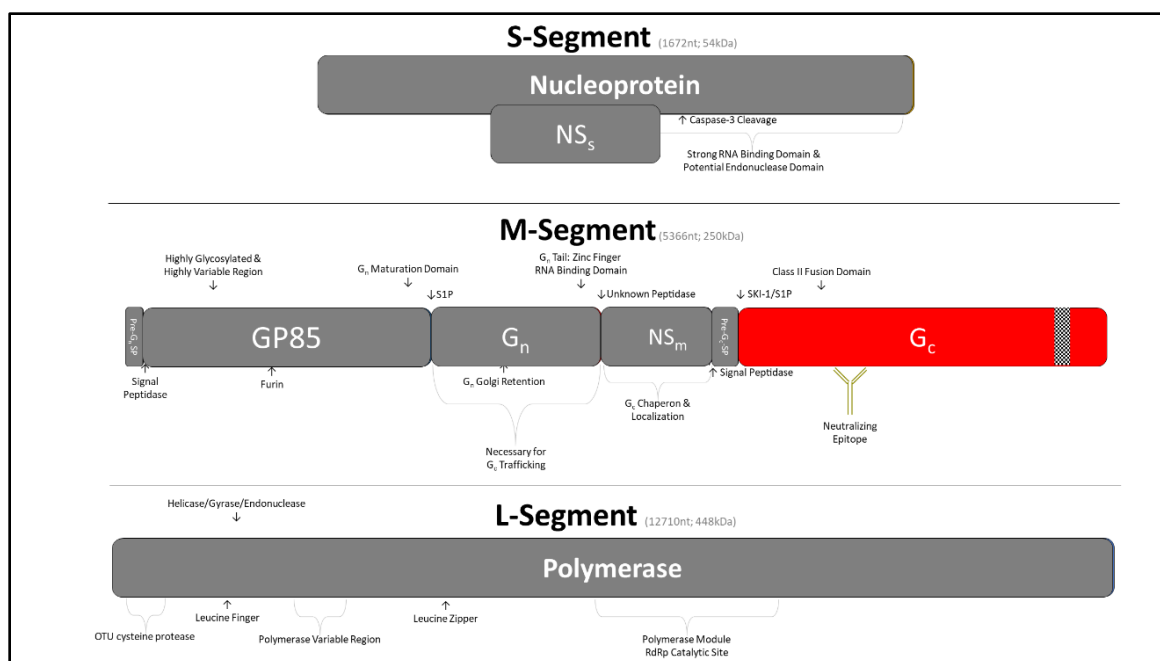


Illustration 9: Areas pertinent to the viral life cycle encoded within the genome of CCHFV

Each of the three genomic segments, their coding regions, and the respective processing and functional domains. The NP contains demonstrated RNA binding domains and a Caspase-3 cleavage site. The GPC contains signal peptides, proprotein convertase cleavage sites, a heavily glycosylated and hypervariable region, maturation domains, retention signals, and RNA binding domains. The RdRp contains ovarian tumor-like deubiquitinase, several RNA/protein interaction regions, and a catalytic module.

As for antibody binding, it has been demonstrated *in vitro* and *in vivo* that monoclonal antibodies can neutralize^{111,113}, and to a certain extent protect against CCHFV infection if administered as an experimental therapeutic¹¹³. Convalescent human sera have also demonstrated targeting of the ectodomain of CCHFV-GC^{114,115}. The GPC also contains numerous maturation areas such as glycosylation^{23,31}, proteolytic cleavage^{30,33,42,116}, signal peptide recognition and processing of the polypeptides across various intracellular membranes (e.g., ER and Golgi)²³. This dependency of the CCHF virus on host cell processing can be exploited by compounds that may disrupt elements that are responsible for this processing. As mentioned above in Table 1, four experimental countermeasures have targeted the NP and RdRp of the various pathogenic members of *Bunyavirales*; however, approximately ten unique compounds have been designed against the GPCs. This, along with the many roles of the viral life cycle which the GPC plays, the family level

conservation of antigenic and processing sites, make it an appropriate target for antigenic and vaccine developments, as well as for antiviral drug discovery efforts.

CHAPTER 4: Developing Tools to Study the Crimean-Congo Hemorrhagic Fever

Virus Glycoprotein Precursor⁴

AVAILABLE TOOLS TO STUDY THE CRIMEAN-CONGO HEMORRHAGIC FEVER VIRUS GLYCOPROTEIN PRECURSOR

Aside from Hazara virus (HAZV) and Dugbe virus (DUGV), the closest relatives to CCHFV, there are no surrogate models available to study the CCHFV-GPC without sacrificing the similarity of GPC by more than 50%²³. A reverse genetics system has been developed for CCHFV that has shown great utility in being able to mutate or label live virus for use in attenuation and functionality studies, as well as drug discovery efforts using fluorescently labeled viruses^{116–118}. However, as CCHFV is categorized as a Risk Group 4 agent, and the handling of live viruses requires the maximum biosafety level 4 (BSL-4) biocontainment. This facet has hampered extensive work into exploring countermeasure designs against the CCHFV-GPC, given that there are very few laboratories around the world with BSL-4 types of biocontainment capabilities. There have been studies aimed at creating low containment surrogates to study CCHFV at BSL-2. A minigenome system has been developed^{34,119,120}, which can be used to study viral transcription, and RNA replication via exchanging viral ORFs with reporter genes. This system is non-infectious and relies on transfection of various plasmids under control of the T7 or Pol-I promoter. Another promising avenue, that has also been useful for both antibody screening and vaccine development has been the virus-like particle (VLP) system^{34,62,121}. This system has enabled CCHFV particles that are capable of entry but not genome RNA replication or further assembly. These particles can carry reporter tags and can be quantified using these reporters or via staining.

⁴ Portions of this chapter are written as a manuscript and *in prep.* for *Scientific Reports* as the following: **Rodriguez S.E.***, Cross R.W.*, Fenton K.A., Bente D.A., Mire C.E., and Geisbert T.W. (*est.* 2018) Single injection pseudotyped vesicular stomatitis virus provides 100% protection to Crimean Congo hemorrhagic fever (*Co-first authors)

A disadvantage of the minigenome and VLP systems for CCHFV is the dependency on transfection reagents which can be costly to optimize and to scale for larger production. Other groups have examined pseudotyped viruses for CCHFV, such as the recombinant vesicular stomatitis virus (rVSV) platform, with a CCHFV-GPC ORF inserted into VSVΔG backbone. A luciferase reporter pseudotype with *in trans* expression of the CCHFV-GPC was developed in 293T cells by Shtanko *et al.*¹²². Suda *et al.*, also did similar pseudotyping with *in trans* expression in 293T cells with various full-length GPC and modified GPC constructs containing truncated G_C, C-terminal/endodomain tails¹¹⁴. These pseudotypes also had a luciferase or GFP ORFs genomically encoded in the VSVΔG backbone¹¹⁴. Both published pseudotyping CCHFV-GP*-ΔGrVSV systems had demonstrated functionality in examining neutralization and entry/infection studies, however, these constructs were not fully characterized by western blot or immune electron microscopy with respect to what was on the exterior of the pseudotypes; nor were either constructs self-replicating nor capable of further expressing CCHFV-GP post infection^{114,115,122}. One of the goals of this dissertation was to expound on this type of work and create a replication competent version that could be used as a screening tool and as an experimental countermeasure.

DEVELOPING RECOMBINANT VESICULAR STOMATITIS VIRUSES EXPRESSING THE CRIMEAN-CONGO HEMORRHAGIC FEVER VIRUS GLYCOPROTEIN PRECURSOR

VSV is a non-segmented, negative sense RNA virus belonging to the genus *Vesiculovirus*, family *Rhabdoviridae*¹²³. VSV has been a powerful tool of molecular and cell biologists for the last 40 years. Its relatively simplistic and linear molecular biology has allowed for the establishment of a reverse genetic system where infectious viral clones can be generated from cDNA¹²⁴. This system relies on the transfection of plasmids encoding the VSV genome and helper plasmids encoding various VSV proteins, into host cells. These plasmids are under specific ‘control’ polymerase (e.g. T7-RNA polymerase),

which allows *in vitro* control and assembly of virions inside eukaryotic cells once introduced. Upon the assembly of virions, VSV RNA genome transcribed from the plasmid DNA can be packaged, and budding occurs as wild-type VSV does. Rescued VSV generated from the *in vitro* system are termed recombinant VSV (rVSV) ¹²⁴.

In addition to a robust reverse genetics system, VSV also has a remarkable tolerance to multiple transcription units and substitution of native genes ^{125–127}. This tolerance makes VSV a suitable system for ‘pseudotype’ construction of foreign soluble and transmembrane glycoproteins. Pseudotyping involves the swapping of viral glycoproteins between species. In relation to VSV, it involves the deletion of a VSV glycoprotein gene (Δ VSV-G), effectively removing the downstream protein it encodes. However, proteins that share homologous functions to the deleted VSV protein can be expressed *in trans* and incorporated or used by VSV. This gives VSV the unique ability to utilize, or ‘pick-up,’ glycoproteins of other viral species to produce progeny virions. Pseudotypes are typically limited in their capability of propagation, because genomic RNA does not encode glycoproteins. This allows for only a single round of infection without generation of infectious progenies. Pseudotyping has allowed for new insights into structure and function of viral genes and analysis of promoter elements in viral infection ^{126,128,129}.

Many groups have taken pseudotyping a step further and used the reverse genetics system to develop replication-competent rVSVs via replacing VSV G ORF with foreign glycoprotein ORF in the rVSV genome. This has allowed for a far more authentic and powerful infection model. In addition to serving as an infection model, many rVSVs have also shown promise as vaccines ¹³⁰; this is due to several reasons. VSV is not known to naturally cause disease in humans, as it is typically an agricultural pest and ailment of livestock ^{123,130}. In the rare instances that humans have become infected with VSV, the disease course was mild or asymptomatic ¹³⁰. Pre-existing immunity to VSV in the general population is also low ^{131,132}. Many other characteristics also make VSV an attractive

vaccine platform as it can replicate in almost all known mammalian cell lines, yield high viral titers, can generate potentiated innate, humoral, and cellular immune responses and has demonstrated safety profiles in both NHP and humans ^{130,133–140}.

Studies have shown the ability of VSV to pseudotypically acquire foreign glycoproteins from several bunyavirus members. Glycoproteins from Seoul, Hantaan, Andes, and Puumula, all members of the genus *Orthohantavirus*, have each been successfully incorporated into VSV lacking its glycoprotein and some have shown promise as experimental vaccine in their respective animal models ^{141–143}. These pseudotypes were demonstrated to be infectious. Several rVSVs expressing glycoproteins or antigens of human pathogens have been created and tested in animal models with promising success ¹³⁰. The pathogen list for the rVSV application includes: Ebola virus ^{132,139,144,145}, Marburg virus ^{132,144}, Lassa virus ^{132,146}, influenza virus ¹⁴⁷, HIV ¹³¹, measles virus ¹⁴⁸, respiratory syncytial virus ¹⁴⁹, hepatitis C virus ¹⁵⁰, Sindbis virus ¹³¹, and *Yersinia pestis* ¹⁵¹, all of which tested in animals and all of which have generated a potentiated immune response. Although many viruses have been successfully adapted to the rVSV system, Nairoviruses like CCHFV have presented a challenge due to a unique CCHFV glycoprotein biology.

CHARACTERIZING THE RECOMBINANT VESICULAR STOMATITIS VIRUSES PSEUDOTYPE

To ensure robust expression of the CCHFV-GPC antigen, we chose to use a codon-optimized CCHFV-GPC (strain: IbAr10200) containing plasmid and subsequently examined the expression of CCHFV-GPC in Huh-7, a human hepatocarcinoma cell line, transiently expressing the codon optimized CCHFV-GPC from a pCAGGs plasmid. Previous studies by Garrison *et al.*, have shown via immunofluorescence stained, unpermeabilized cells observed via flow cytometry, will stain for the CCHFV-G_C if the CCHFV-GPC is codon optimized ¹⁵². I confirmed this by immunocytochemistry, staining both the plasma membrane and CCHFV-G_C on unpermeabilized cells—demonstrating cell surface staining of CCHFV-G_C on transfected cells (Figure 5). These initial data suggested

over-expression under a strong promoter (such as the CAG promoter within the pCAGGS plasmid), as well as codon optimization, could uncharacteristically localize CCHFV-GP to the plasma membrane in addition to the Golgi^{113,153} where VSV could acquire the GP when budding from the cell surface¹⁵⁴.

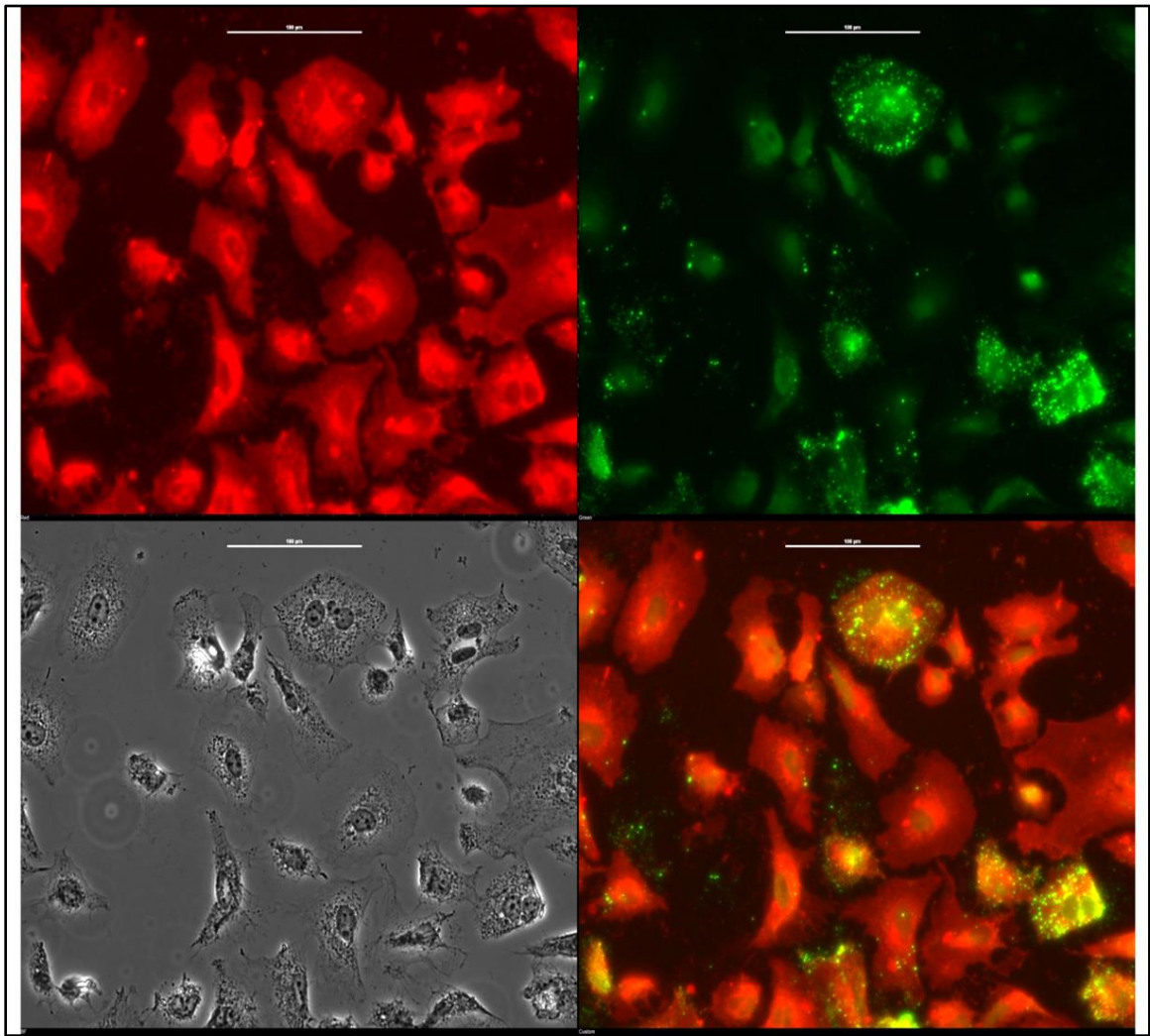


Figure 5: Cell surface expression of CCHFV-G_c from codon optimized CCHFV-GPC

Transfected Huh-7 cells with 1 μg of pCAGG-CCHFV-GPC codon-optimized, fixed briefly with paraformaldehyde and unpermeabilized. Stained with a CellMask Deep Red Plasma Membrane Stain (ThermoScientific), as well as CCHFV-GC Mab 8A1 and an AlexaFluor488 secondary antibody. Plasma membrane stain is indicated in red, while CCHFV-GC is indicated in green. Bright field is included for comparisons. All images were taken at x20 objective with a white bar indicating 50 μm.

Encouraged by these over-expression results using the codon optimized CCHFV-GPC; we cloned and recovered ΔGrVSV-CCHFV-GPC. Our initial attempts using the

DNA clone recovery system designed by Lawson *et al.*, failed to produce infectious Δ GrVSV-CCHFV-GPC (Illustration 10A) ¹²⁴. To overcome this hurdle, we used a modification based on a system described by Whitt ¹⁵⁵ relying on *in trans* VSV glycoprotein (G) complementation (VSV-G*) of Δ GrVSV virions. This technique allowed for VSV-G*, incorporation into recoveries to facilitate efficient assembly of the VSV Δ G-CCHFV-GPC genome without the need for elements of CCHFV-GPC *in trans* to participate in initial infection of recovered virions (Illustration 10A). Recovery of this virus was termed VSV-G*- Δ GrVSV-CCHFV-GPC (VSV-G* for the *in trans* complementation of VSV-G on the virion, - Δ GrVSV- for the recombinant VSV genomic backbone lacking native VSV-G encoded, and the CCHFV-GPC ORF which was swapped for the VSV-G's ORF position). This virus was limited to a single-cycle infection; unless VSV-G* was provided *in trans*, and would not effectively replicate in cell culture.

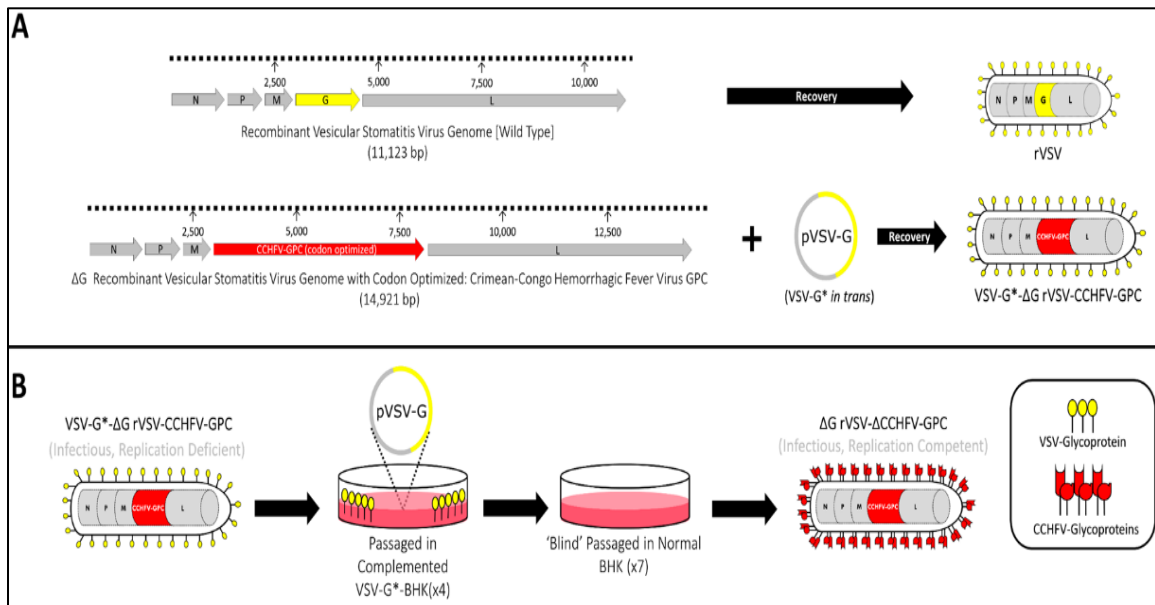


Illustration 10: rVSV-CCHFV-GPC vectors design and creation

(A) Generating a replication deficient vaccine vector: Genome organization comparing VSV (wild-type) genome (in grey arrows) and the rVSV vector expressing the CCHFV-GPC codon optimized open reading frame. N; nucleoprotein, P; phosphoprotein, M; matrix protein, and L; large polymerase protein. The rVSV-CCHFV-GPC vector had natural VSV glycoprotein gene (yellow arrow) exchanged with the open reading frame coding for the full glycoprotein precursor gene (GPC) of CCHFV (red arrow). Using a T7 driven DNA clone recovery system, complemented VSV-G* recombinant was generated containing the CCHFV-

GPC open reading frame (VSV-G-ΔGrVSV-CCHFV-GPC). (B) Generating a replication competent vaccine vector: VSV-G*-ΔGrVSV-CCHFV-GPC is infectious due to the VSV-G complementation; however, VSV-G is needed in trans to effectively replicate in cell culture. Multiple passages of this vector through VSV-G complemented and un-complemented BHK cells resulted in a replication competent vaccine vector (ΔGrVSV-ΔCCHFV-GPC).*

After the initial recovery of VSV-G*-ΔGrVSV-CCHFV-GPC, this virus was passaged four times on VSV-G* complemented BHK cells for stock creations and characterizations (Illustration 10B). During these characterizations, simultaneous passages of VSV-G*-ΔGrVSV-CCHFV-GPC supernatants were placed onto cell cultures containing un-complemented ('normal') BHK cells. I was unable to isolate infectious virus from initial supernatants, however, seven total serial passages of supernatants on un-complemented BHK cells (Illustration 10B), resulted in cytopathic effect (CPE) consistent with VSV CPE, within cell cultures, as well as with plaque formations on several of the monolayers. These monolayers with CPE were harvested for RNA and stained positive for CCHFV-G_C antigen via immunofluorescence assay (data not shown).

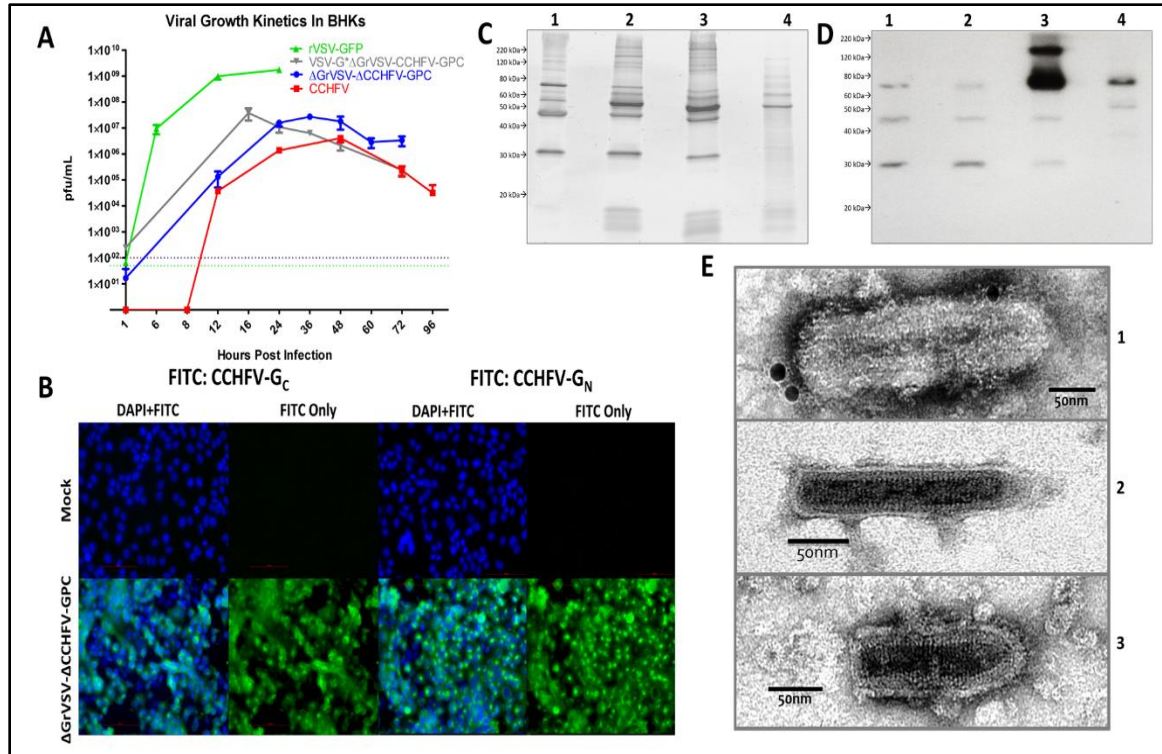


Figure 6: Characterization of the rVSV-CCHFV-GPC vectors

(A) Single-cycle growth kinetics comparing rVSV wild-type (Isolate: Indiana) tagged with GFP (rVSV-GFP), VSV-G*-ΔGrVSV-CCHFV-GPC, ΔGrVSV-ΔCCHFV-GPC, and CCHFV (Isolate: IbAr10200) all at MOI 0.1 in BHK cells. Data shown are a mean \pm standard deviation from three biological replicates, titrated by plaque assay in duplicate. Complemented VSV-G* BHK (via transfection with pCAGGS-VSV-GIndiana) were used for VSV-G*-ΔGrVSV-CCHFV-GPC kinetics and plaque assays. (B) Phase and fluorescence microscopy of MOI 3 and MOI 0.01 infected SW-13-CDC (VSV-G*-ΔGrVSV-CCHFV-GPC) and BHK (ΔGrVSV-ΔCCHFV-GPC) cells at 10x objectives, stained with α -CCHFV-Gc Mab 8A1 using a FITC-conjugated secondary at 24 and 96 hpi, respectively. (C) Coomassie of approximately 100 ng of loaded 20% sucrose cushioned/semi-purified and gradient purified particles on 4-16% gradient TGX gels. 1: rVSV-GFP, 2: VSV-G*-ΔGrVSV-CCHFV-GPC, 3: ΔGrVSV-ΔCCHFV-GPC, and 4: CCHFV. Particle preps were stained with Coomassie Fluor Orange. (D) Western blot of approximately 100 ng of loaded 20% sucrose cushioned/semi-purified and iodixanol gradient purified particles on 4-16% gradient TGX gels. 1: rVSV-GFP, 2: VSV-G*-ΔGrVSV-CCHFV-GPC, 3: ΔGrVSV-ΔCCHFV-GPC, and 4: CCHFV. Particle preparations were stained with α -CCHFV-GC Mab 11E7 using an HRP-conjugated secondary. (E) Transmission electron micrographs of 1: ΔGrVSV-ΔCCHFV-GPC, 2: VSV-G*-ΔGrVSV-CCHFV-GPC, 3: rVSV-GFP and replication competent particles from BHK cells, semi-purified using a 20% sucrose cushion or purified using iodixanol gradient centrifugation, negatively stained with 2% aqueous uranyl acetate, immunolabeled with α -CCHFV-Gc Mab 11E7 and a secondary 15nm gold labeled secondary. Samples were fixed with 2% glutaraldehyde. Images were adjusted for brightness, contrast, and formatted for size for display purposes. Size markers are indicated in each image for reference.

To assess the growth kinetics of the rVSV vectors compared to authentic CCHFV, we performed single-cycle growth curve analysis on BHK cells infected with respective viruses at various time intervals up to 96 hpi or full monolayer destruction. The rVSV-GFP (wild-type control) peaked in titer at approximately 24 hpi, while CCHFV prototype-

strain: IbAr10200 peaked at 48 hpi (Figure 6A). Using VSV-G* complemented BHK cells, enabled replication, spreading, and formation of plaques for VSV-G*- Δ GrVSV-CCHFV-GPC, permitting growth kinetics assays and subsequent titrations. VSV-G*- Δ GrVSV-CCHFV-GPC replicated to highest titer in these BHK VSV-G* complemented cells, around similar peak times for wild-type VSV titers, 16 hpi (Figure 6A). Both Δ GrVSV- Δ CCHFV-GPC and CCHFV had peak titer, at approximately 36 hpi (Figure 6A).

To assess the expression of the CCHFV-GPC in the Δ GrVSV-CCHFV-GPC vector, Huh-7 cells were infected with Δ GrVSV- Δ CCHFV-GPC, and analyzed by indirect immunofluorescence assay, using an antibodies that binds CCHFV-G_C or CCHFV-G_N. Both antibodies revealed strong *in vitro* expression of these respective antigens, where both G_C and G_N were diffuse throughout the cell, though higher staining (*i.e.*, localization) of G_N was noted perinuclearly—suggesting a stronger antigen presence for G_N in the ER (Figure 6B). We additionally examined if CCHFV-G_C was incorporated onto gradient purified rVSV virions, VSV-G*- Δ GrVSV-CCHFV-GPC and Δ GrVSV- Δ CCHFV-GPC, and semi-purified virions of both rVSV-GFP and CCHFV (as controls), by Coomassie staining and western blot analysis. Through Coomassie staining, differences in number and mobility of protein bands were detected among VSV-G*- Δ GrVSV-CCHFV-GPC and Δ GrVSV- Δ CCHFV-GPC. The two CCHFV-GPC recombinants both had additional protein bands below 20kDa with analogous bands detected in CCHFV virion pellets (Figures 6C, Lanes 2, 3, and 4). Both CCHFV-GPC recombinants also possessed more pronounced protein bands around 60kDa, compared to the wt rVSV-GFP (Figure 6C). CCHFV structural glycoproteins G_N and G_C present as bands of approximately at 37 kDa and 75 kDa, respectively, on SDS-PAGE gels. There was no observable G_N band found on either CCHFV-GPC recombinant at 37 kDa, however, there were two distinct bands between 60-80 kDa in both recombinants (Figures 6C-2, -3). The VSV-G*- Δ GrVSV-CCHFV-GPC was expected to possess a VSV-G as one of these bands. The Δ GrVSV- Δ CCHFV-GPC did not encode for a VSV-G, nor would it be complemented with VSV-G

after seven rounds of BHK passaging. A duplicate run protein gel was run and further probed by western blotting using a monoclonal antibody previously identified to be specific for CCHFV G_C by western blot (Mab 11E7, BEI Resources)¹¹³. These western blot data demonstrated limited, non-specific binding to three VSV proteins as observed in lanes rVSV-GFP and VSV-G*-ΔGrVSV-CCHFV-GPC (Figure 6D, Lanes 1 and 2), but showed strong signal to CCHFV-G_C at approximately 75 kDa and 150kDa for ΔGrVSV-ΔCCHFV-GPC, however the replication deficient VSV-G*-ΔGrVSV-CCHFV-GPC did not display these CCHFV-G_C protein mobility shift profiles (Figure 6D, Lanes 2 and 3). Indicating that mature CCHFV-G_C and potentially a precursor molecule or an oligomeric form of CCHFV-G_C (due to the lack of β-mercaptoethanol in antigen preparations), are incorporated in/on ΔGrVSV-ΔCCHFV-GPC virions. The semi-purified CCHFV also showed limited non-specific binding to antigens at 57 kDa (CCHFV-NP) and 37 kDa (CCHFV-G_N), but distinct signal at 75 kDa (CCHFV-G_C) (Figure 6D, Lane 4).

To examine the ultrastructure of the replication competent recombinant, ΔGrVSV-ΔCCHFV-GPC, transmission electron microscopy studies were conducted. Consistent with other rVSV pseudotyped with bunyavirus GP¹⁴¹, our rVSV maintained rhabdovirus morphology and classical bullet shape with coiled intra-virion structure (Figure 6E). Particles of ΔGrVSV-ΔCCHFV-GPC and VSV-G*-ΔGrVSV-CCHFV-GPC were observed to have lengths of particles ranging between 210-260 nm (Figures 6E, Images 1 and 2). Particles of rVSV-GFP ('wild-type' VSV electron microscopy control) were observed between 170-200 nm (Figure 6E, Image 3). This apparent length increase of the ΔGrVSV-ΔCCHFV-GPC and VSV-G*-ΔGrVSV-CCHFV-GPC is likely due to the genome containing approximately 4,000 extra nucleotides in comparison to the rVSV-GFP genome (which is also slightly larger than native wt VSV Indiana [GenBank number NC_001560.1]). Additionally, immunolabeling of ΔGrVSV-ΔCCHFV-GPC was employed with either CCHFV-G_C Mab 11E7, 12A9, or 8A1 and counterstained with 15 nm gold conjugated secondary Mab (Figure 6E, Image 1). Immunolabeling demonstrated

labeling of G_C spikes on the virion surface of Δ GrVSV- Δ CCHFV-GPC (Figure 6E, Image 1).

Studies have had varied success expressing CCHFV-GPC *in trans* on viral vectors^{114,115,122}. rVSV with CCHFV-GPC has likely been challenging due to the numerous post-translational modifications required to mature, and provide functional, CCHFV-GPC^{30,31,33,156}. Additionally, CCHFV-GPC form immature CCHFV particles at the Golgi and egress via vesicular transport^{24,113,153}. Unlike CCHFV, VSV buds from the plasma membrane¹⁵⁴, which hampers efforts to recover a Δ GrVSV CCHFV-GPC vector. To approach this issue, we used a mammalian codon optimized CCHFV-GPC (strain: IbAr10200). This platform has been observed to provided robust CCHFV GPC production in mammalian tissue culture¹⁵², while maintaining native CCHFV maturation factors. My data from Figure 5, confirmed that codon optimization, could result in shuttling of CCHFV-G_C to the plasma membrane, where VSV could likely acquire and bud with functional components of the GPC in the viral envelope. Though, we were able to drive strong expression CCHFV-GPC *in vitro*, we were unable to generate a replication competent pseudotype without VSV-G* *in trans*. With the tools currently available for our analysis, we were able to detect by western blotting and electron microscopy, a form of CCHFV-G_C that was present and functional on the surface of the Δ GrVSV- Δ CCHFV-GPC virion. Immunolabeled electron micrographs demonstrated that CCHFV-G_C was incorporated on the surface of the virion. While we were able to immunolabel for CCHFV-G_C, PAGE and Coomassie staining analysis of our purified virion lysates, did not reveal prominent protein bands at the 37 kDa position, the estimated size of mature G_N. However, we did have three smaller protein bands in our VSV-G*- Δ GrVSV-CCHFV-GPC and Δ GrVSV- Δ CCHFV-GPC preparations. Similar protein profiles have been shown in other CCHFV preparations, as shown by Buttigieg et al., 2014. Though, it is possible that these protein bands may also correspond to VSV-M2 and -M3 by alternative initiation at downstream start codons present in the ORF of VSV-M¹⁵⁷. While not the focus of this current study, these

observations warrant further characterization if this vector is to be used as a tool to further study CCHFV-GPC mechanisms.

GENOMIC AND *IN TRANS* STUDIES INTO REPLICATION COMPETENCE OF THE Δ GrVSV- Δ CCHFV-GPC PSEUDOTYPE

Sanger sequencing of both constructs, using primers for the CCHFV-GPC ORF, was carried out which revealed several single nucleotide polymorphisms (Illustration 11). Next generation sequencing (NGS) was then performed to confirm Sanger sequencing results and revealed further details of the signal nucleotide polymorphisms within the entire genomes of both constructs (Table 4, Illustration 11).

Table 4: Synonymous and non-synonymous mutations within the genomes of the replication-deficient and replication-competent pseudotypes

Viruses	VSV-G* Δ GrVSV-CCHFV-GPC (Replication Deficient)	Δ GrVSV- Δ CCHFV-GPC (Replication Competent)
Viral Passage Histories	vp. 3	vp. 11
Single Nucleotide Polymorphisms	14	20
Non-Coding Regions	(3)	(3)
Synonymous	(2)	(4)
Non-Synonymous	(9)	(13)
Non-Synonymous Mutations within Open Reading Frames		
Nucleoprotein (VSV-N)	I14V	I14V
Phosphoprotein (VSV-P)	Q77P, P110Q	Q77P, P110Q
Matrixprotein (VSV-M)	T133A, S226G	T133A, S226G
Glycoprotein Precursor (CCHFV-GPC)	S368T, STOP1685Q	S368T, L518V, L1638R, R1648Q, R1671STOP , STOP1685Q
RNA-Dependent RNA-Polymerase (VSV-L)	T689S, T2026I	T689S, T2026I

Next generation sequencing (NGS) was carried out from Trizol extractions of clarified supernatant stocks of vp3 replication deficient pseudotype and vp11 replication competent pseudotype. Bolded residues indicate changes unique to replication competent (vp11) pseudotype.

NGS sequencing demonstrated fourteen identical single nucleotide polymorphisms (SNP) preserved between the replication deficient and replication competent constructs; with the replication competent construct possessing four additional non-synonymous mutations within the CCHFV-GPC (Table 4). Two of these mutations within the CCHFV-GPC of the replication competent construct, resulted in the truncation of fourteen amino acids off the C-terminal tail of the G_C (Illustration 11).

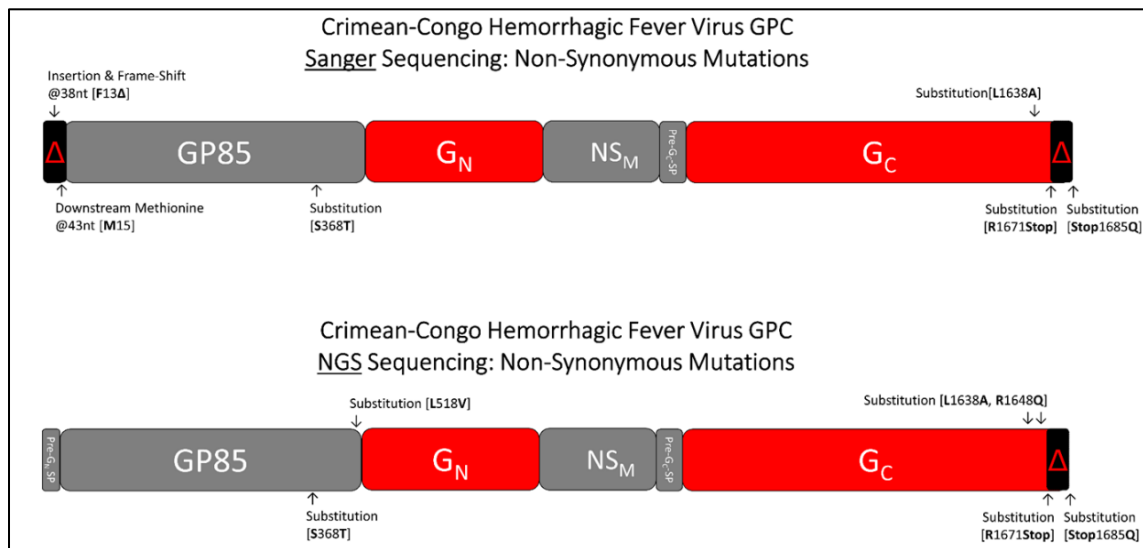


Illustration 11: Sanger and next generation sequencing of the CCHFV-GPC

Illustration of the non-synonymous mutations found by Sanger and next generation sequencing (NGS) on the CCHFV-GPC of the replication competent pseudotype, viral passage 11 (vp11). While both sequencing methods outlined several substitutions in the C-terminus of the GPC, effectively truncating the G_C tail—Sanger sequencing had insertions that ablated the N-terminal signal peptide of the GPC.

Suda *et al.*, have shown an increase in the amount of infectious pseudotype the more the G_C tail is truncated, up to a deletion of 53 residues at the end of the C-terminal GC tail¹¹⁴. Our data supports this region as a probable, or at the very least, contributory mechanism which enables the replication competent ΔGrVSV-ΔCCHFV-GPC pseudotype formation (Illustration 11). There is likely a localization or retention signal within the transmembrane region or endodomain tail which is aberrated and fails to shuttle G_C to solely the intracellular compartments and this perhaps allows shuttling to the plasma membrane. It is interesting to note, that a similar motif has been demonstrated by other

bunyaviruses^{44,158} and has also been demonstrated with other VSV pseudotypes¹⁵⁹. While Sanger sequencing and NGS confirmed the mutations on the C-terminus that resulted in the G_C tail truncation, Sanger sequencing also indicated an insertion that resulted in the ablation of the N-terminal signal peptide of the CCHFV-GPC. The purposes behind these two truncations were unclear, and therefore investigated further.

Plasmids under the CAG promoter-enhancer elements, encoding solely the CCHFV-GPC (not codon optimized) with the N-terminal and C-terminal truncations, were created to investigate the potential roles behind these mutations. Additionally, I wanted to understand if the codon optimization of the GPC was playing a role in pseudotype formations versus the non-codon optimized version of the CCHFV-GPC (strain: IbAr10200). To first evaluate these cloned plasmids, an immunofluorescence microscopy assay was done in Huh-7 to stain for the presence of Pre-G_N or Pre-G_C using the previously published and characterized monoclonal antibodies (MAb) 13G8 or 11E7, respectively¹¹¹⁻¹¹³. Figure 7 demonstrates that all constructs can express a form of Pre-G_C in transfected cells which is localized to similar intracellular environments as both the Δ GrVSV- Δ CCHFV-GPC pseudotype and wild-type CCHFV (strain: IbAr10200). However, the Pre-G_N was found only in the codon optimized, non-codon optimized, and C-truncation plasmid transfected cells. It was not detected in the N-terminal truncation.

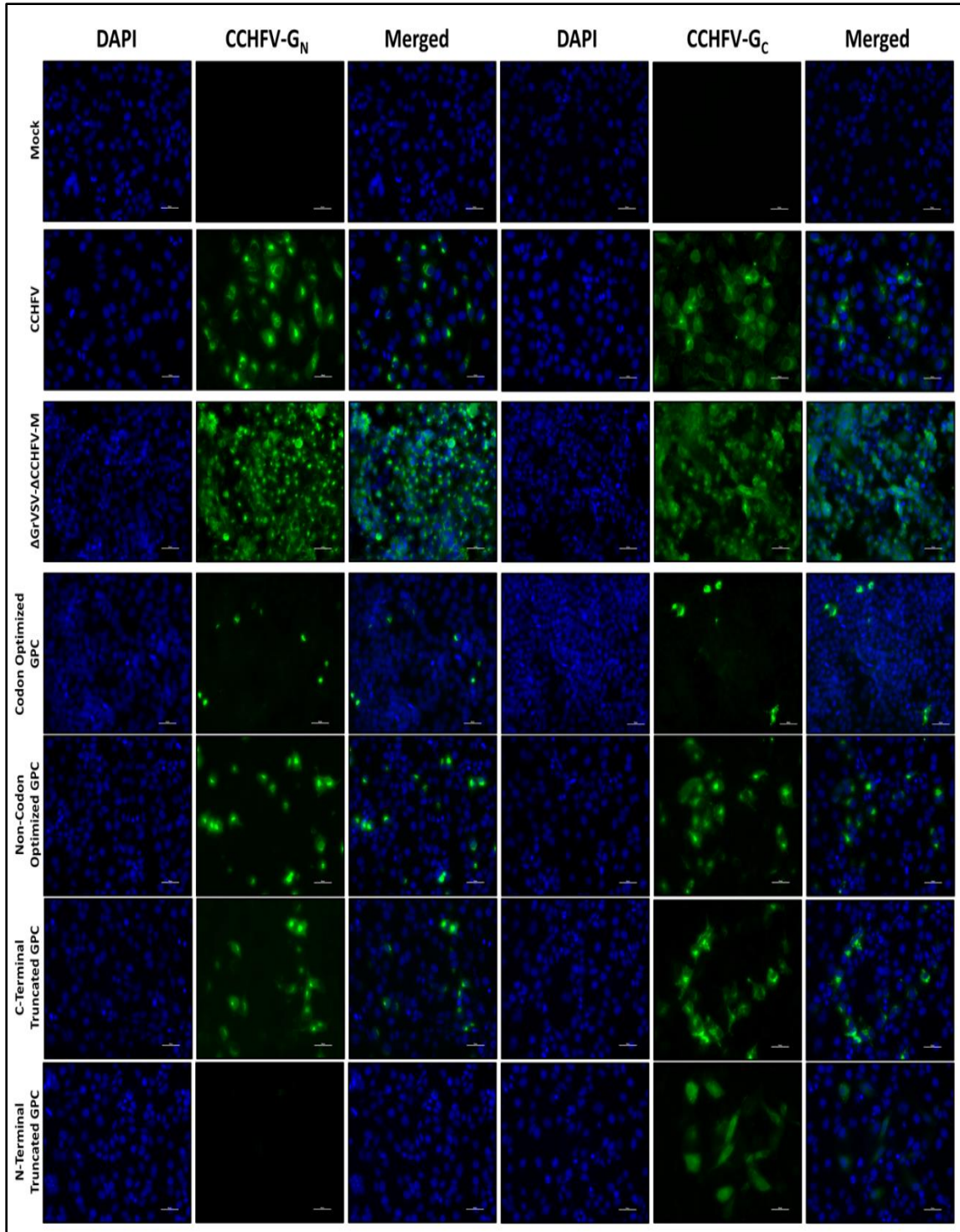


Figure 7: Immunofluorescence microscopy of G_N and G_C antigens expressed by plasmids encoding the N-terminal and C-terminal CCHFV-GPC truncations

Human hepatocarcinoma cells (Huh-7) were transfected with pCAGGs plasmids encoding either a codon optimized or wild-type (non-codon optimized) CCHFV-GPC, along with both the truncation of the N-terminus and C-terminus separately. The replication competent Δ GrVSV-ACCHFV-GPC pseudotype and

wild-type CCHFV (strain: IbAr10200) were used as controls along with mock. All cells were permeabilized and stained with either CCHFV-PreG_N MAb 13G8 or CCHFV-PreG_C MAb 11E7.

Subsequently, an *in trans* assay was set up with a single-round infectious reporter VSV which lacks a glycoprotein encoded within its genome but has been complemented previously with VSV-G *in trans* (designated VSV-G* ΔGrVSV-GFP). The goal of this experiment was to transfect the various CCHFV-GPC plasmids (codon optimized, non-codon optimized, C-terminal truncation, and N-terminal truncation) into cells and to infect these cells with the VSV-G* ΔGrVSV-GFP reporter. Supernatants from these transfected/infected cells should demonstrate if CCHFV-GPC *in trans* can facilitate VSV egress and subsequent re-infection—potentially revealing which facet of the CCHFV-GPC is contributing to the formation of the replication competent ΔGrVSV-ΔCCHFV-GPC pseudotype. Figure 8 illustrates the subsequent titers from these transfected/infected cells, where foci forming units were calculated using fluorescence microscopy of the GFP tag.

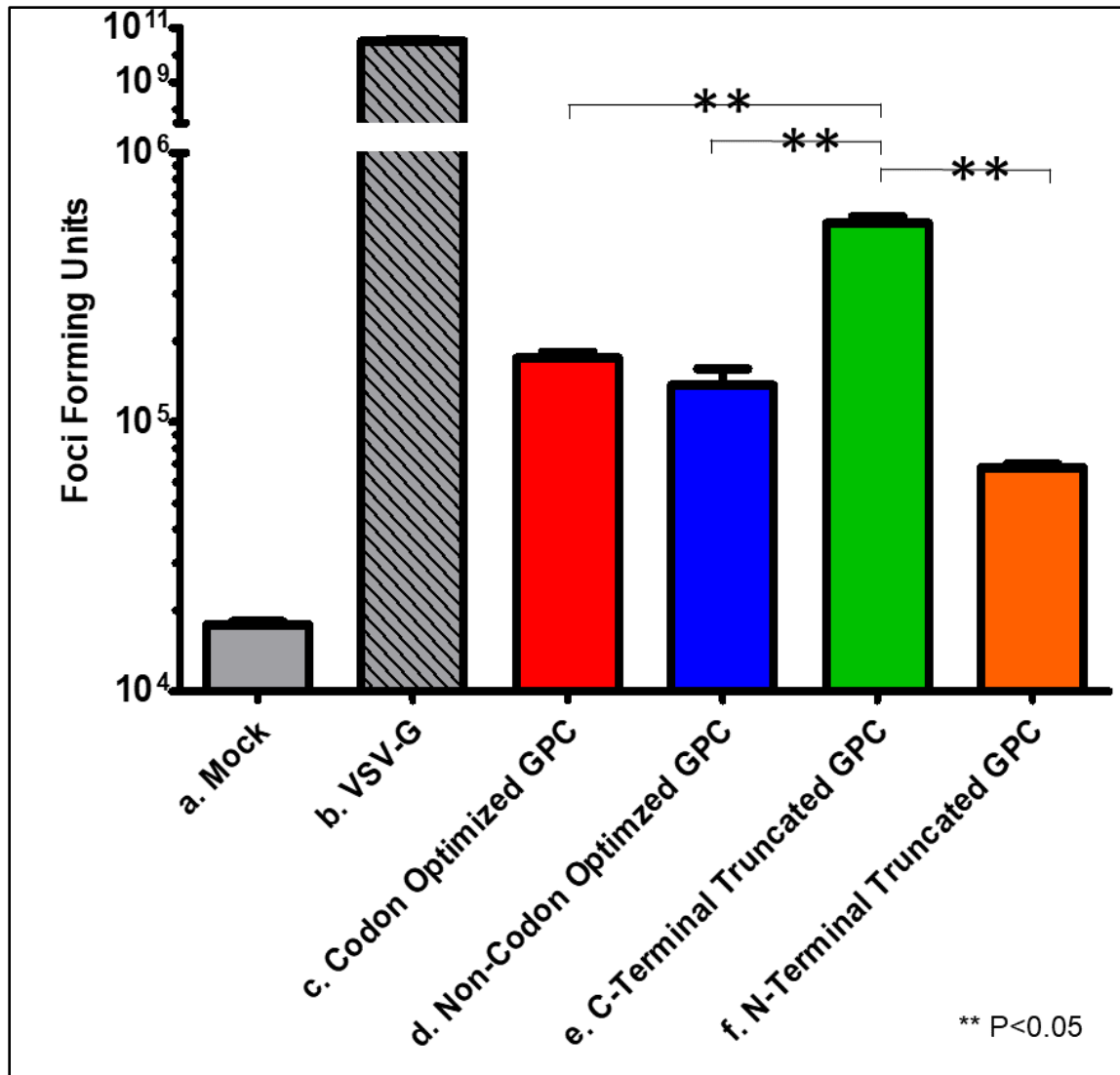


Figure 8: Titers from *in trans* complemented cells using a single-round replicative reporter VSV

Baby hamster kidney (BHK) transfected with pCAGG plasmids encoding either VSV-G or codon optimized, non-codon optimized, C-terminal truncated, or N-terminal truncated CCHFV-GPC. BHK were infected with a MOI of 1 with the single-round infectious VSV-G* Δ GrVSV-GFP reporter and extensively washed and incubated for 20 hours. Supernatants were harvested and clarified of cellular debris and supernatants were overlaid onto either normal BHK for the observation of fluorescence/GFP foci using fluorescence microscopy. Statistical significance at $p<0.05$ was designated with double asterisk (**).

While extensive washing was accomplished ~10⁴ foci forming units (ffu) per mL were observed from mock (no plasmid) cells. As expected with the positive control of transfected VSV-G* cells had titers >10⁹ ffu/mL. While most of the titers from the *in trans* CCHFV-GPC constructs were above mock at ~10⁵ ffu/mL, a statistically significant

increase in the CCHFV-GPC C-truncation construct was observed compared to the other constructs. This data is in agreement with those Suda *et al.*, have observed with the G_C tail truncation in their mutants.

These *in trans* constructs were also harvested and semi purified for protein mobility shift profiling as well as western blotting using the MAb 11E7 for CCHFV-G_C.

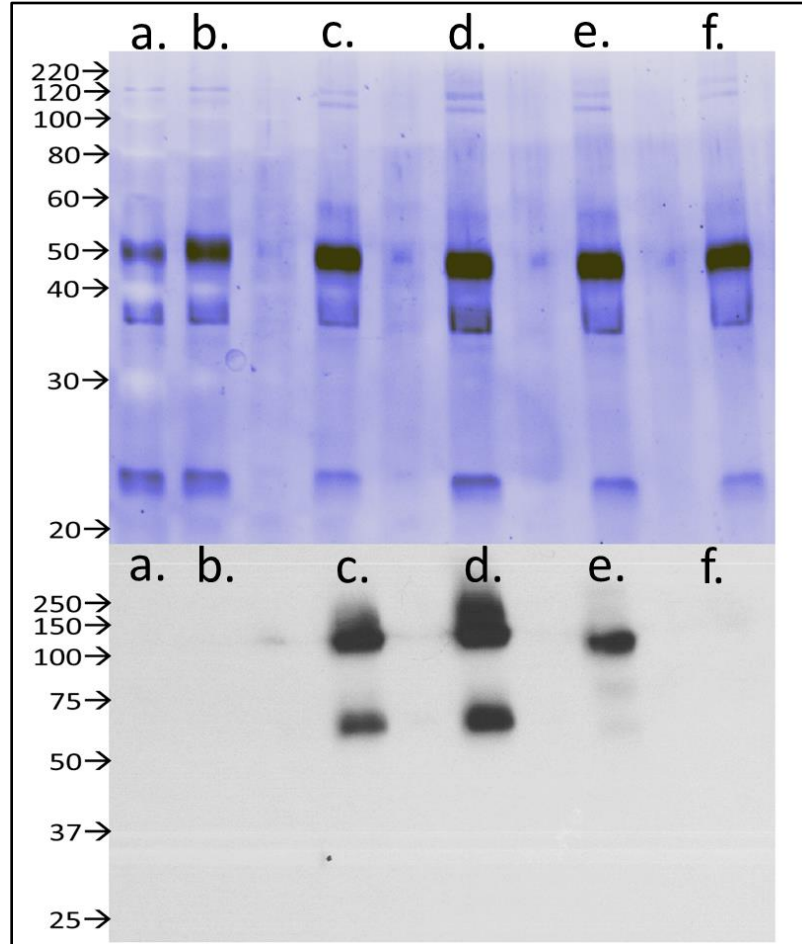


Figure 9: Coomassie and western blot of in trans-expressed, semi-purified

Top image: Coomassie of approximately 100 ng of loaded 20% sucrose cushioned/semi-purified particles on 4-16% gradient TGX gels. Particle preps were stained with Coomassie Fluor Orange. Bottom image: Western blot of approximately 100 ng of loaded 20% sucrose cushioned/semi-purified particles on 4-16% gradient TGX gels. Blots were stained with α -CCHFV-G_C MAb 11E7 using an HRP-conjugated secondary. a: Δ GrVSV-GFP, b: VSV-G* Δ GrVSV-GFP, c: CCHFV-GPC_(codon optimized)* Δ GrVSV-GFP, d: CCHFV-GPC_(non-codon optimized)* Δ GrVSV-GFP, e: CCHFV-GPC_(C-terminal truncation)* Δ GrVSV-GFP, and f: CCHFV-GPC_(N-terminal truncation)* Δ GrVSV-GFP.

As shown in Figure 9, the banding profiles of VSV, similar to those illustrated in Figure 6C, were observed. For the western blot, both the codon optimized, and non-codon optimized constructs showed two forms of CCHFV-G_C that were present on these semi-purified virion preps. Interestingly, the N-terminal truncation did not express detectable CCHFV-G_C on virion preparations, though the C-terminal truncation did express multiple forms incorporated onto virion preparations (Figure 9).

These *in trans* experiments demonstrate that the N-terminal truncation was likely not a major player in the formation of the replication competent Δ GrVSV- Δ CCHFV-GPC pseudotype. Especially given, one of the controls of the assay presented in Figure 6, was the actual pseudotype, which produced a robust CCHFV-PreG_N, indicating that this insertion is likely not expressed in the pseudotype. Despite duplicates and multiple primer reads, that the insertion the yielded the N-terminal truncation in Sanger sequencing is likely an artifact. However, the C-terminal truncation appears to offer some utility in permitting a higher titer of *in trans* reporter viruses coming from C-terminal truncated CCHFV-GPC expressed cells. This C-terminal truncation is likely not the sole mediator of what is expressed on the virion surface, as the western blots comparing both this C-terminal *in trans* construct (CCHFV-GPC_(C-terminal truncation)* Δ GrVSV-GFP) and the actual Δ GrVSV- Δ CCHFV-GPC pseudotype provide different CCHFV-GC staining in western blotting (Figures 6 and 9). The reason for this is unclear and will require future studies.

USING THE RECOMBINANT VESICULAR STOMATITIS VIRUS PSEUDOTYPE FOR ANTIBODY TESTING

In addition to characterizing the Δ GrVSV- Δ CCHFV-GPC pseudotype as to the phenotype and expression of various CCHFV-GPC antigens, additional functionality studies were also undertaken. To determine if the G_C that was proven to be on the Δ GrVSV- Δ CCHFV-GPC pseudotype virion surface was biologically similar in nature to

wild-type CCHFV-G_C, a plaque reduction neutralization test (PRNT) using a panel of antibodies with publish neutralization capacities was performed.

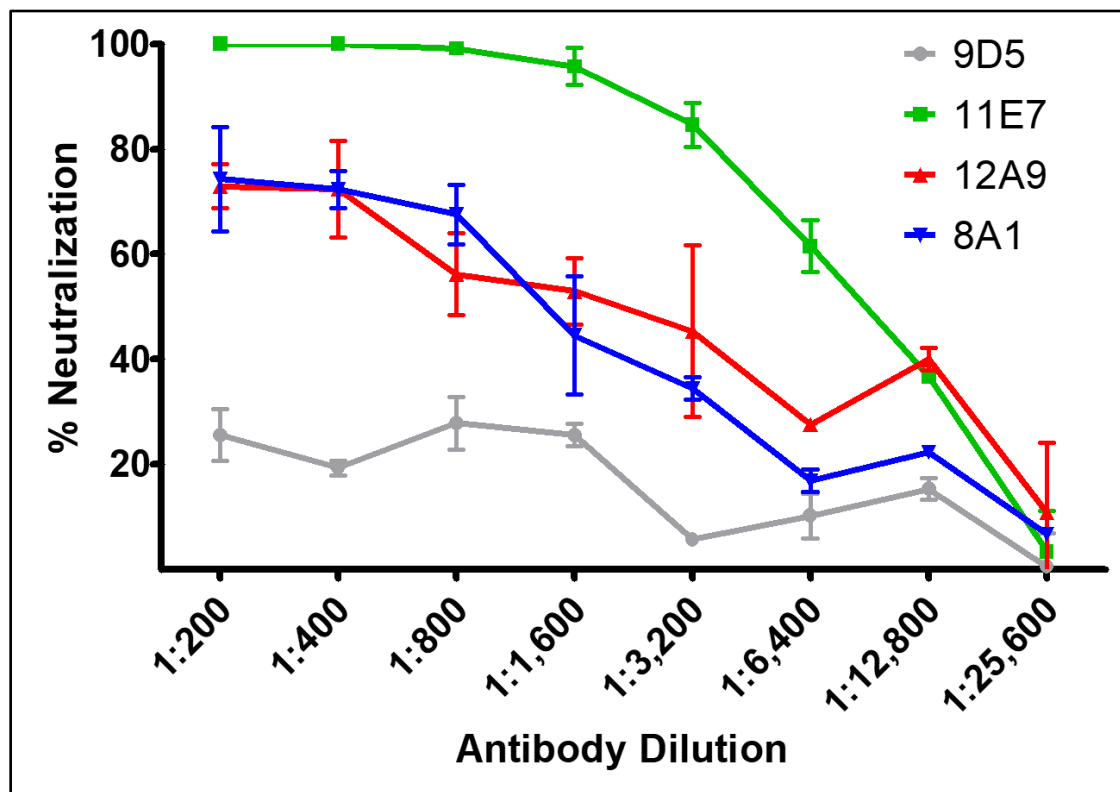


Figure 10: Neutralization of Δ GrVSV- Δ CCHFV-GPC by CCHFV monoclonal antibodies (MAb)

Percent neutralization expressed from a plaque reduction neutralization test (PRNT) on replication competent Δ GrVSV- Δ CCHFV-GPC pseudotype using various dilutions of MAb 11E7, 12A9, and 8A1. These CCHFV-PreG_C antibodies have been previously characterized in Ahmed et al., 2005, Bertolotti-Ciarlet et al., 2005, and Zivcec et al., 2017 as potent neutralizing antibodies to wild-type CCHFV. As a control, MAb 9D5, an antibody against the CCHFV-NP was used to determine non-specific neutralization.

As depicted in Figure 10, the replication competent Δ GrVSV- Δ CCHFV-GPC pseudotype could be neutralized in PRNT assays using wild-type CCHFV characterized neutralizing MAb. The most potent neutralizing antibody was 11E7, while MAb 8A1 and 12A9 performed similarly with observed neutralizing properties on the pseudotype.

Lastly, I investigated the diagnostic potential of the Δ GrVSV- Δ CCHFV-GPC pseudotype by using purified virion preparations to design an enzyme linked immunosorbent assay (ELISA) for the CCHFV-G_C. For this experiment, 96-well plates

were coated with either wild-type VSV, or with the Δ GrVSV- Δ CCHFV-GPC replication-competent pseudotype and various antibodies or sera were used to determine if a diagnostic readout could be obtained. As shown in Figure 11, using hyperimmune mouse ascitic fluid (HMAF) raised against wild-type CCHFV, a titer of 12,800 could be obtained on plates coated with Δ GrVSV- Δ CCHFV-GPC versus below detection limit for those with wild-type VSV. Additionally, the MAb 8A1 was used, along with pseudotype vaccinated mouse sera from other experiments, and both produced robust titers in pseudotype coated wells versus wild-type VSV. Naïve mouse sera showed minimal non-specific binding to either the pseudotype or wt VSV.

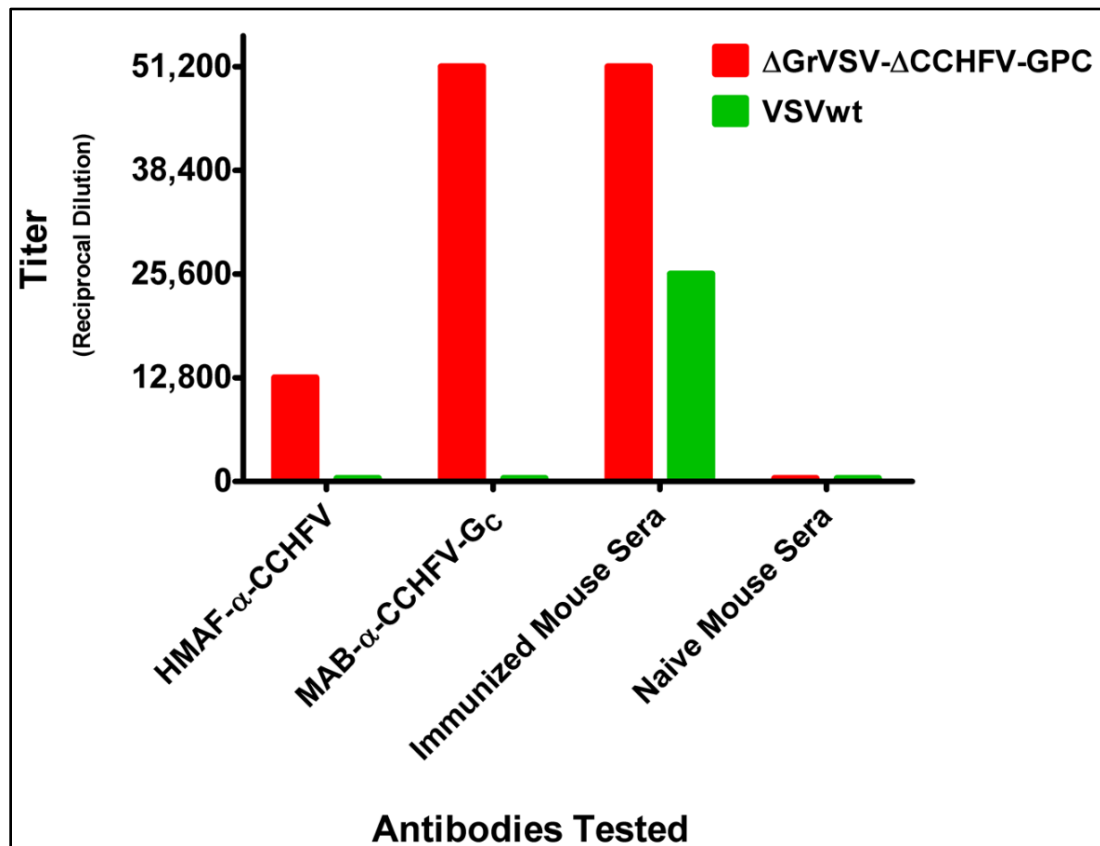


Figure 11: Validating enzyme linked immunosorbent assay coated with CCHFV-GPC pseudotyped or wild-type VSV, against multiple CCHFV antibody reagents

Immunosorbent plates were coated with 1 μ g/mL of either purified Δ GrVSV- Δ CCHFV-GPC pseudotype or wild-type VSV. Plates were optimized using matrices of hyperimmune mouse ascitic fluid (HMAF) and monoclonal antibodies (MAb) raised against CCHFV or CCHFV-G_C, respectively. Matrices were also used to optimize blocking buffer(s), secondary horseradish peroxidase antibody dilutions, and stop times.

Taken together, these experiments in Chapter 4 describe the first instance of a replication competent, CCHFV-GPC pseudotyped rVSV, designated $\Delta\text{GrVSV-}\Delta\text{CCHFV-GPC}$. While the exact mechanism that enables replication competence is still unclear, it does appear that a mutation in the C-terminus of the GPC plays a role to pseudotype rVSV with CCHFV-GPC. This $\Delta\text{GrVSV-}\Delta\text{CCHFV-GPC}$ pseudotype can express both PreG_N and PreG_C antigens in a similar manner to authentic CCHFV. Additionally, the pseudotype also has a form of G_C present on the virion surface as demonstrated by western blotting and immunoelectron microscopy. This form of G_C appears to be biologically functional in terms of entry and diagnostic studies given that antibodies can both recognize and neutralize the $\Delta\text{GrVSV-}\Delta\text{CCHFV-GPC}$ pseudotype in PRNT and ELISA experiments. This pseudotype will be useful as a screening tool in evaluating experimental countermeasures targeting either the CCHFV-GPC or CCHFV- G_C .

CHAPTER 5: Screening Crimean-Congo Hemorrhagic Fever Virus Entry

Inhibitors

VIRAL ENTRY: ROLE OF THE FUSION PEPTIDE

The biological process of fusing lipid membranes is an intricate dance of protein-lipid interactions that dates back to the formation of higher organismal evolution. Biological lipid membranes are stable structures that serve to compartmentalize intracellular contents from the external milieu. In a biologically necessary step, lipid membranes undergo fusion to reorganize, transfer, or mix contents from one membrane bound entity to the next. In the case of higher organisms such as mammals, vesicular transport, placental syncytiotrophoblast formation, and most importantly the fusion of gametes, *i.e.* sperm and egg, must occur for life to occur/propagate^{160–162}. The notion of which came first, the virus or the egg, is a fascinating idea given that the mechanism responsible for gamete fusion in unicellular eukaryotes and plants, is HAP2. HAP2 is a class II fusion protein and it is highly like viral class II fusion proteins found in such viral families such as, *Flaviviridae*^{160,163}. Regardless of which came first, viruses have co-evolved this conserved mechanism of membrane fusion which has become a cornerstone in enveloped virus infectivity and propagation.

Viral fusion proteins exist in metastable conformations, which can be induced by the surrounding environment to undergo a conformational change. This conformational change occurs when an alteration of free energy occurs, which results in a change of peptide arrangement to a conformationally stable form (of the fusion peptide) at a lower energy state³⁸. The trigger of this change in energy occurs for most enveloped viruses at a low pH environment. This pH environment happens due to proton pumps present often present on intracellular vesicles which lower the pH of the intravehicular compartment³⁸. As the vesicle descends further into the cytoplasm of the cell, a lower pH accumulates. Depending

on the type of fusion peptide and the residues surrounding said peptide, this can serve to drive the conformational state of several intermediates that ultimately bring the two membranes of the viral envelope and vesicular envelope to a merger³⁸. This rearrangement ultimately forms a fusion pore which facilitates release and diffusion of the intravirion contents, such as the genome and viral effector proteins, into the cytosol of the infected cell.

CCHFV utilizes its two structural glycoproteins to enter host cells, the G_N and G_C^{30,111,113,122}. Garry and Garry (2004) use *in silico* proteomic modeling to compile the G_C of prototype Bunyaviruses, and postulated a conserved area spanning residues 138-160 of mature G_C served as a class II viral fusion protein³⁹. This cluster of hydrophobic and aromatic amino acids are described as β -penetrenes, which are composed of antiparallel β sheets, *i.e.*, two peptide strands running in opposing directions but held together by hydrogen bonding between strands. The fusion peptide resides in G_C domain II_a of all Bunyaviruses and the fusion peptide is predicted to start with W-X-C-X³⁹. As demonstrated by the conservation of this region among all Bunyaviruses, and the prevalence of this β -penetrene throughout many viral families, demonstrate how critical this domain is to viral infectivity.

These class II viral fusion proteins have been studied in many viral families^{38,39,161,163–166}. The prototype of viral class II fusion is the flavivirus, tick-borne encephalitis virus (TBEV). Upon attachment and uptake of TBEV into host cells, acidification of endocytic vesicles containing a receptor bound viral glycoprotein(s) undergo a pH-dependent conformational change³⁹. In flaviviruses, the envelope protein (glycoprotein) rearranges from a dimeric form to a trimeric form and exposes the hydrophobic and aromatic side chains of the fusion peptide. This causes it to intercalate within the target cellular membrane. A second conformational change occurs which shortens the trimeric complex and brings the viral and cellular membranes into proximity which causes them to fuse and form a fusion pore. Since this act of viral-cell fusion is a unique and near sole

mechanism of infection, this is a phenomenon that can be targeted by experimental strategies for disruption^{163,167–169}. Inhibiting the binding of virus to cell or inhibiting this conformational change of to the fusion state of these peptides to prevent a fusion pore from forming, can be used to develop countermeasures. Further, the various conformational rearrangements that take place from fusion to fusion pore formation, present numerous intermediates of the viral glycoprotein, which are normally not exposed for targeting by antibodies and the like. This presents an opportunity to create a very targeted response to multiple intermediates in this fusion pathway, with the overall goal to inhibit Nairovirus (*i.e.*, CCHFV) glycoprotein attachment or fusion induction.

SMALL PEPTIDES USED AS BROAD-SPECTRUM VIRUS ATTACHMENT AND VIRAL-FUSION INHIBITORS

One class of antivirals that has gone from the applied sciences and into an FDA approved antiviral for human immunodeficiency virus 1 (HIV-1) is Fuzeon™ (DP178; T20; Enfuvirtide)¹⁶⁸. This antiviral compound is a synthesized chain of 36 peptides which have been formulated into a subcutaneous injection. These 36-amino acids correspond to a portion of α helices within the pre-anchor domain of heptad repeat region-2 (HR2) of the HIV-1 envelope glycoprotein 41 (gp41)¹⁶⁸. This mimicry with HR2 prevents its association with HR1 and arrests the formation of the fusion pore, thus reducing infection of HIV-1 and reduces overall viral load¹⁶⁸. Since it is a small synthetic peptide, no hepatic or renal impairments have been observed, nor have significant drug interactions been reported during clinical trials. This is likely due to the rapid catabolism of the drug down to its base amino acids¹⁶⁸.

Besides HIV, inhibitory peptides have proven successful in pre-clinical studies for multiple human pathogenic viruses such as West Nile virus (WNV) and dengue virus (DENV)^{169,170}, severe-acute respiratory syndrome coronavirus (SARS-CoV)¹⁷¹, Zaire Ebolavirus (ZEBOV)¹⁶⁶, respiratory syncytial virus (RSV)^{172,173}, Hendra (HeV) and Nipah

viruses (NiV) ¹⁷⁴, and bunyaviruses such as Hanta (HANTV) and Andes viruses (ANDV) ^{175,176}, and Rift Valley fever virus (RVFV) ¹⁶⁶. For flaviviruses and bunyaviruses, a proposed target area for inhibitory peptides has been the stem region, which directly precedes the single spanning transmembrane region ^{166,169}. It is thought that upon acidification, the rearrangement of the G_C allows for residues to become exposed which can then be bound to the peptides and prevent fusion of the viral and vesicular membranes.

DESIGNING *NAIROVIRIDAE* ENTRY INHIBITOR PEPTIDES: SELECTING RESIDUES IN THE G_C AS PRIMARY TARGETS

Currently, no crystal structure of any Nairovirus G_C exists in published literature. This would be helpful in determining residues which might be exposed during the various pre-fusion and fusion states, which could aid in future inhibitory peptide designs. Since only linear peptide sequences are available, individual G_C and family level consensus G_C were examined *in silico*. I aligned all sequences and set a cut off threshold of 80% identity, shown as highlighted regions in green within Illustration 12. Regions of 15 or more amino acids with this cutoff of 80% similarities, were designated as ‘regions of interest’ and designated with black boxes in Illustration 12. I further overlaid data presented in Koehler *et al.* (2013) to model regions of interest with the RVFV-G_C, onto a consensus mapping between RVFV and CCHFV (Illustration 12). These RVFV-G_C regions of interest were conserved regions for RVFV that Koehler *et al.*, designed inhibitory peptides to ¹⁶⁶. The predicted fusion domain for both the RVFV-G_C and CCHFV-G_C were designated with a white box.

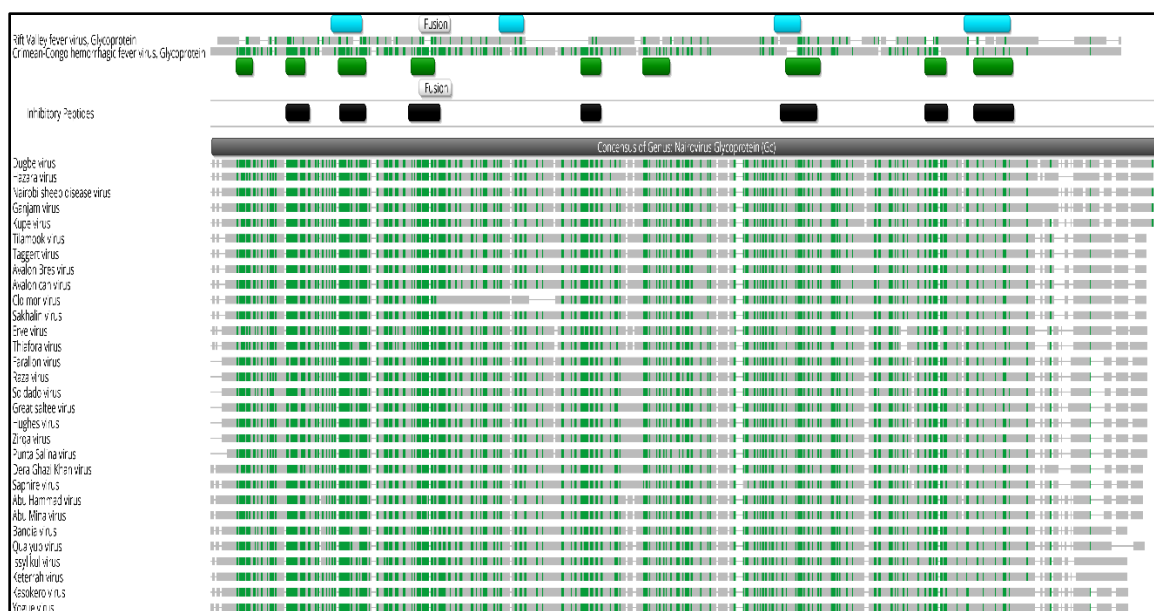


Illustration 12: Selecting CCHFV regions of interest from successful RVFV inhibitory peptide regions and from Nairovirus conserved regions within the G_C

At the top of the figure, a comparison among the consensus sequences of RVFV- G_C and CCHFV- G_C with the color cyan (light blue) indicating regions of interest for inhibitory peptides from Koehler et al. (2013). The green bars below the CCHFV- G_C indicate areas of similarity (>80%) from a Geneious alignment as previously described. These green regions of interest were analyzed for a positive Wimley-Whit interfacing hydrophobicity scoring using in silico Membrane Protein eXplorer. Those with a positive Wimley-Whit were designated with black bars and sent off to our collaborator at Columbia University, New York, New York, USA, Matteo Porotto, for synthesis.

Use of Sterol Groups to Enhance Uptake and Inhibition Efficacy

Many enveloped viruses undergo fusion in the confined space of internalized cell endosomes/vesicles. This compartment can be strikingly different from that of the plasma membrane on the cell surface. Sphingolipids and cholesterol are enriched depending on the vesicle and can be segregated into microdomains known as lipid rafts during endocytosis. This action can cause sequestering of various lipids and associated proteins to be endocytosed. It has been demonstrated by experimental studies that the antiviral efficacy of inhibitory peptides for HIV and paramyxoviruses can be increased by facilitating these peptides to intercalate into formation of these lipid rafts^{177–179}. This can be accomplished by PEGylating and tagging a sterol group onto the peptides. Various molecular weight PEGs and various types of sterols can be used, as it is unclear which

types of lipid domains are required for endosomal-dependent entry into infected host cells. Previous studies have shown the importance of clathrin-mediated endocytosis in CCHFV entry into mammalian host cells^{36,37,122}. This requires both clathrin and clathrin pit adaptor protein-2 complex but is independent of caveolin-1^{36,37,122}. For CCHFV, this internalization process has been shown to be dependent on cholesterol³⁷. With this knowledge, the peptides were conjugated to various sized PEGs and both cholesterol and tocopherol, another sterol that plays a role in the formation of ordered domains on cellular membranes.

Creating inhibitory peptides

Using the regions of interest outlined in Illustration 12 (black bars), a series of seven sequences between 15 and 23 residues long was selected for peptide synthesis. The peptide locations were designed against the prototype CCHFV strain IbAr10200, and the mature G_C residues for sequences were sequence 1: 147-169aa, sequence 2: 319-333aa, sequence 3: 412-432aa, sequence 4: 508-523aa, sequence 5: 542-560aa, sequence 6: 546-562aa, and sequence 7: 553-570aa. Cysteines present in the various peptide sequences were replaced with serines. The side chain for cystine, which contains this sulfhydryl (thiol) group, can lead to the formation of disulfide bonds among the peptides which can form oligomers that may negatively affect the solubility or functionality of lyophilized or resuspended inhibitor peptides. Of these seven selected sequences, only four were able to be produced in sufficient quantities for downstream applications (Illustration 13).

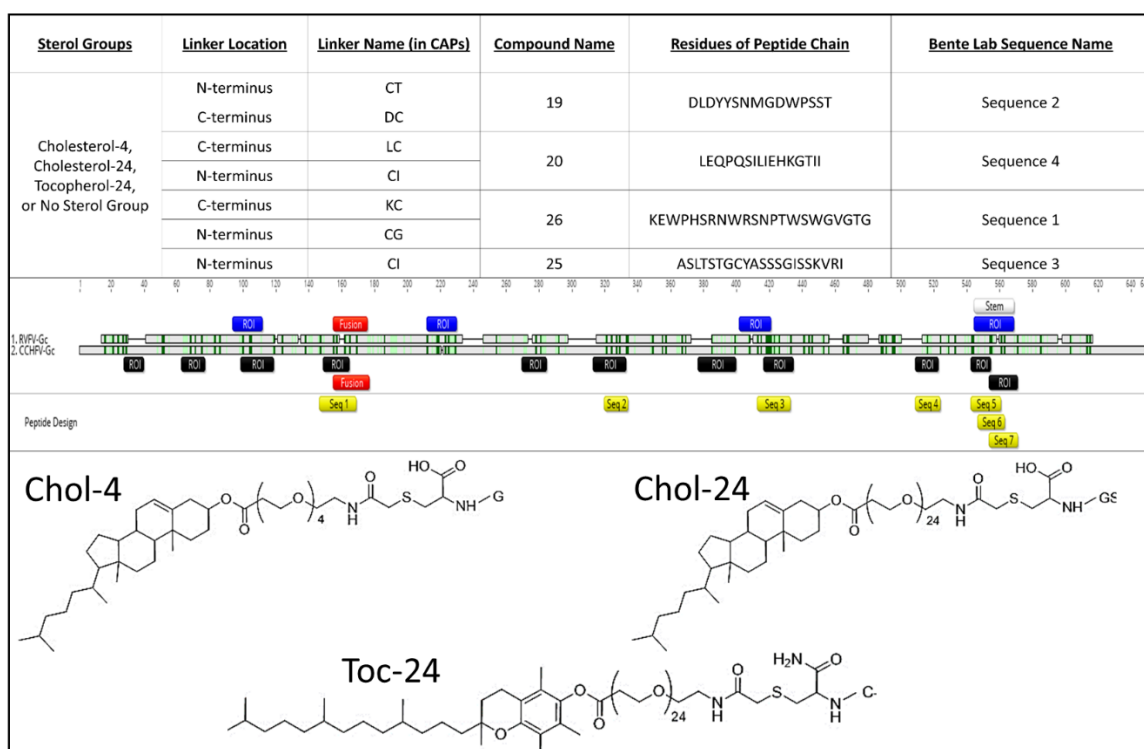


Illustration 13: CCHFV inhibitory peptide selection and linker group descriptions

Regions of interest (ROI) within the CCHFV- G_C which had a positive Wimley-Whit score, were selected for peptide synthesis and are depicted in yellow. Each of the regions of interest (ROI) that were used in selecting these peptides, were the RVFV- G_C (in blue) and CCHFV- G_C (in black). The fusion domain for both the RVFV- G_C and the CCHFV- G_C are outlined in red. Of the seven selected regions, only four sequences were yielded due to purity issues with the other three sequences. These four remaining sequences (1 through 4), were linked on either the N- or C- terminus of the peptide chain with either a various molecular weighted PEG, and/or cholesterol and tocopherol. Sequence 1: 147-169aa, sequence 2: 319-333aa, sequence 3: 412-432aa, sequence 4: 508-523aa, sequence 5: 542-560aa, sequence 6: 546-562aa, and sequence 7: 553-570aa

These four peptides were created using solid-phase conventional N-a-9-fluorenylmethyloxycarbonyl chemistry and linked on either the N- or C-termini using high performance liquid chromatography. Each linker was attached to either a polyethylene glycol 4,000 kDa (PEG-4) or 24,000 kDa (PEG-24) molecule, respectively. The linker and PEG molecules were then attached to either a cholesterol, tocopherol or lacked the sterol groups altogether. In the case of the absence of sterol group, only PEG-24 was left linked. The addition of the PEG molecules is hypothesized to play a role in longevity and half-life of the peptides, similar to other small molecule therapies such as PEGylated interferon

gamma (IFN- γ) therapy. In total, twenty-eight peptides were reconstituted using pipetting and ultrasonication to 100 μ M aliquots in DMSO.

SCREENING PEPTIDES ON PSEUDOTYPED RECOMBINANT VESICULAR STOMATITIS VIRUS

To first assess the inhibitory effects of the twenty-eight peptides, an initial screening was performed using a plaque reduction neutralization test (PRNT) and the replication competent pseudotype. Each peptide was suspended in cell culture media with a final concentration of 10 μ M peptide and 1% DMSO and incubated onto cells for 90 minutes. Cells were then infected with a known concentration of the pseudotype Δ GrVSV- Δ CCHFV-GPC in medium containing the peptides. Figure 12 demonstrates that several peptides worked to reduce the overall number of plaques forming. Two controls were incorporated into the assay. The first was hyper-immune mouse ascitic fluid (HMAF) at 1:160 dilution, which has a PRNT₈₀ value with the pseudotype (data not shown). Additionally, 10 μ M of chloroquine was also incorporated into the assay as a control to disrupt the pH reduction of endocytic vesicles, and potentially impact viral fusion. Both the controls showed a level of impact on the percent reduction of the pseudotype plaques (Figure 12). Several compounds from the CT19, DC19, LC20, and CI20 performed well in reducing the overall number of plaques in the PRNT assay (Figure 12). Interestingly, the cholesterol and PEG-4 groups of both KC26 and CG26 enhanced the number of plaques formed within the assay. The cause or mechanism for this is unknown, though KC26 and CG26 are analogues of Sequence 1 (Illustration 13) which is the peptide targeting the putative class II fusion peptide on the CCHFV-G_C. Further curious, is that CI25, the only peptide with overlap on a RVFV-G_C ROI, all sterol and non-sterol linked peptides, enhanced the formation of plaques as well. This region that was targeted in the Koehler *et al.*, (2013) article, details this region as RVFV-G_C domain III (332-350aa), and 30% plaque reduction was demonstrated from peptides targeting this region¹⁶⁶.

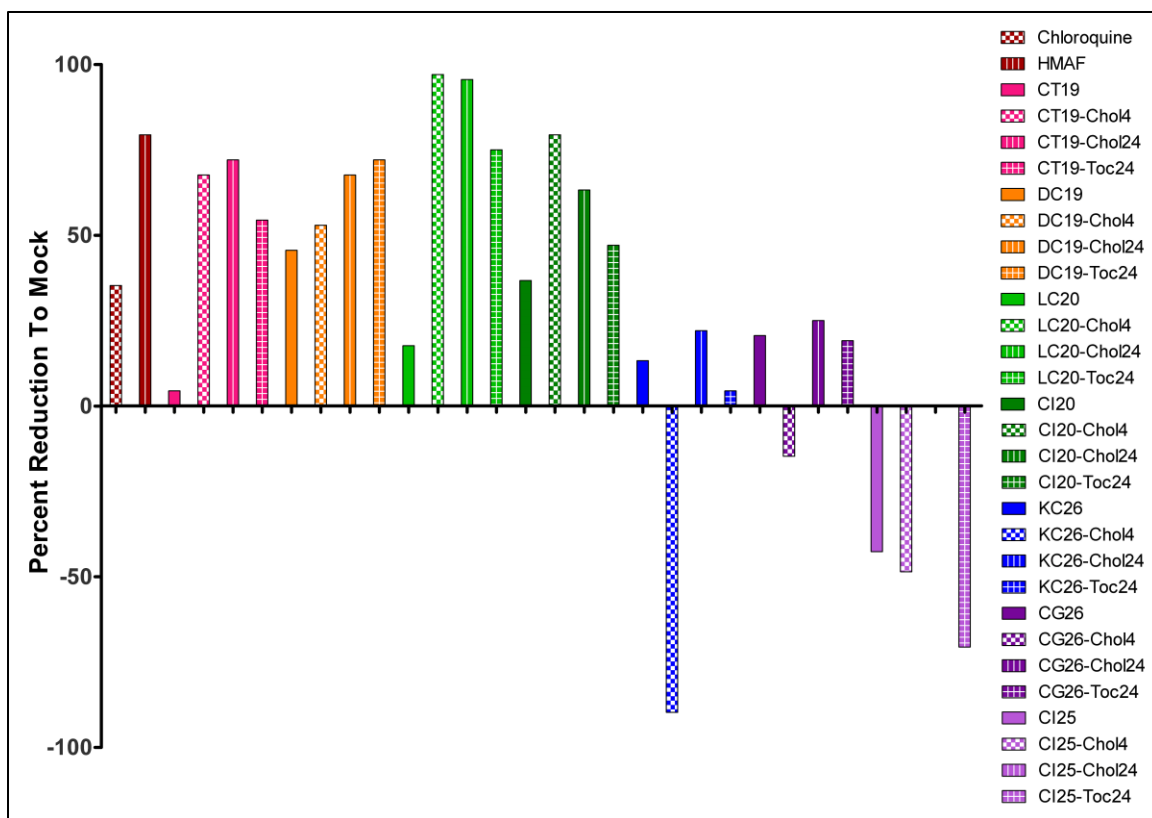


Figure 12: Percent plaque reduction neutralization test of 10 μ M of inhibitory peptides on pseudotyped Δ GrVSV- Δ CCHFV-GPC

A plaque reduction neutralization test of each of the twenty-eight inhibitory peptides at 10 μ M, screened on the pseudotyped Δ GrVSV- Δ CCHFV-GPC on BHK cells. A starting titer of virus was 50 pfu, though all compounds are compared at baseline to the mock of virus only (as shown on the far most left of the treatment groups). Compounds that inhibited plaque formations resulted in an increase in the percent of plaque reduction, all the way up to 100% reduction which resulted in 0 plaques forming. In some instances, the reverse happened, where the number of plaques increased up to approximately 80 pfu. Chloroquine (10 μ M) and hyper-immune mouse ascitic fluid (HMAF) (1:160 dilution) were used as positive controls, an uninfected mock, and virus only well were used as baseline controls.

To assay specificity, a sample of four peptides that had >70% inhibition of the pseudotyped virus were chosen (LC20-cholesterol/PEG4 [designated LC-20 Chol 4], CI20-cholsterol/PEG4 [designated CI-20 Chol 4], DC19 tocopherol/PEG24 [designated DC-19 Toc 24], and CT19-cholesterol/PEG24 [designated CT-19 Chol 24]) and the same experiment was carried out on wild-type VSV, strain: Indiana. As demonstrated in Figure 13, the peptides had minimal effect, all <40% on inhibiting plaques from forming, demonstrating that these peptides were specific for the CCHFV-G_c present on the pseudotype Δ GrVSV- Δ CCHFV-GPC.

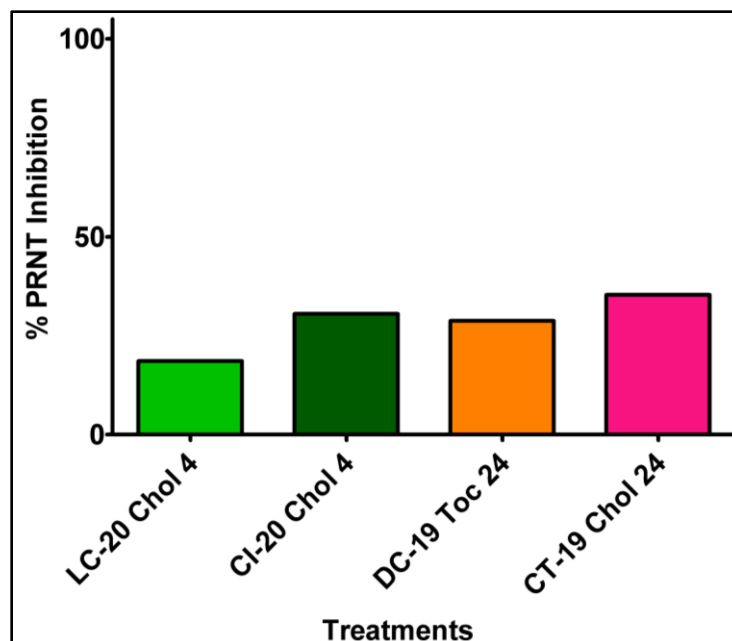


Figure 13: Specificity of inhibitory peptides on wild-type vesicular stomatitis virus (VSV)

A plaque reduction neutralization test of each of the six inhibitory peptides at 10 μ M, screened on wild-type VSV, strain: Indiana on BHK cells. A starting titer of virus was 50 pfu, though all compounds are compared at baseline to the mock of virus only. Compounds that inhibited plaque formations resulted in an increase in the percent of plaque reduction, all the way up to 100% reduction which resulted in 0 plaques forming.

EVALUATING SELECTED PEPTIDES ON CRIMEAN-CONGO HEMORRHAGIC FEVER VIRUS

Six of the top inhibitory peptides (LC20-cholesterol/PEG4, CT19-cholesterol/PEG24, DC19-cholesterol/PEG24, CI20-cholesterol/PEG4, DC19-tocopherol/PEG24, DC19-cholesterol/PEG24) which were screened on the pseudotype Δ GrVSV- Δ CCHFV-GPC, were then tested multiple times on wild-type CCHFV, strain: IbAr10200. The results are displayed in Figure 14. The two peptides that inhibited the most at 10 μ M concentrations on CCHFV were LC20 linked to cholesterol/PEG4 and CT19 linked to cholesterol/PEG24.

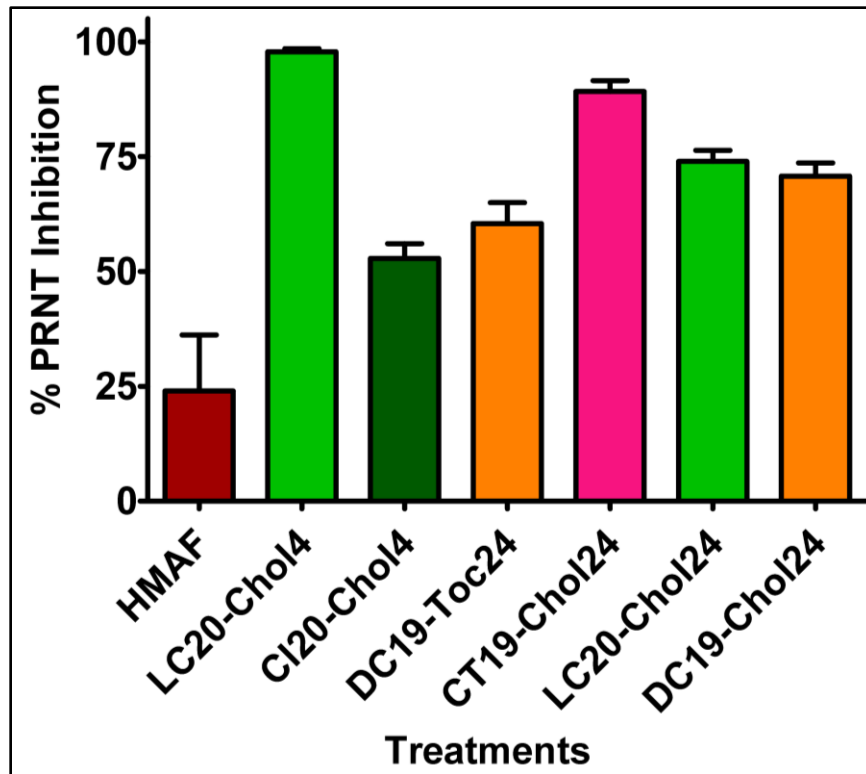


Figure 14: Percent plaque reduction neutralization test of selected inhibitory compounds on wild-type CCHFV

A plaque reduction neutralization test of each of the six inhibitory peptides at 10 μ M, screened on wild-type CCHFV, strain: IbAr10200 on SW13CDC cells. A starting titer of virus was 50 pfu, though all compounds are compared at baseline to the mock of virus only. Compounds that inhibited plaque formations resulted in an increase in the percent of plaque reduced, all the way up to 100% reduction which resulted in 0 plaques forming. Hyperimmune mouse ascitic fluid (HMAF) (1:640 dilution) were used as positive controls, an uninfected mock, and virus only well were used as baseline controls. Assay was done twice with each parameter measured in duplicate.

Interestingly, both LC20 and CI20 are the same sequence, however the linker and cholesterol placement are on different termini. For LC20, the linker is on the C-terminus versus for CI20 where the linker is on the N-terminus. It is unknown why this would cause a 40% difference in percent reduction of CCHFV, though it could be due to potential folding or interactions depending on linker placement. This peptide sequence for LC20 is sequence 4, which corresponds to 508-523aa on the CCHFV-G_C, it is the shortest peptide sequence designed for these experiments. This region is directly upstream of the original targeted ‘stem’ region which in ANDV and RVFV inhibitory peptide studies, reduced the infectivity of both viruses the most out all regions targeted. For these studies, sequences

5-7 were not synthesized to sufficient quantities for downstream applications such as screening, though it would be curious in the future, if sufficient quantities could be generated, to test this region as well.

CT19 is the C-terminus of sequence 2, from region 319-333aa of the CCHFV-G_C. This region was not targeted by either the ANDV or RVFV inhibitory peptides studies, though this selected region has a high degree of similarity among nairoviruses. On CCHFV-G_C, this region is directly downstream of an N-linked glycan epitope, the linear binding region of the MAb 11E7, and the region that supposedly binds cell surface nucleolin^{35,113}. Aside from these epitopes preceding this area that sequence 2 is based off, this region warrants additional studies in the future as it appears to be an influential site for at the very least neutralization.

DEVELOPING AND EVALUATING A *NAIROVIRIDAE* FUSION ASSAY

After screening and identifying peptides that are functionally inhibitory to both pseudotype and wild-type CCHFV, I sought to understand if these neutralizing peptides could affect viral fusion. To assess the impacts of these peptides on fusion, a Nairovirus fusion assay had to be developed as one did not exist in currently published literature. Given that CCHFV relies on the early endosomal trafficking and multivesicular bodies^{36,37,122}, the pH during these steps can range down to approximately 6.0¹⁸⁰. Therefore, an immunofluorescence assay was designed which stained cytoplasmic content and nuclei, with separate stains. Cells would express the G_C of various nairoviruses via either transfection, vectored viruses (pseudotyped Δ GrVSV- Δ CCHFV-GPC) or wild-type nairoviruses. pH would be altered in these cell culture systems with medium buffered at 0.2 increments descending from 7.4 (approximate basal pH of the body) down to 5.2, the late endosomal pH¹⁸⁰, which nairoviruses are not expected to induce fusion at. Cells would then be fixed and stained, and a fusion index calculated to determine the relative number of fused cells, or polykaryocytes formed per field of view using the following equation:

$$Fusion\ index = 1.0 - \frac{number\ of\ cells}{number\ of\ nuclei}$$

First, Huh-7 were transfected with a CAGGs plasmid encoding the CCHFV-GPC. These liver cells were chosen for three reasons. The first is that at a approximately 80% subconfluent conditions, they form large umbonate cells with defined plasma membranes and higher cytoplasmic content vs. nuclear content. This should make polykaryocyte counting for the fusion index easier for discerning purposes. The second reason, was that these cells are the susceptible and permissive to CCHFV infection ¹¹⁶. Our group has also shown that these cells are also susceptible and permissive to infection by other nairoviruses such as Hazara, Qualyub, Dugbe, Clo Mor, and Tillamook viruses (data not shown). Lastly, many cytotoxicity studies for drug development have been done in liver cells like HuH-7 or HEPG2 cells. While cytotoxicity studies were not undertaken due to compound exhaustion, they are planned for future work. Compounds are being re-synthesized and further studies such as cytotoxicity assays and inhibitory concentration assays, including the calculation of IC50 values, are planned. Figure 15 demonstrated a few polykaryoctes beginning to form at pH 5.8 and increasing down to pH 5.2 (Figure 15). These findings were not in line with the current published data supporting that fusion occurs during the early endosomal pathway. A rational for this, is that the expression system does not adequately allow for fusion events at the cell surface using the CCHFV-G_C, or that transfection expression efficiencies limit the quantity of CCHFV-G_C that can act at the cell surface in a biologically functional manner. While, overall, transfection may achieve the goal of Nairovirus fusion, it may not be the most straight forward approach to be able to assay fusion inhibitors with.

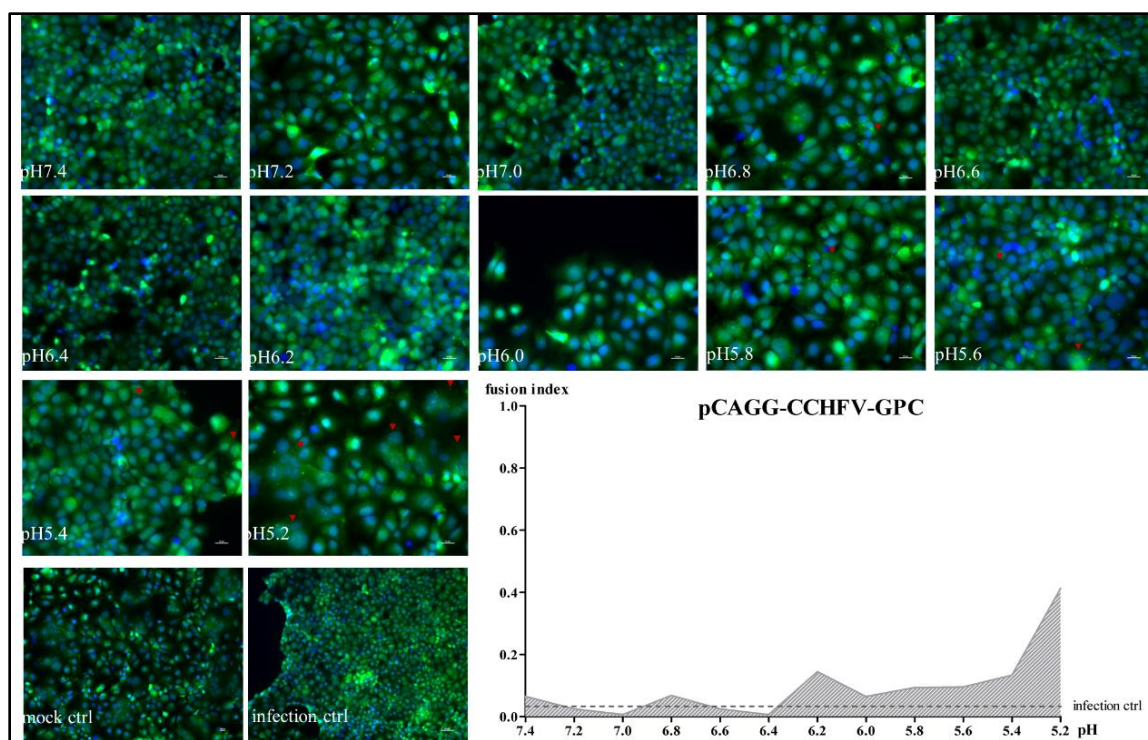


Figure 15: Nairovirus fusion assay using pCAGG-CCHFV-GPC

Human hepatocarcinoma cells (HuH-7) were transfected with 750 ng of codon optimized pCAGG-CCHFV-GPC (strain: IbAr10200) per well of an eight well chamber slide. Each well was exposed to variable pH from 7.4 to 5.2, along with a mock control and infection only control that had normal media. Cells were stained with Cell Mask Green, and counterstained during mounting with DAPI in the mountant. Representative fields of view were imaged and were coded. Two blinded analyzers counted nuclei and individual cells/polykaryocytes. Using the fusion index formula, fusion indices were plotted for each pH 0.2 incremental step of the assay.

To examine fusion with ‘live’ virus, a BSL-2 Nairovirus called HAZV (strain: JC280) was utilized. HAZV is a tick-borne isolate from the Hazara valley of Pakistan. It has no association to human disease, but it is serogrouped with CCHFV due to its relative similarity (~49% identity within the G_C 's)^{23,181}. Recent work has been done on Hazara virus entry by Punch *et al.*, (2018), whom have demonstrated the need of potassium (K^+) ions and a pH of 6.3 to promote viral infectivity¹⁸². Utilizing various nairoviruses in this type of fusion assay, it was unclear the mechanism which might induce cell-to-cell fusion events. As the Nairovirus G_C is the mediator of this phenomena, it is hypothesized that either shuttling of this G_C to the plasma membrane, or nairoviruses being ejected from infected cells and encountering adjacent cells in a paracrine manner, could induce fusion

events if the virus infects the space between two neighboring cells. Accordingly, a higher MOI was chosen to maximize antigen production and hopefully localization of the G_C to the plasma membrane to induce fusion. Multiple attempts at several time points were made to optimize conditions for polykaryocyte formations using Hazara virus. Ultimately, it was discovered that infected cells with Hazara virus can induce polykaryocytes between 16 and 20 hours when the pH is changed for approximately 15 minutes. Once the pH is 6.4, polykaryocyte formations begin to occur with increasing frequency as pH decreases. (Figure 17).

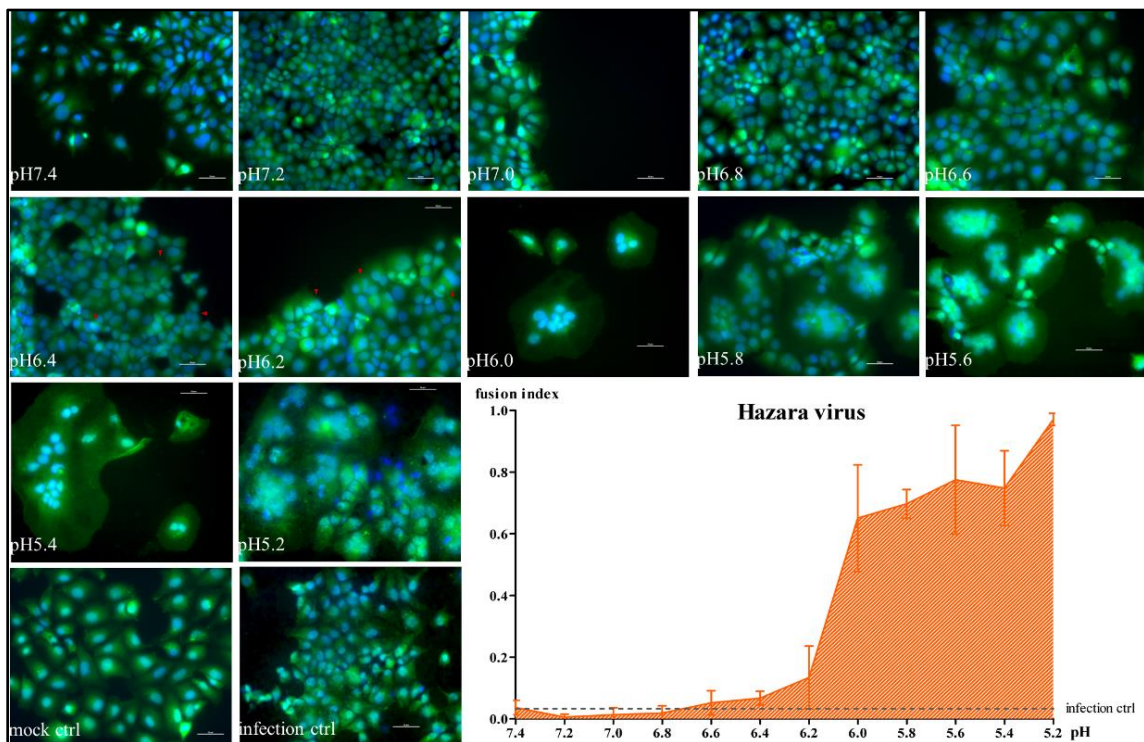


Figure 16: Nairovirus fusion assay using Hazara virus

Human hepatocarcinoma cells (HuH-7) infected at a MOI of 3 with the BSL-2 Nairovirus, Hazara virus, per well of an eight well chamber slide. Each well was exposed to variable pH from 7.4 to 5.2, along with a mock control and infection only control that had normal media. Cells were stained with Cell Mask Green, and counterstained during mounting with DAPI in the mountant. Representative fields of view were imaged in triplicate and were coded. Two blinded analyzers counted nuclei and individual cells/polykaryocytes. Using the fusion index formula, fusion indices were plotted for each pH 0.2 incremental step of the assay.

An assay was developed to determine whether infected cells with Δ GrVSV- Δ CCHFV-GPC could also induce fusion. One limitation that changed the overall

experimental design for the pseudotyped virus, is that while it infects human liver cells (Huh-7), it induces syncytial formations within 16 hours of infection (data now shown). These syncytial formations confound fusion indices, therefore BHK cells were substituted in this assay, as fusion does not occur at physiologic (~7.4 pH) conditions like in the Huh-7. In our fusion assay, polykaryocytes begin to form below pH 6.4 and increase as pH decreases (Figure 17), similarly to the Hazara virus fusion assay.

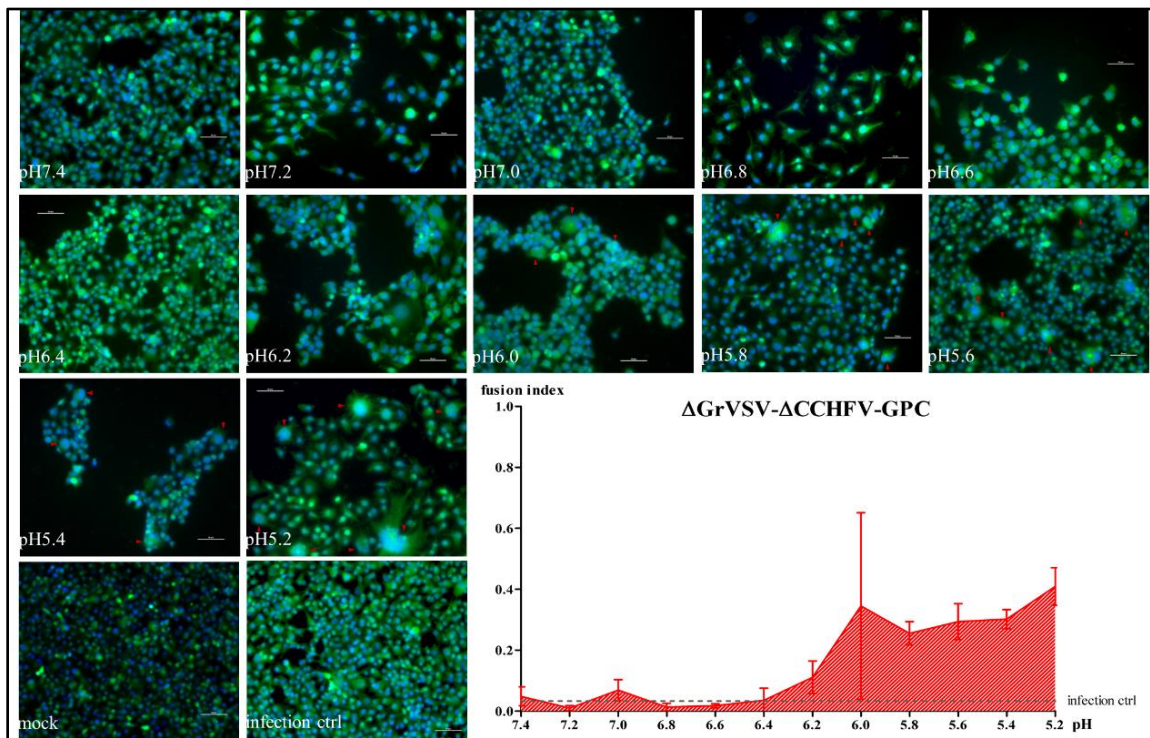


Figure 17: Nairovirus fusion assay using $\Delta\text{GrVSV-}\Delta\text{CCHFV-GPC}$

Baby hamster kidney cells (BHK) infected at a MOI of 3 with the pseudotype $\Delta\text{GrVSV-}\Delta\text{CCHFV-GPC}$ per well of an eight well chamber slide. Each well was exposed to variable pH from 7.4 to 5.2, along with a mock control and infection only control that had normal media. Cells were stained with Cell Mask Green, and counterstained during mounting with DAPI in the mountant. Representative fields of view were imaged in triplicate and were coded. Two blinded analyzers counted nuclei and individual cells/polykaryocytes. Using the fusion index formula, fusion indices were plotted for each pH 0.2 incremental step of the assay.

An additional pathogenic Nairovirus was also examined for fusion assay. The BSL-3 Dugbe virus (DUGV), a human pathogenic Nairovirus, was similarly infected on to human liver cells with exposures to gradient pH. Dugbe virus began polykaryocyte

formations at $\text{pH} \leq 6.6$ (Figure 18). It formed large polykaryocytes at pH 6.4 and eventually formed a full fused monolayer.

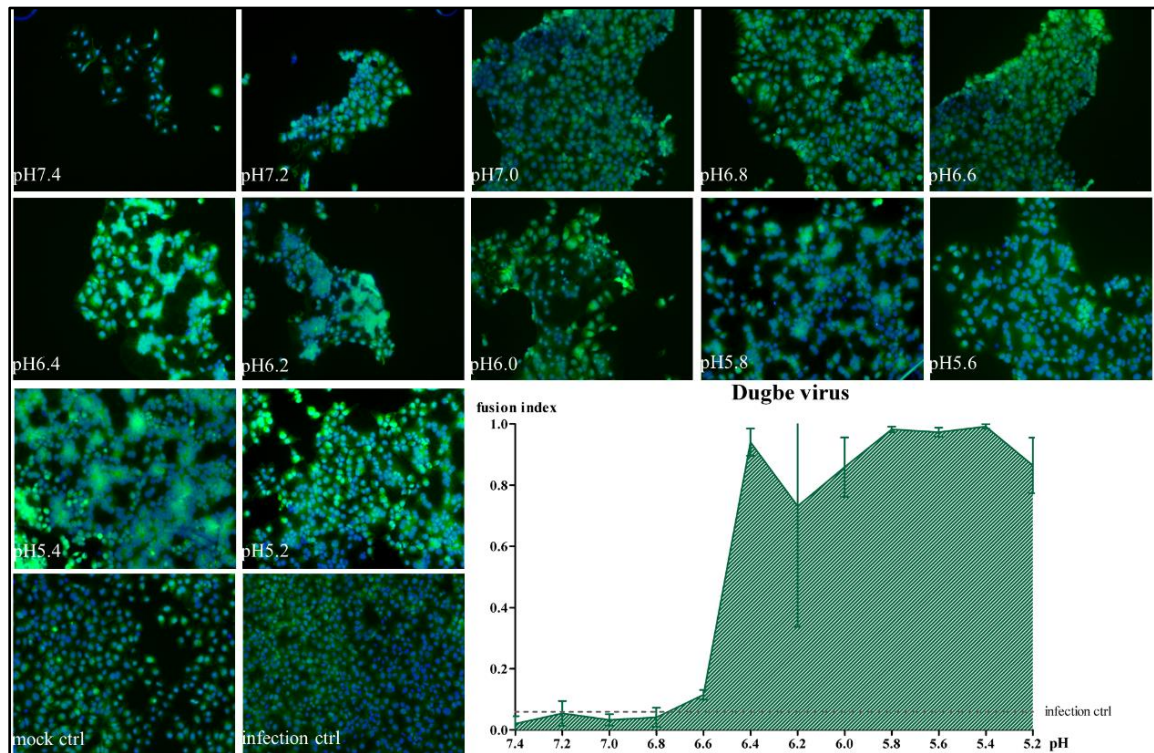


Figure 18: Nairovirus fusion assay using Dugbe virus

Human hepatocarcinoma cells (HuH-7) infected at a MOI of 3 with the BSL-3 prototype Nairovirus, Dugbe virus, per well of an eight well chamber slide. Each well was exposed to variable pH from 7.4 to 5.2, along with a mock control and infection only control that had normal media. Cells were stained with Cell Mask Green, and counterstained during mounting with DAPI in the mountant. Representative fields of view were imaged in triplicate and were coded. Two blinded analyzers counted nuclei and individual cells/polykaryocytes. Using the fusion index formula, fusion indices were plotted for each pH 0.2 incremental step of the assay.

Lastly, a fusion assay was developed for CCHFV. A recombinant CCHFV (rCCHFV) that encodes the fluorescent protein mCherry, a *Discosoma* sea anemone protein, was placed in the N-terminus nonstructural protein portion of Pre-G_N. This recombinant virus was used to determine if polykaryocytes could be overlaid with active CCHFV infection (Figure 19).

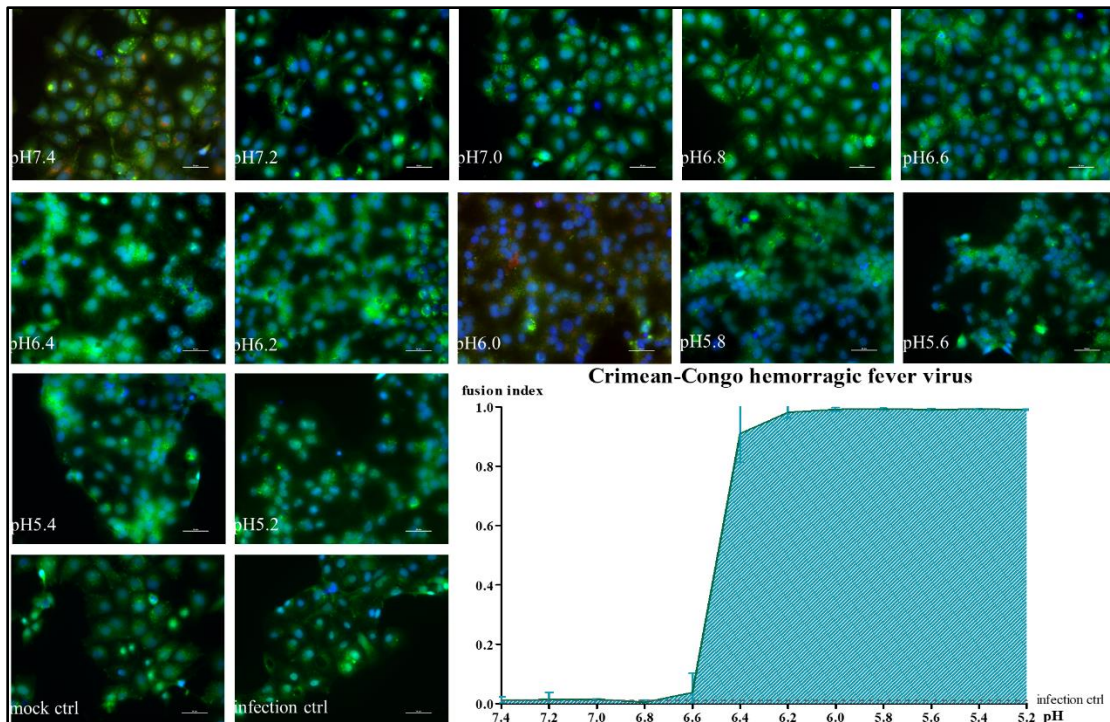


Figure 19: Nairovirus fusion assay using CCHFV virus

Human hepatocarcinoma cells (HuH-7) infected at a MOI of 3 with the recombinantly fluorescently labeled BSL-4 Nairovirus, rCCHFV-M/Cherry, per well of an eight well chamber slide. Each well was exposed to variable pH from 7.4 to 5.2, along with a mock control and infection only control that had normal media. Cells were stained with Cell Mask Green, and counterstained during mounting with DAPI in the mountant. Representative fields of view were imaged in triplicate and were coded. Two blinded analyzers counted nuclei and individual cells/polykaryocytes. Using the fusion index formula, fusion indices were plotted for each pH 0.2 incremental step of the assay.

Like DUGV, the fusion index for CCHFV also began to rise at a $\text{pH} \leq 6.6$ indicating a higher proportion of nuclei vs number of cell bodies indicating increasing cell-to-cell fusion events. Cumulatively, these data presented within Figures 16-19 demonstrate that Nairovirus fusion occurs between pH 6.6-6.2. This experimental design and the data support a fusion event for nairoviruses during the early endosomal compartment as studied by Garrison *et al.*, (2013) and Shtanko *et al.*, (2014) for CCHFV^{36,122}. The pseudotyped $\Delta\text{GrVSV-}\Delta\text{CCHFV-GPC}$ also demonstrated utility in both examining fusion using the CCHFV-G_C in a different cell type and had a similar pH range as wild-type CCHFV, whereas the plasmid base system (pCAGG-CCHFV-GPC) did not perform in a similar manner.

Based off the results from the Nairovirus fusion assays the pseudotype was used as a screening tool to examine the effects of the top five peptide compounds on the fusion index. Figure 20 illustrates the fusion inhibition of the top five peptides. LC-20 linked to cholesterol and PEG4, along with CT-19 linked to cholesterol and PEG24, inhibited the fusion index the strongest. These results align with the overall inhibitory capacities of the peptides on both the pseudotype and wild-type CCHFV as outlined in Figures 12 and 14.

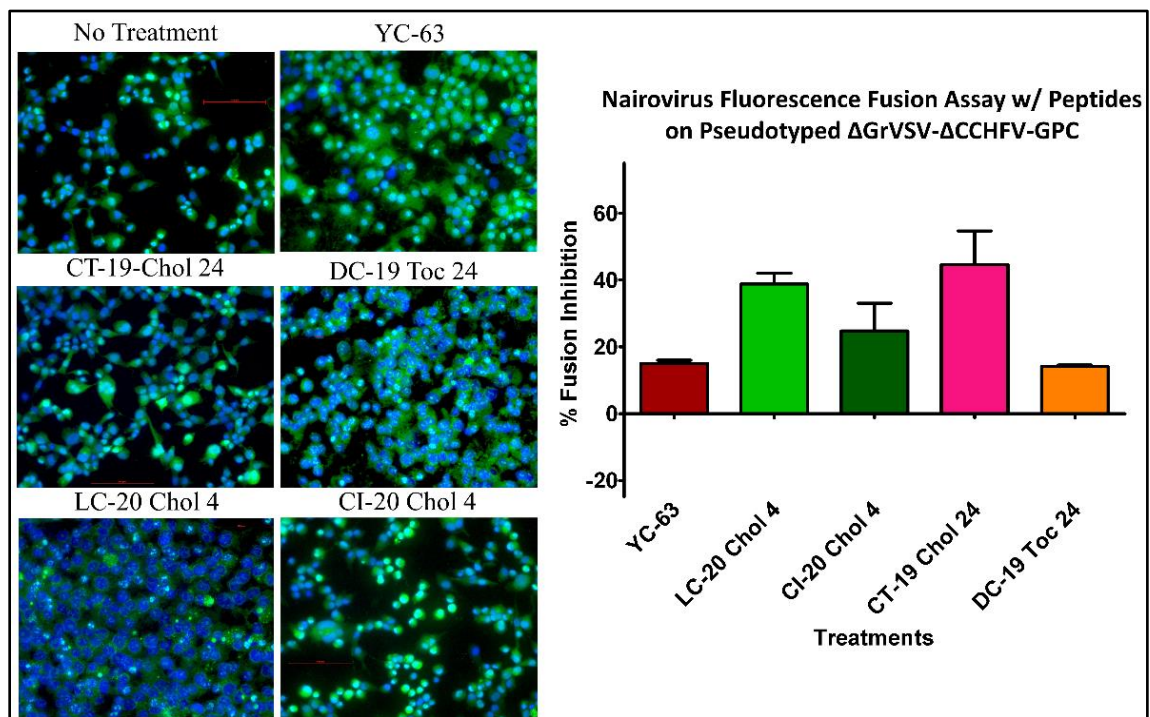


Figure 20: Role of inhibitory peptides on nairovirus fusion using pseudotyped Δ GrVSV- Δ CCHFV-GPC

Baby hamster kidney cells (BHK) infected at a MOI of 3 with pseudotyped Δ GrVSV- Δ CCHFV-GPC, per well of an eight well chamber slide. Each well was exposed to variable pH from 7.4 to 5.2, along with a mock control and infection only control that had normal media. Cells were stained with Cell Mask Green, and counterstained during mounting with DAPI in the mountant. Representative fields of view were imaged in triplicate and were coded. Two blinded analyzers counted nuclei and individual cells/polykaryocytes. A fusion index was calculated for each treatment and was expressed as a percent fusion subtracted from infected only wells. This experiment was done twice. A control scramble peptide YC-63 was included in the assay to account for non-specific inhibition of fusion.

These five peptides (LC-20, CI-20, CT-19, and DC-19), showing evidence of inhibiting fusion, were further examined on wild-type CCHFV. Figure 21 demonstrates that LC-20 has the highest fusion inhibition with an 80% knockdown of cell-to-cell mediate

fusion in using the Nairovirus fusion assay, while CT-19 cholesterol 24 appeared to have a milder fusion inhibition on wild-type CCHFV of approximately 40% fusion inhibition (Figure 21).

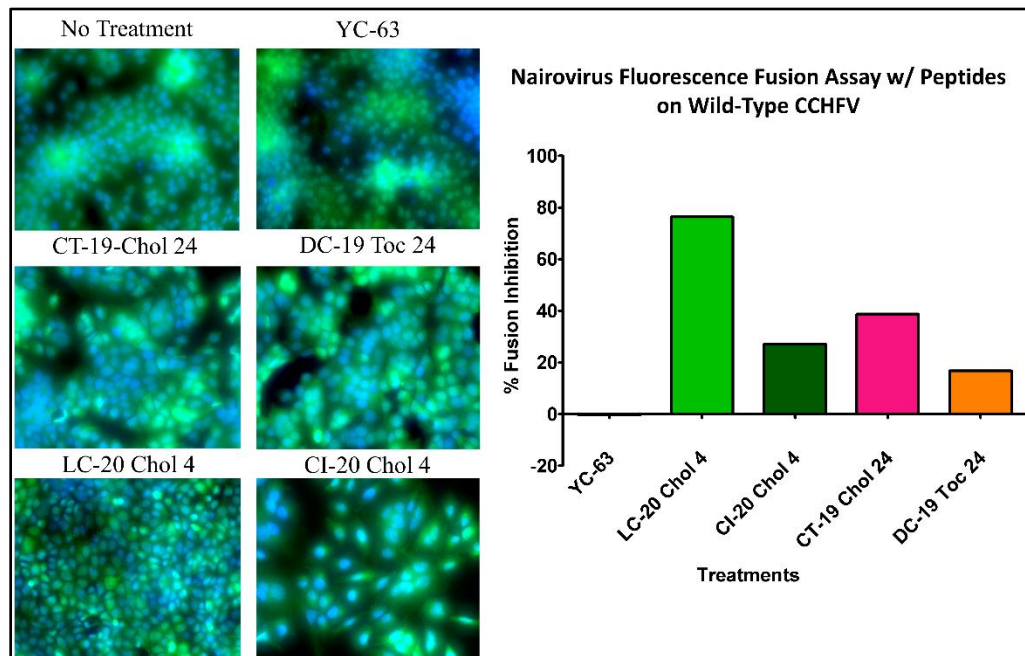


Figure 21: Role of inhibitory peptides on nairovirus fusion using CCHFV

Human hepatocarcinoma cells (HuH-7) infected at a MOI of 3 with the recombinantly fluorescently labeled BSL-4 Nairovirus, rCCHFV-M/Cherry, per well of an eight well chamber slide. Each well was exposed to variable pH from 7.4 to 5.2, along with a mock control and infection only control that had normal media. Cells were stained with Cell Mask Green, and counterstained during mounting with DAPI in the mountant. Representative fields of view were imaged in triplicate and were coded. Two blinded analyzers counted nuclei and individual cells/polykaryocytes. A fusion index was calculated for each treatment and was expressed as a percent fusion subtracted from infected only wells.

Overall, two areas, sequence 2 (targeted by CT-19) and sequence 4 (targeted by LC20) both demonstrated inhibition of PRNT, and inhibition of fusion, with LC-20 (sequence 4) demonstrating the highest inhibition in both assays. Neither of these portions of the G_C has have been extensively studied with relation to mechanism or function, however this data revealed that these two conserved areas are prime targets for further studies and for further countermeasure designs. It would be interesting, to alternatively design antibody reagents to these peptide chains to look at other ways of inhibiting CCHFV entry by targeting these regions.

Another interesting note from these studies, is the termini linkage of these peptides. LC-20 cholesterol/PEG4 versus CI20 cholesterol/PEG4, though designed against the same sequence, have starkly different PRNT and fusion inhibitions. This study supports the notion that a multipronged approach at the linker location, and linker type—as is the case with CT19 with cholesterol/PEG24, should be undertaken, when countermeasures, such as peptide inhibitors, are designed. This study further demonstrates the utility of pseudotyped VSV with the CCHFV-GPC, as given much of the inhibition (either PRNT or fusion indices) trends were similar between Δ GrVSV- Δ CCHFV-GPC and wild-type CCHFV. Lastly, this study provides two new peptide inhibitors for CCHFV which warrant further studies to examine inhibitory concentrations and *in vivo* studies.

CHAPTER 6: Screening Crimean-Congo Hemorrhagic Fever Virus Glycoprotein

Precursor Processing Inhibitors

PATHOGEN BOX

Drug discovery costs an average of ~\$800,000,000 and can require nearly a decade of research from discovery to clinical development ¹⁸³. Recent ventures in the private sector have explored the facets of ‘open-source’ drug discovery platforms to reduce both the time of preclinical development and the economic burden. The Pathogen Box is one such venture which serves as a free and open-source drug discovery platform developed by the Medicines for Malaria Venture (MMV) in Geneva, Switzerland ¹⁸⁴. Funded by the Bill & Melinda Gates Foundation, MMV provides a series of 96-well plates of over 400 diverse, FDA approved drug, or drug-like analogues that are active against an array of neglected tropical diseases such as tuberculosis, malaria, burkholderia, kinetoplastids, helminths, cryptosporidiosis, toxoplasmosis, and dengue virus ^{185–187}. The principle advantage of the Pathogen Box is that it allows for the repurposing of FDA-approved drugs or closely related analogues ¹⁸⁴.

The goal of using the Pathogen Box in this CCHFV drug discovery study, involved screening the large panels of compounds for off-label efficacies on the target outlined in Chapter 3, the CCHFV-GPC. Given that the CCHFV-GPC requires numerous host factors for maturation to yield mature GP, the hypothesis was that given the diverse array of compounds included in the Pathogen Box, some of these might function as non-traditional treatments in impeding CCHFV-GPC processing and GP maturation. Compounds tested include proprotein convertase inhibitors for dengue virus, which relies on similar furin cleavage in the Golgi ¹⁸⁸, similar to the CCHFV-GPC. Other compounds function to arrest protein translation for short periods of time, which can derail the viral ‘life’ cycle. Viral pseudotypes have been used in multiple published studies, such as with influenza virus

(H5N1, 1918, *etc.*) or SARS-CoV to run drug-discovery screens for their more virulent counterparts^{189–192}. As demonstrated in Chapters 4 and 5, pseudotyped Δ GrVSV- Δ CCHFV-GPC possessed utility both in expressing and processing the CCHFV-GPC and in serving as a screening tool for inhibitory peptides against CCHFV-G_C. Thus, the pseudotype was a prime candidate to evaluate and screen which compounds might be effective against the CCHFV-GPC and in turn wild-type CCHFV.

SCREENING PATHOGEN BOX COMPOUNDS ON PSEUDOTYPED RECOMBINANT AND WILD-TYPE VESICULAR STOMATITIS VIRUSES

A set of screening experiments was designed to evaluate the inhibition efficacies of the various compounds of the Pathogen box on pseudotyped Δ GrVSV- Δ CCHFV-GPC. Human liver cells (HuH-7) were seeded into 96-well plates and infected with the pseudotyped Δ GrVSV- Δ CCHFV-GPC at a low MOI. Infected cells were incubated with the various Pathogen Box compounds which were re-suspended to a final volume of 5 μ M in 1% DMSO. Infected and treated cells were incubated for 48 hours and cell monolayers were fixed with formalin and crystal violet. Stained monolayers were examined by a 570 nm absorbance reading and a percent inhibition was calculated by comparing treatment wells to mock wells. The published inhibitory compounds for CCHFV, ribavirin and chloroquine, were incorporated that have demonstrated inhibition of CCHFV to validate the screens. All compounds were run, totaling more than 1,200 screening evaluations and an arbitrary cutoff of 20% inhibition was selected for further evaluation. Figures 22 through 26 demonstrate a number of ‘hits’ using this experimental design.

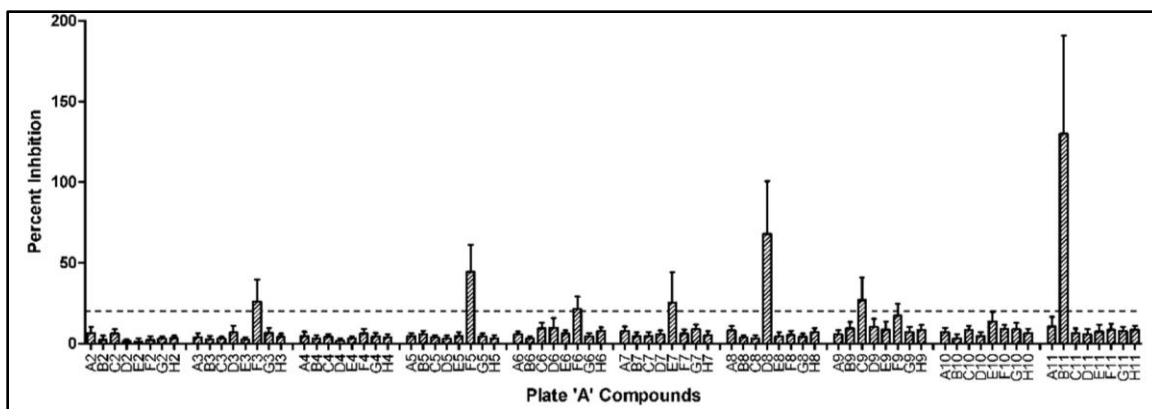


Figure 22: Screening of Pathogen Box, plate 'A' compounds using Δ GrVSV- Δ CCHFV-GPC pseudotype

Percent inhibition compared to mock (no compound) infected cells. All compounds were run in biological duplicates and the assay was run in triplicate. An arbitrary cutoff of 20% inhibition was designated by a dashed line.

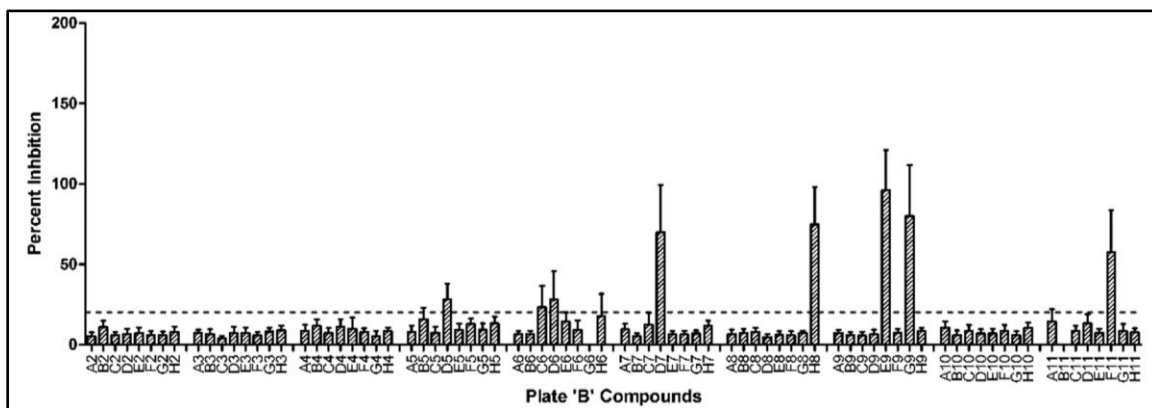


Figure 23: Screening of Pathogen Box, plate 'B' compounds using Δ GrVSV- Δ CCHFV-GPC pseudotype

Percent inhibition compared to mock (no compound) infected cells. All compounds were run in biological duplicates and the assay was run in triplicate. An arbitrary cutoff of 20% inhibition was designated by a dashed line.

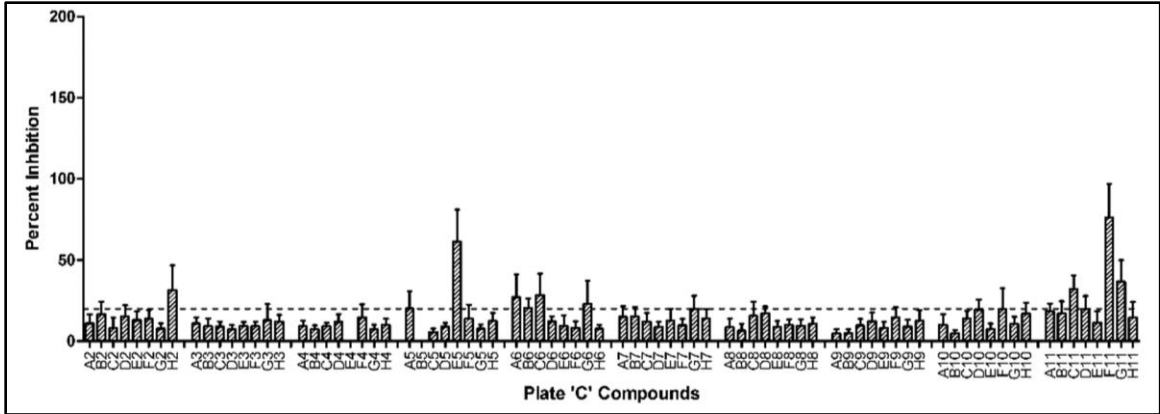


Figure 24: Screening of Pathogen Box, plate 'C' compounds using Δ GrVSV- Δ CCHFV-GPC pseudotype

Percent inhibition compared to mock (no compound) infected cells. All compounds were run in biological duplicates and the assay was run in triplicate. An arbitrary cutoff of 20% inhibition was designated by a dashed line.

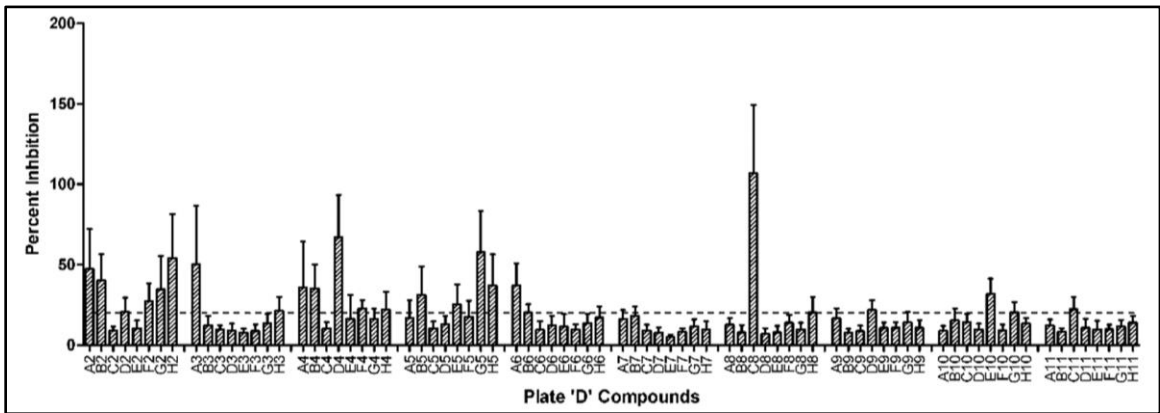


Figure 25: Screening of Pathogen Box, plate 'D' compounds using Δ GrVSV- Δ CCHFV-GPC pseudotype

Percent inhibition compared to mock (no compound) infected cells. All compounds were run in biological duplicates and the assay was run in triplicate. An arbitrary cutoff of 20% inhibition was designated by a dashed line.

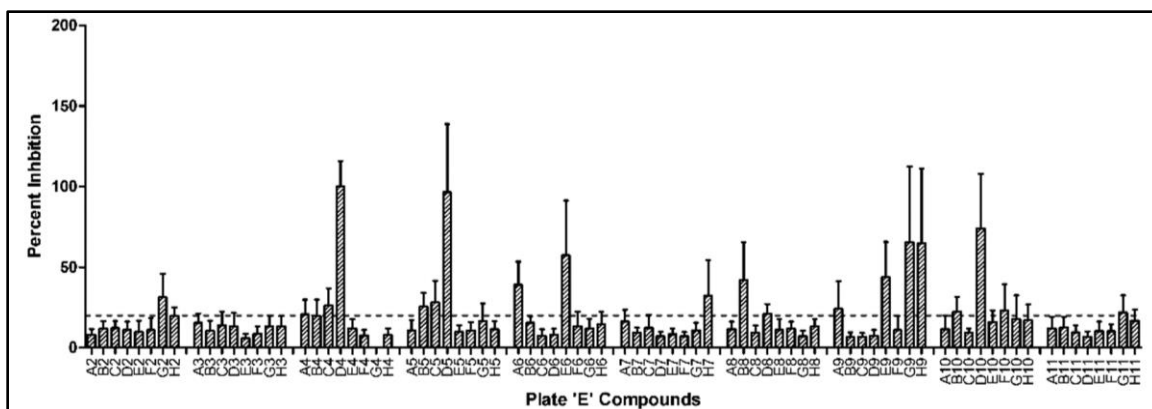


Figure 26: Screening of Pathogen Box, plate 'E' compounds using Δ GrVSV- Δ CCHFV-GPC pseudotype

Percent inhibition compared to mock (no compound) infected cells. All compounds were run in biological duplicates and the assay was run in triplicate. An arbitrary cutoff of 20% inhibition was designated by a dashed line.

Based on the results from Figures 22 through 26, a total of 88 compounds were identified which, to some degree, inhibited cytopathic effects and destruction of human liver cell monolayers caused by Δ GrVSV- Δ CCHFV-GPC pseudotype after 48 hours of incubation. These 88 compounds were then screened in a similar manner on wild-type VSV (strain: Indiana) and were in tandem, re-run on the Δ GrVSV- Δ CCHFV-GPC pseudotype. Percent inhibitions were calculated for both and wild-type VSV percent inhibitions were subtracted from the pseudotype's to yield percent difference in inhibition (Figure 27). Using a cutoff of 50% difference in inhibition, eighteen compounds were selected for further analysis on wild-type CCHFV.

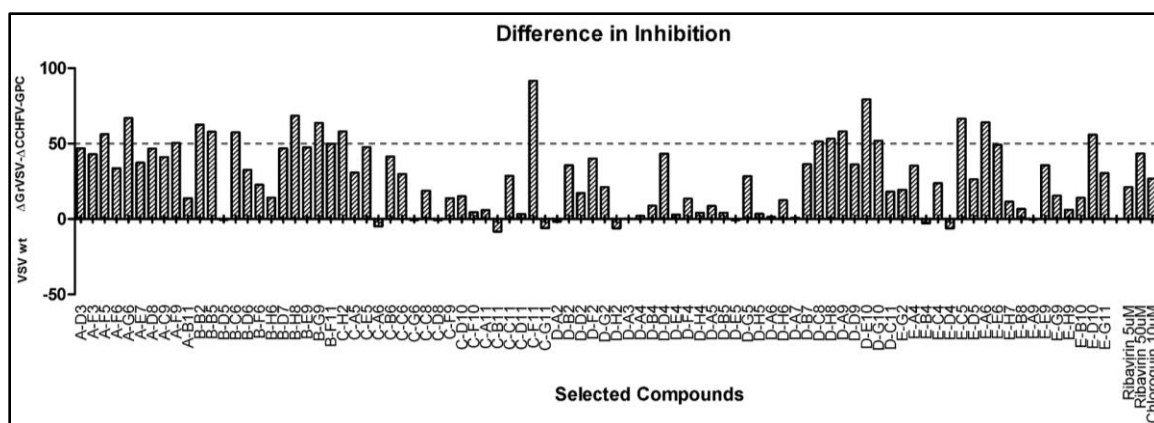


Figure 27: Difference in inhibition between wild-type VSV and Δ GrVSV- Δ CCHFV-GPC pseudotype

Percent inhibition compared to mock (no compound) infected cells of the Δ GrVSV- Δ CCHFV-GPC pseudotype with percent inhibition of wild-type VSV subtracted. All compounds were run in biological duplicates and the assay was run in triplicate. An arbitrary cutoff of 50% inhibition was designated by a dashed line.

EVALUATING SELECTED COMPOUNDS ON WILD-TYPE CRIMEAN-CONGO HEMORRHAGIC FEVER VIRUS

Of the 400 compounds screened by the Δ GrVSV- Δ CCHFV-GPC pseudotype, 88 demonstrated at least 20% inhibition of the pseudotype in the developed assay. In order to improve the specificities of the drug screen to the encoded CCHFV-GPC, rather than the VSV backbone, wild-type VSV was also tested against the 88 compounds. This narrowed down the 88 compounds to eighteen compounds as detailed in Table 5.

Table 5: Details of selected inhibitory Pathogen Box compounds on Δ GrVSV- Δ CCHFV-GPC pseudotype

Position	Compound ID	Disease Set	Trivial Name	Molecular Formula
A-F05	MMV202553	KINETOPLASTIDS		C15H15N3O2
A-F09	MMV676406	TUBERCULOSIS		C26H29N5O2S
A-G06	MMV063404	TUBERCULOSIS		C19H24N3OCI
B-B02	MMV012074	TUBERCULOSIS		C16H14N3OCI
B-B05	MMV687776	LYMPHATIC FILARIASIS		C28H23N2O4BCl2F4
B-C06	MMV001493	ONCHOCERCIASIS	Isradipine	C19H21N3O5
B-G09	MMV006741	MALARIA		C22H26N4O2
B-H08	MMV006901	MALARIA		C18H18N4O
C-F11	MMV688921	DENGUE		C23H18N3O5CI
C-H02	MMV675969	ONCHOCERCIASIS		C21H28N2O2
D-A09	MMV688362	KINETOPLASTIDS		C21H20N4O2
D-C08	MMV688467	KINETOPLASTIDS		C22H26N4O2S
D-E10	MMV688271	KINETOPLASTIDS		C18H16N6OCl2
D-G10	MMV676182	CRYPTOSPORIDIOSIS		C22H24N6
D-H08	MMV023388	MALARIA		C21H18N3OF3
E-A06	MMV688775	REFERENCE COMPOUNDS	Rifampicin	C43H58N4O12
E-C05	MMV676599	CRYPTOSPORIDIOSIS		C20H21N5
E-D10	MMV687700	TUBERCULOSIS		C17H18N6O8S

Pathogen Box compound IDs, molecular formulas, reference names (if available), and pathogens each compound targets, as provided by <https://www.pathogenbox.org/about-pathogen-box/composition>. Bolded compounds were identified as those with the highest percent inhibition on the Δ GrVSV- Δ CCHFV-GPC pseudotype.

Multiple attempts were made to examine wild-type CCHFV in a similar screen method relying on infecting human liver cells and observing cytopathic effect/cell monolayer destruction. I was unable to reproduce the same type of read out with wild-type CCHFV, as CCHFV did not induce cytopathic effects at low MOI on the liver cells. Instead, a recombinant CCHFV expressing a ZsGreen tag (rCCHFV-ZsG) was optimized with the assay controls, ribavirin and chloroquine, and mean fluorescence intensity was calculated using 488nm absorbance. This new method, rather than relying on cell death, relied on inhibiting CCHFV viral spread within infected monolayers. Using this experimental design, the eighteen compounds were evaluated using rCCHFV-ZsG over a 72-hour time course (Figure 28).

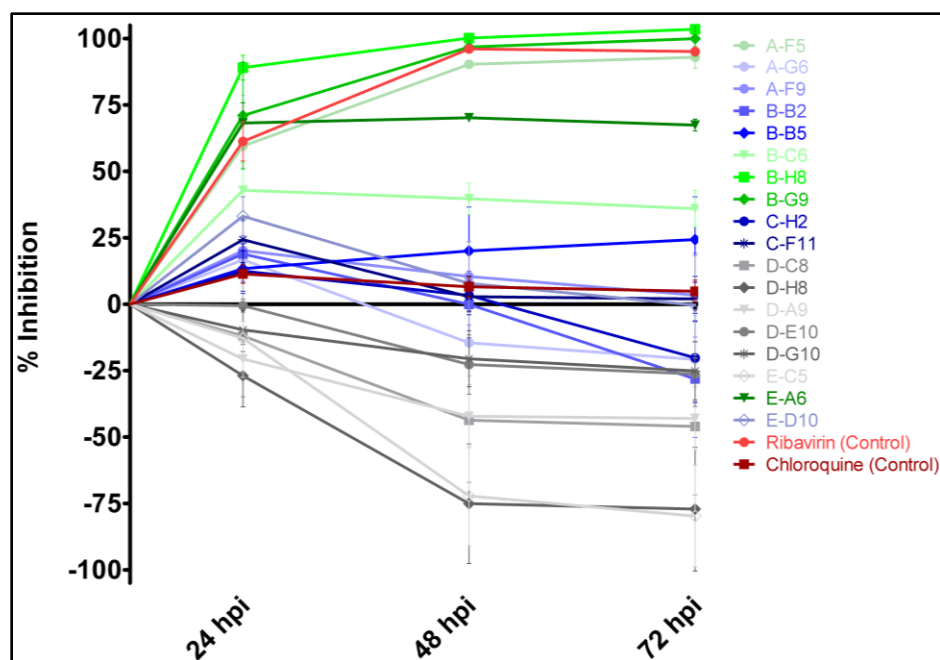


Figure 28: Time course experiment using selected inhibitory Pathogen Box compounds from Δ GrVSV- Δ CCHFV-GPC pseudotype screening

Percent inhibition of mean fluorescence intensity of treatment wells compared to infected only well (0%). Compounds were stratified based on their percent inhibitions with shades of green being the highest in inhibition of CCHFV spread, shades of blue being elevated inhibition, shades of grey showing either minimal

inhibitory effects or enhanced viral spread. Controls (ribavirin at 100 μ M and chloroquine at 10 μ M) were shown in red.

Overall, five compounds (B-H8, B-G9, A-F5, E-A6, and B-C6) demonstrated between 40% and 100% inhibition of CCHFV spread via mean fluorescence intensities (Figure 28). These five compounds had similar inhibitions compared to 100 μ M of the control ribavirin, which has shown potent *in vitro* inhibition of CCHFV. The 72-hour time point from Figure 28 was selected for further comparison to the screening results from wild-type VSV and Δ GrVSV- Δ CCHFV-GPC pseudotype (Figure 29).

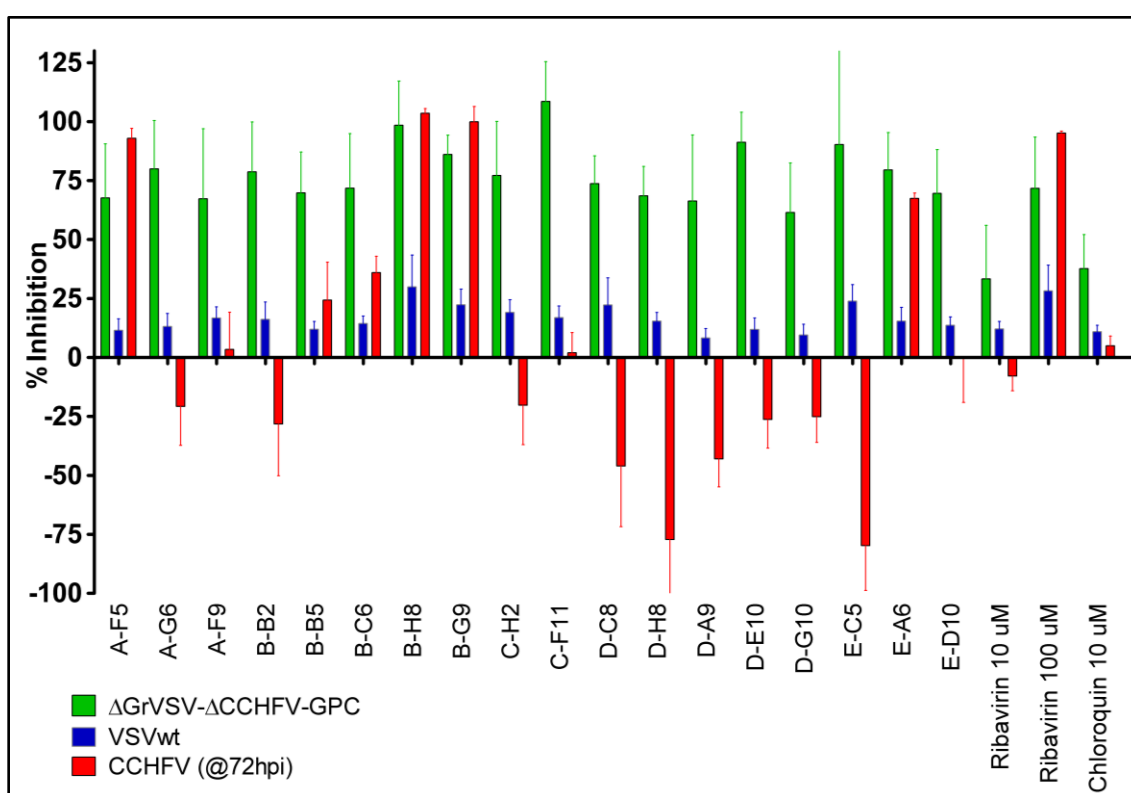


Figure 29: Comparison of wild-type VSV, Δ GrVSV- Δ CCHFV-GPC pseudotype, and wild-type CCHFV on selected inhibitory Pathogen Box compounds

Percent inhibitions comparisons of the eighteen selected compounds on wild-type VSV, Δ GrVSV- Δ CCHFV-GPC pseudotype, and on the labeled wild-type CCHFV (rCCHFV-ZsG) at 72 hours post infection.

Three compounds that had a high degree of inhibition on the Δ GrVSV- Δ CCHFV-GPC pseudotype also had potent inhibition on CCHFV (A-F5, B-H8, B-G9). Though many of the Pathogen Box compounds are proprietary and therefore encoded as to exact drug names, their molecular formulas are provided by MMV (listed in Table 5). These

three most inhibitory compounds to CCHFV were A-F5 a proprietary compound raised against kinetoplastids and B-H8 and B-G9 proprietary compounds against malaria. The Pathogen Box screen demonstrated several other promising candidates such as B-C6 and E-A6. B-C6 is the FDA approved drug called Dynacirc (Isradipine), a dihydropyridine calcium channel blocker used to treat high blood pressure ¹⁹³. E-A6 is another promising drug candidate identified in this assay was the widely used tuberculocidal, rifampicin. Rifampicin, a guanosine-analogue which has been approved as an FDA approved drug since 1971, is available at a reduced cost in developing countries as it has been declared an ‘essential medicine’ by the WHO ¹⁷. This drug has been demonstrated to have antiviral properties in poxviruses and is being evaluated as a potential therapeutic for vaccinia virus infections ¹⁹⁴.

Overall, the Δ GrVSV- Δ CCHFV-GPC pseudotype served once again as a useful tool to in drug discovery. The pseudotype was used, in tandem with wild-type VSV, to screen over 400 compounds of FDA approved drugs or drug-analogues. This screen led to the identification of five compounds which successfully inhibited CCHFV, two of which are already prescribed by physicians to treat the neglected tropical diseases tuberculosis and onchocerciasis. Future studies are warranted to examine inhibitory concentrations and potentially *in vivo* studies to determine if these compounds can impart benefit in a CCHFV animal model.

CHAPTER 7: Experimental Vaccine Development for Crimean-Congo

Hemorrhagic Fever Virus ⁵

CURRENT APPROACHES IN EXPERIMENTAL VACCINE DEVELOPMENT FOR CRIMEAN-CONGO HEMORRHAGIC FEVER VIRUS

Developed Experimental Vaccines

Currently, there are several experimental vaccine candidates that have relied on the GPC as an antigenic component, which have been evaluated in immunocompromised signal transducer and activator of transcription 1 knock-out (STAT-1-/-), interferon α/β receptor knock-out (IFNAR), or interferon receptor antibody transiently suppressed (IS) mouse models for CCHFV, as they recapitulate clinical illness and are uniformly lethal models for CCHF ^{152,195–197}. Vaccine candidate approaches have focused on either DNA expression of CCHFV antigens in host tissues, replication deficient viral-like particles, inactivated whole virus preparations, subunit antigen preparations, or vectored vaccinia virus vaccines ^{121,152,195,198–201}. Two of these preparations, a prime and boost strategy using modified recombinant Vaccinia virus (strain: Ankara) [MVA] encoding the GPC, and a prime, boost, and boost strategy with a DNA based vaccine encoding separate NP, G_N, and G_C antigens, have provided promising results with up to 100% protection in the IFNAR animal model ^{121,200}. Although published NP studies suggest this antigen alone in the MVA platform has failed to provide protection ²⁰². Recently published data, however, suggests that an Adenovirus system expressing CCHFV NP can also provide protection ²⁰³. Published and unpublished data on CCHFV experimental vaccines is outlined below in Table 6.

⁵ This chapter is written as a manuscript and *in prep.* for *Scientific Reports* as the following: Rodriguez S.E*, Cross R.W.*, Fenton K.A., Bente D.A., Mire C.E., and Geisbert T.W. (*est.* 2018) Single injection pseudotyped vesicular stomatitis virus provides 100% protection to Crimean Congo hemorrhagic fever (*Co-first author)

Table 6: Published and unpublished CCHFV experimental vaccines and animal models

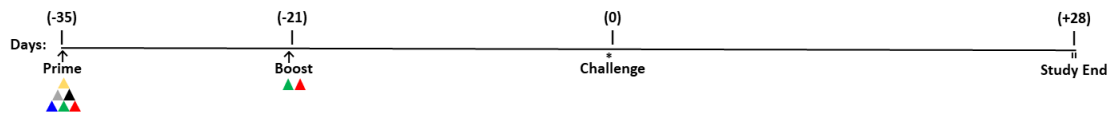
Type	Antigen (Strain)	Additives	Adjuvants	Prime	Boosts	Challenge (Isolate)	Protection	Model	References
Inactivated	Whole virus (V42/81)	Mouse brain derivatives, chloroform, thiomersal	Aluminum hydroxide	2 doses, S.C.	≥2x	-	-	Human	Rousseau-Lacoste et al., 2012; Ghase et al., 2011
	Whole virus (Turkey-Kelkit06)	Monkey kidney cell culture derivatives, formalin	Aluminum hydroxide	1 dose, I.P.	2x	1,000 pfu (Turkey-Kelkit06)	80%	IFNAR Mice	Caneroglu et al., 2015
Live Attenuated	rCCHFVΔMucin (lbAr0200)	Human adrenocarcinoma cell culture derivatives	-	1 dose, I.P.	0	100 pfu (lbAr10200)	100%	STAT-1 K/O Mice	Bente and Borgeau, Unpublished
Virus-like Particle (VLP)	NP+GPC (lbAr10200)	Human liver cell culture derivatives	-	1 dose, I.P.	2x	440 ffu (lbAr10200)	40%	IFNAR Mice	Hissulali et al., 2017
Subunit	Gn, Gc, Gc-ΔTail (lbAr10200)	Baculovirus and fruit-fly cell culture derivatives	Sigma Adjuvant System	2 doses, I.P.	1x	100 pfu (lbAr10200)	0%	STAT-1 K/O Mice	Kurtulbas et al., 2015
	GPC (Iran-53)	Transgenic tobacco leaf and hairy root pellet derivatives	-	4 doses, P.O.	1x	-	-	BALB/c Mice	Ghase et al., 2011
	Gn (Iran-53)	Amy-worm cell culture derivatives	Freund's complete adjuvant	1 dose, S.C.	2x	-	-	BALB/c Mice	Ratnayake et al., 2017
	NP (lbAr10200)	???	-	1 dose, I.P.	0	100 pfu (lbAr10200)	0%	STAT-1 K/O Mice	Bente and Turk, Unpublished
Vectored	GPC (lbAr10200)	Modified Vaccinia virus and hamster kidney cell culture derivatives	-	2 doses, I.M.	1x	~140 pfu (lbAr10200)	100%	IFNAR Mice	Bullinger et al., 2014
	NP (lbAr10200)						0%		
	Gn (lbAr10200)	Human adenovirus and human kidney cell culture derivatives	-	1 dose, I.M.	0	~35 pfu (lbAr10200)	0%	IFNAR Mice	Zivcec et al., Unpublished
	Gc (lbAr10200)						0%		
	GPC (lbAr10200)						0%		
	NP (lbAr10200)						33%		
	NP+GPC (lbAr10200)				1x, I.N.		78%		
	GPC (lbAr10200)						0%		
	NP (lbAr10200)						78%		
	NP+GPC (lbAr10200)						100%		
	GPC (lbAr10200)	Vesicular stomatitis virus and hamster kidney cell culture derivatives	-	2 doses, I.P.	1x	100 pfu (lbAr10200)	40%	STAT-1 K/O Mice	Rodriguez et al., Unpublished
	GPC (lbAr10200)				0	50 pfu (Turkey2004)	100%		
Plasmid Based	UTR+GPC (lbAr10200)	2um gold beads	-	4 doses, I.D.	2x	-	-	BALB/c Mice	Saï et al., 2006
	GPC (lbAr10200)	25 ug DNA in saline	-	1 dose, I.M.	2x	100 pfu (lbAr10200)	71%	IFNAR Mice	Garrison et al., 2017
	NP, Gn, Gc (lbAr10200)	150 ug DNA	-	1 dose, I.D.	2x	400 ffu (lbAr10200)	100%	IFNAR Mice	Hissulali et al., 2017
Heterologous Blend (Plasmid + VLP)	NP, Gn, Gc, GPC (lbAr10200)	150 ug DNA + Human liver cell culture derivatives	-	1 dose, I.D.	2x, I.P.	400 ffu (lbAr10200)	80%	IFNAR Mice	Hissulali et al., 2017

A review of published and unpublished CCHFV experimental vaccines and animal models. The table details the type, antigen, any additives/adjuvants, and the dosing regimen in the specific CCHFV animal models.

EVALUATING PSEUDOTYPED RECOMBINANT VESICULAR STOMATITIS VIRUSES AS EXPERIMENTAL VACCINES FOR CRIMEAN-CONGO HEMORRHAGIC FEVER VIRUS

With the data supporting that the replication-deficient construct expressed CCHFV-GP *in vitro* and the replication-competent construct additionally expressed CCHFV-G_C on the surface of the virion, an *in vivo* study was designed to test the ability of either construct to function as an experimental vaccine. The STAT-1^{-/-} mouse model for CCHFV was selected to test these constructs for safety and protective efficacy. A pilot study was designed to test a range of conditions, doses, and boosting response (Illustration 14) as it was unclear whether the rVSV expressing CCHFV-GPC would be tolerated in the STAT-1^{-/-} model. Similar rVSV vectors encoding Ebola and Marburg hemorrhagic fever virus

GP, have resulted in lethal outcomes following vaccination of STAT-1^{-/-} mice ²⁰⁴. Three groups of five mice were vaccinated with a prime dose of 10⁶ pfu of the replication deficient VSV-G*-ΔGrVSV-CCHFV-GPC construct. One of these groups was boosted at two weeks post prime with a 10⁶ pfu of the replication competent ΔGrVSV-ΔCCHFV-GPC. To avoid a limiting anamnestic response in the boosted replication deficient vaccinations, a VSV complemented with a different serogroup VSV-G (Indiana and New Jersey) between prime and boosting was also used, as previous studies have suggested immune responses can vary between serogroup VSV-G ²⁰⁵. This group was boosted with a 10⁶ pfu dose of VSV-GNJ*-ΔGrVSV-CCHFV-GPC, where the *in trans* complemented VSV-G on the boosting was from the New Jersey VSV serogroup in comparison to prime (prime: Indiana, boost: New Jersey). Two additional groups were primed with the replication competent construct at a ‘low’ (10² pfu) and ‘high’ (10⁶ pfu) dose of ΔGrVSV-ΔCCHFV-GPC. A final group of five STAT-1^{-/-} mice in the pilot experiment was administered PBS for mock control purposes.



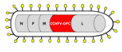

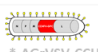
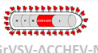
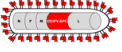
Animal	Groups (n=5)	Prime	Prime Dose (i.p.)	Boost	Boost Dose (i.p.)	Challenge	Challenge Dose (i.p.)
STAT-1 K/O Mice	▲ 1	 VSV-G _(Ind) *-ΔGrVSV-CCHFV-M (Replication Deficient)	10 ⁶ pfu/500uL	—	—	 CCHFV Strain: IbAr10200	10 ² pfu/500uL
	▲ 2			 VSV-G _(Ind) *-ΔGrVSV-CCHFV-M (Replication Deficient)	10 ⁶ pfu/500uL		
	▲ 3			 ΔGrVSV-ΔCCHFV-M (Replication Competent)	10 ⁶ pfu/500uL		
	▲ 4	 ΔGrVSV-ΔCCHFV-M (Replication Competent)	10 ⁶ pfu/500uL	—	—		
	▲ 5		10 ² pfu/500uL	—	—		
	▲ 6	PBS	—	—	—		

Illustration 14: Pilot *in vivo* CCHFV experimental vaccine study

Experimental conditions including animal type, number, group, prime/boost/challenge conditions, routes, dose amounts, and schedule. Flow chart showing vaccination (triangles), sampling days (arrows), and day of challenge (*).

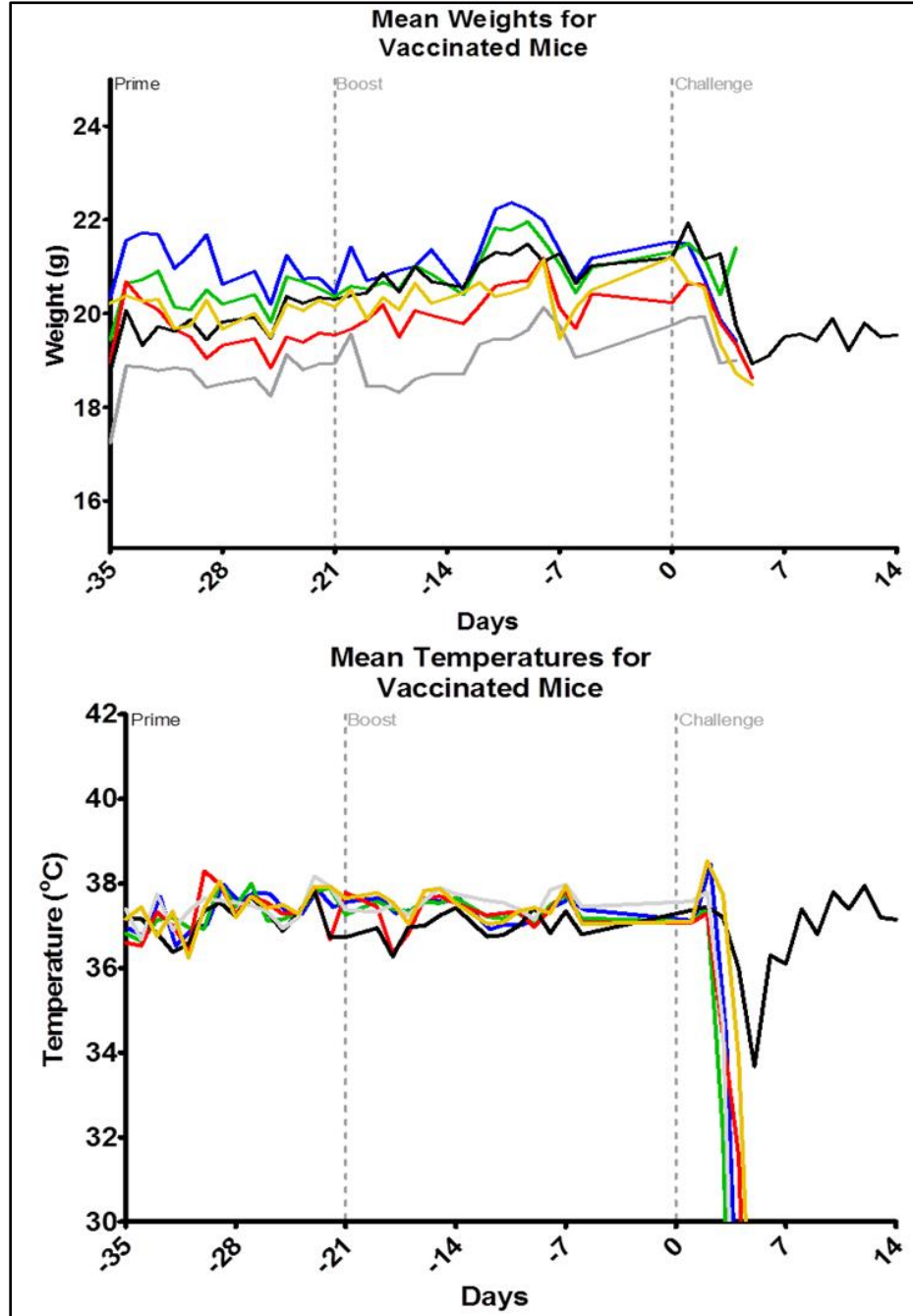


Figure 30: Mean weights and temperatures from pilot study mice

Top panel: Averaged weights from all groups collected each day for 35 days pre-challenge and 28 days post challenge total. Bottom panel: Averaged temperatures from all groups collected each day for 35 days

pre-challenge and 28 days post challenge total. Group is indicated by color which corresponds to the colored triangles outlined in Illustration 14.

Mice were observed daily for 35 days for clinical signs, body weights, and temperatures. All mice survived vaccination of prime and boost regimens, with no attributed fever, and approximately 5% weight loss observed in three of the five mice in the 10^6 pfu replication competent group across two days (Figure 30).

All mice were challenged with 100 pfu of CCHFV strain IbAr10200 at 35 days post prime and monitored for weight and temperatures. Time-to-death for the animals occurred between 3-5 days post challenge for all groups. The 10^6 pfu high dose of replication competent Δ GrVSV- Δ CCHFV-GPC had 40% observed survival while all other groups succumbed to CCHF (Figure 31).

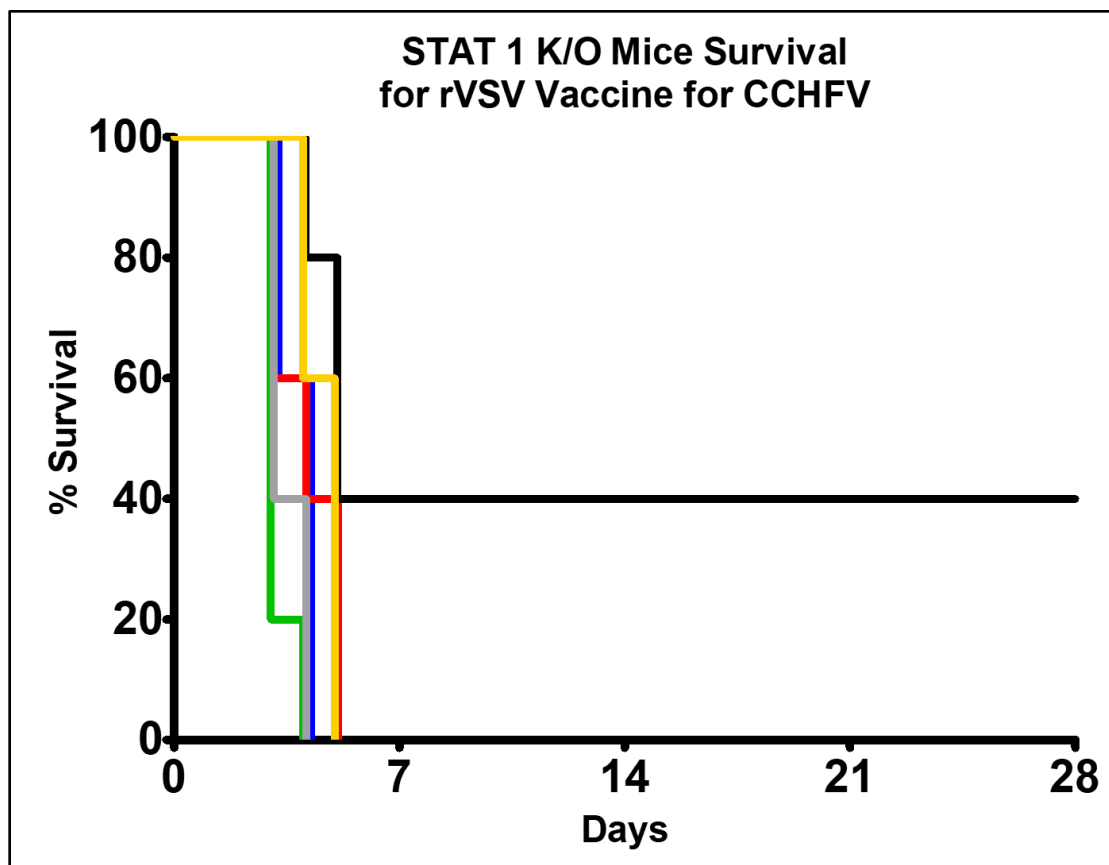


Figure 31: Pilot study mice survival following CCHFV challenge

Kaplan-Meier survival curve of challenged animal groups. Group is indicated by color which corresponds to the colored triangles outlined in Illustration 14.

Another experiment was designed to increase the prime only dose and incorporate a boost of only the replication competent virus (Illustration 15), as this was the sole construct to offer protection (40%) against the lethal challenge outlined from the first *in vivo* experiment shown in Figures 30 and 31. For the *in vivo* experiment outlined in Illustration 15, we challenged with a clinical strain, Turkey200406546, designated throughout this work as Turkey2004; which has previously been published in GenBank with the accession numbers KY362517 (S-segment), KY362519 (M-segment), and KY362515 (L-segment) (45). We conducted NGS on our Turkey2004 isolate and found the genomes were highly similar to what had been published by Spengler et al ²⁰⁶. Our deep sequencing revealed four nonsynonymous mutations compared to published sequences (S-segment: R68A, M-segment: R709A and A4039G, L-segment: A2804G). As the rVSV constructs were designed from a codon optimized GPC from the IbAr10200 strain, we examined the GPC genomic alignments between the vaccination strain and challenge strain to assess the residue conservation among antigenic regions of the GPC between the IbAr10200 and Turkey2004 isolate.

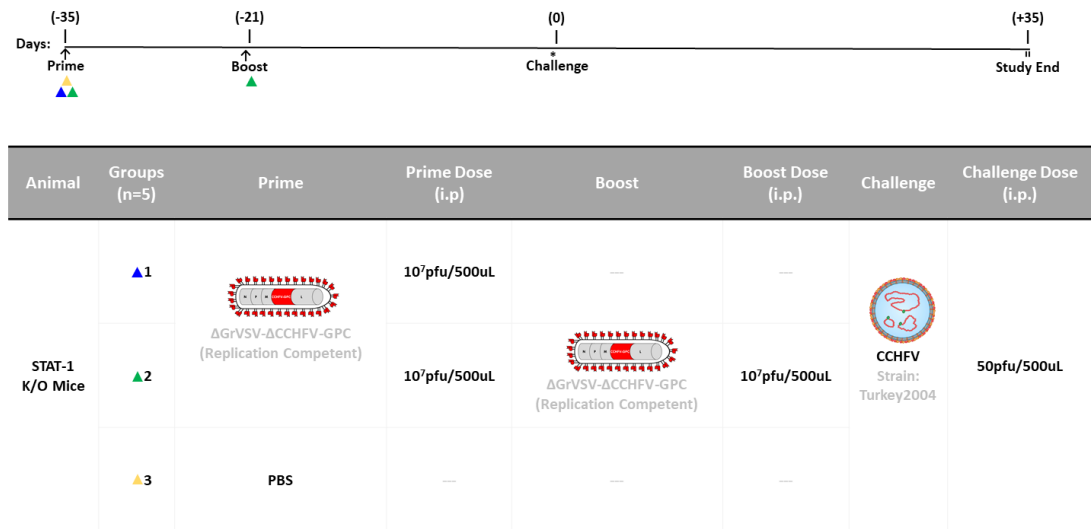


Illustration 15: Follow up *in vivo* CCHFV experimental vaccine study

Experimental conditions including animal type, number, group, prime/boost/challenge conditions, routes, dose amounts, and schedule. Flow chart showing vaccination (triangles), sampling days (arrows), and day of challenge (*).

Genomic alignments of all published (and complete) CCHFV-GPCs demonstrate 44.0% amino acid identity observed between all strains GPCs (Table 3, Illustration 16A). Despite Turkey2004 and IbAr10200 being from separate M-segment clades, clade V and III respectively, the genomic alignment demonstrates 84.4% identify between the GPCs of Turkey2004 and IbAr10200 (Illustration 16B). Much of this variability is attributed to the non-structural components of the GP. Further analysis revealed that the antigenic regions to be examined for countermeasure developments are largely the ectodomains of the structural G_N and G_C regions. These regions alone are conserved between the two isolates with 91.8% and 95.2% identity, respectively (Table 3, Illustration 16A).

conservation). (A) The similarities map of all published (and complete) CCHFV strains, GPC. (B) The similarities map of the CCHFV-GPC from strains IbAr10200 and Turkey2004.

Informed by the genetic alignment and conserved residue data between strains, we proceeded to vaccinate two groups of five STAT-1^{-/-} mice with the replication competent Δ GrVSV- Δ CCHFV-GPC construct at an increased dose of 10^7 pfu and boosted one of these groups with the same construct and dose at 14 days post prime (Illustration 15). As a control, we again used PBS as a mock vaccination. A single mouse succumbed in the boosted group (leaving only four mice to be challenged in the boosted group) on the day of boosting. At 35 days post prime, all mice were challenged with 50 pfu of CCHFV strain Turkey2004 and were monitored for clinical signs, weights, and temperatures.

For this CCHFV strain, the observed mean survival time was between five- and six-days post infection (dpi), as demonstrated with the PBS control group (Figure 32A). For both prime and boosted groups, 100% protection was observed out to 35 dpi (Figure 32A). The prime and PBS group displayed weight loss, while the boosted group did not (Figure 32B). All three groups displayed elevated temperatures for the first three days post challenge (Figure 32C). Additionally, the prime group did have two mice that scored 'rough' on days 5 and 6 post challenge (Figure 32D). These results indicate that the primed group displayed a marked illness, while the boosted group displayed a milder form of illness post-challenge.

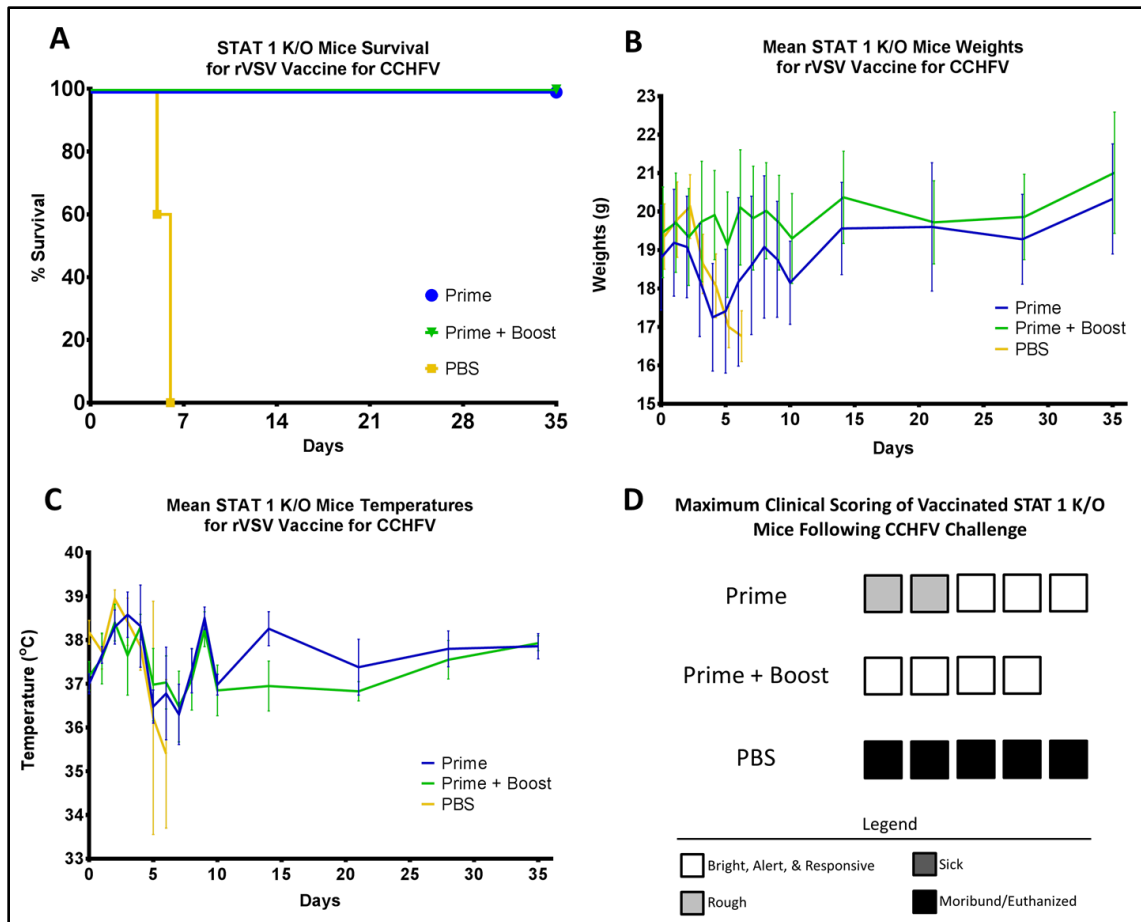


Figure 32: Follow up *in vivo* CCHFV experimental vaccine study data: animal survival, average weights, average temperatures, and maximum clinical scoring

(A) Kaplan-Meier survival curve of challenged animal groups. Group is indicated by color which corresponds to the colored triangles outlined in Figure 4. (B) Averaged weights with error bars from all groups collected each day for 14 days post challenge and every 7 days after that for 35 days post challenge total. (C) Averaged temperature with error bars from all groups collected each day for 14 days post challenge and every 7 days after that for 35 days post challenge total. (D) The highest clinical scoring assigned to the mice is reported via colored boxes. White boxes indicate no clinical scoring (i.e., bright, alert, and responsive). Light grey boxes indicate mild illness with roughed appearance. Dark grey boxes indicate moderate to severe illness. Black boxes indicate moribund animals which were humanely euthanized per study protocols. The boosted group only had four animals due to a single animal succumbing for unknown reasons during the day of boosting.

To examine the humoral response in mice, all groups were bled at study end points and sera were analyzed on an IgG ELISA for CCHFV-GPC. Circulating IgG to CCHFV-GP were detected in sera of both vaccinated groups (Figure 33A). A reciprocal dilution titer was reported for all tested sera to account for IgG response to VSV antigens. Curiously, the prime group displayed higher CCHFV-GPC titers compared to the prime

plus boosted group (Figure 33A). This indicates the prime only group had a higher concentration of IgG at the study endpoint which recognized CCHFV-GPC, compared to the boosted group. The PBS group had negligible IgG responses to CCHFV-GPC (Figure 33A). To determine the neutralizing capacity of these sera, a plaque reduction neutralization test (PRNT) was carried out using the Turkey2004 challenge isolate. As depicted in Figure 33B, the prime only group had neutralizing antibody titers with a PRNT80 of <160 and the boosted group a PRNT80 of <80 at the study endpoint (Figure 33B). The PRNT positive control, hyper-immune mouse ascitic fluid (HMAF) raised against CCHFV exposed mice, showed a PRNT80 of <80 while the PBS control mice did not demonstrate a PRNT80 value (Figure 33B).

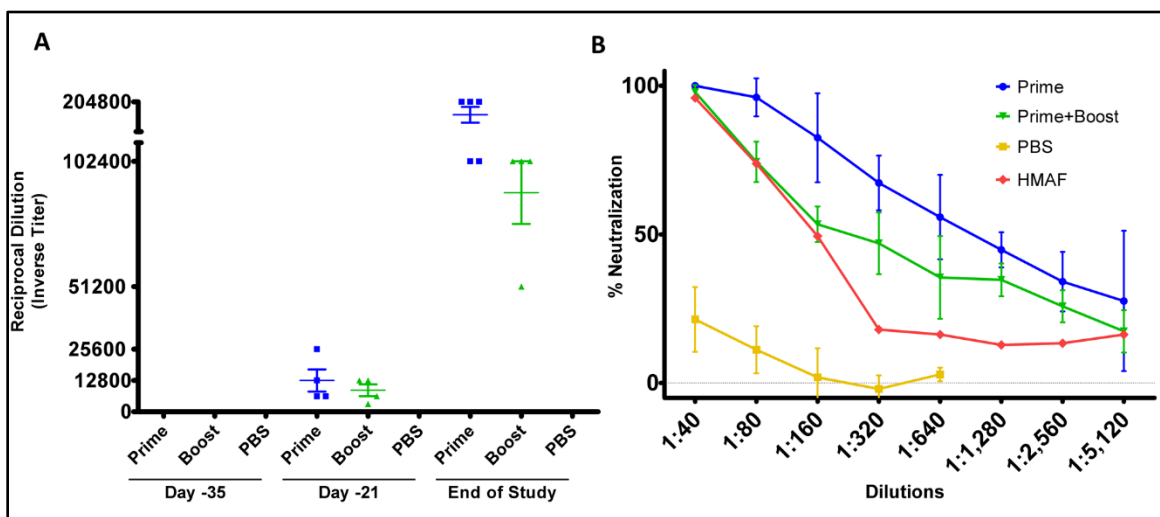


Figure 33: Follow up *in vivo* CCHFV experimental vaccine study humoral immune responses

Study endpoint mouse sera collected from second *in vivo* experiment outlined in Illustration 15. Mice sera were run in duplicate with each group indicating four separate animal sera tested for humoral responses. (A) Enzyme linked immunosorbent assay (ELISA) using plates coated with 1 μ g of purified rVSV-GFP and Δ GrVSV-CCHFV-GPC antigens. Adjusted OD values were calculated by subtracting VSV antigens (from rVSV-GFP coated ELISA plates) from Δ GrVSV-CCHFV-GPC coated ELISA plates. (B) Plaque reduction neutralization test (PRNT) from diluted endpoint sera with CCHFV (Strain: Turkey2004) incubated on SW-13-CDC cells. Hyper-immune mouse ascitic fluid (HMAF) was used as a positive control.

At study endpoints for each cohort, we examined tissues by immunohistochemistry (IHC) for CCHFV-NP antigen. The control cohort had marked CCHFV-NP immunolabeling in hepatocytes within the liver sections (Figure 34A) while liver sections

from the prime only and boosted cohorts had no observable CCHFV-NP immunolabeling (Figure 34A and B). We further examined the spleen tissue sections and observed that the control cohort had marked CCHFV immunolabeling in mononuclear cells (Figure 34D), and that the prime cohort had a cytoplasmic, mild, and diffuse immunolabeling of mononuclear cells primarily in the red pulp (Figure 34E). The boosted cohort had no specific CCHFV immunolabeling within the spleen sections (Figure 34F).

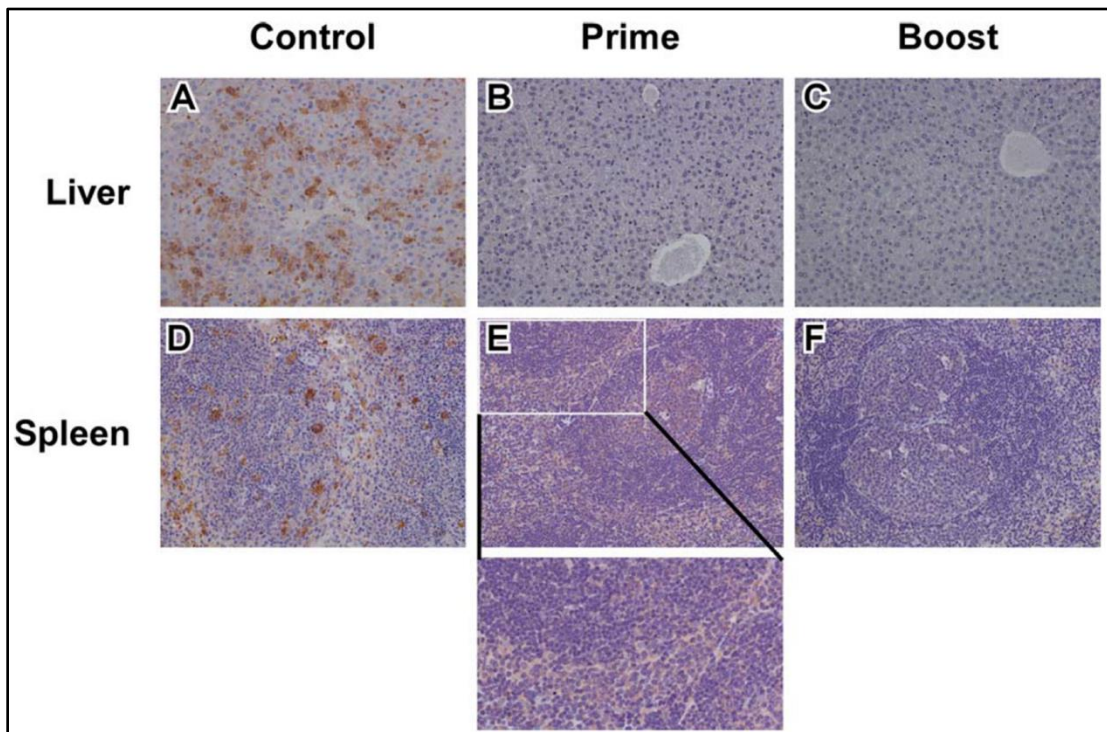


Figure 34: Immunohistochemistry of murine tissues

Representative study endpoint liver tissue sections for the control (A), prime (B), and boost (C) cohorts with observable marked CCHFV immunolabeling of hepatocytes in the control group (A) and no observable labeling in the prime (B) or boost (C) cohorts. Representative study endpoint spleen tissue sections for the control (D), prime (E), and boost (F) cohorts with observable marked CCHFV immunolabeling in mononuclear cells (D), cytoplasmic, mild, and diffuse immunolabeling of mononuclear cells primarily in the red pulp (E, inset), and no specific CCHFV immunolabeling in the boost cohort (F).

When exploring the use of rVSV expressing CCHFV-GP as potential vaccines, there was a concern of murine virulence, which has been observed for wild-type VSV^{207,208}. Studies with rVSV expressing hemorrhagic fever virus GP have also demonstrated lethal outcomes in the STAT-1^{-/-} model²⁰⁴. This has hampered the STAT-1^{-/-} animal

platform from serving as a vaccine development tool, as ‘vaccinated’ mice succumb to a prime dosing ²⁰⁴. Because of this information, in our studies (Illustration 14) we tested three doses at 10^7 , 10^6 and 10^2 pfu, for the replication competent Δ GrVSV- Δ CCHFV-GPC construct and selected a traditional 10^6 pfu dose for our replication deficient VSV-G*- Δ GrVSV-CCHFV-GPC construct. Demonstrating the safety profile of both constructs, no group had any attributed fatality due to the vaccines.

In the pilot studies (Illustration 14) the time-to-death for challenged mice, ranged between 3-5 dpi (Figure 30). It was hypothesized that time-to-death was occurring too rapidly in the model due to the challenge virus, CCHFV isolate IbAr10200, and may be overwhelming the immune response too quickly. The IbAr10200 strain has been widely used as the prototype strain for CCHFV research, despite it being passaged substantially in mice and without any record of human disease. The IbAr10200 strain used in this study has a documented history of thirteen passages in suckling mice, plus several passages in Vero and SW-13-CDC cell cultures. These passages, specifically in suckling mice, may have induced murine adaptation and enhanced virulence in the STAT-1-/- model. The history behind the IbAr10200 strain also reveals that this strain was isolated from a tick which had engorged on a camel and has no associated human clinical disease attributed ²⁰⁹. As there is ongoing debate in the field about the pathogenicity among circulating CCHFV strains ^{7,210-212}, a human/clinical isolate with lower passage history may be more pertinent at evaluating medical countermeasures. Additionally, our unpublished studies have shown that certain CCHFV isolates, particularly isolates from human/clinical cases, have a delayed time-to-death in the STAT-1-/- murine model, compared to the prototype CCHFV isolate IbAr10200. To delay time-to-death in our model, we decreased the challenge dose and changed the CCHFV challenge strain to a human clinical disease isolate. Based on CCHFV isolate availability, we selected an isolate with a much lower passage history, clinical relevance (*i.e.*, documented history of disease in humans), and one that has a prolonged time-to-death in the STAT-1-/- mouse model, relative to the IbAr10200 isolate.

The Turkey2004 strain has a lower passage history of four passages in Vero cells and one in SW-13-CDC cells with no passaging in murine tissues and has only four nucleotide changes in the genome when compared to the Genbank published Turkey 2004 isolate²⁰⁶. Despite the geographic and phylogenetic clade differences between Turkey2004 and IbAr10200, we hypothesized that there is residue conservation in the GPC in general, but a high degree of residue conservation among the antigenically important regions of the G_N and G_C. As our genomic analysis demonstrates, the GPC contains approximately 84% amino acid variability between the IbAr10200 and Turkey2004 strains. However, the variability of the structural G_N and G_C proteins is more conserved (>90%) and thus have lower residue variability. Altering the strain with a less passaged and human/clinical isolate, prolonged the time-to-death window to up to 7 days. This challenge strain switch and increasing the prime dosing improved the initial 40% protection to 100% protection in vaccinated mice. It is curious to speculate that if structural components of the CCHFV-GPC are preferred antigens for CCHFV vaccine design, than a multiple clade vaccine approach might be feasible for cross protection between circulating strains and across geographic areas. The construct expressed a notable and useable form of CCHFV-G_C, and elicited a protective response against two strains, additional countermeasure studies regarding this structural GP should also be explored.

ELISA and PRNT experiments on study endpoint sera, demonstrate a humoral IgG response to CCHFV-GPC with observed neutralizing antibodies produced from the prime group that received a high (10^7 pfu) dose of Δ GrVSV- Δ CCHFV-GPC. Curiously, the boosted (10^7 pfu) group had lower detectable antibodies to the CCHFV-GPC with lower neutralization titers. Clinical data for these groups following CCHFV challenge show that the prime only group had elevated temperatures and weight loss, indicating illness from the CCHFV challenge. While the boosted group did display elevated temperatures, there was neither substantial weight loss detected nor clinical scoring. Further analysis of tissues at study end point for these cohorts, also revealed that while there was no immunolabeling

in the liver of the vaccinated animals the prime cohort had diffuse cytoplasmic immunolabeling of mononuclear cells in the spleen sections, suggesting, along with the clinical scores, that there was more replication of CCHFV in this group compared to the boosted group. This could potentially lead to the higher anti-CCHFV-GPC IgG titers in the prime cohort at the study endpoint as the CCHFV challenge may have “boosted” these levels when compared to the boost cohort. Regardless, protection was achieved by both regimens, though the boosted group data supports the notion that at study endpoint, the observed IgG titers against CCHFV-GPC along with lower neutralizing titers (PRNT₈₀ of <160) are sufficient in combating lethal CCHFV infection in the STAT-1^{-/-} mouse model.

Correlates of protection against CCHF have been difficult to define due to the multiple vaccine and delivery platforms examined to date, along with the lack of an immunocompetent animal model ¹⁹⁵. Several CCHFV experimental vaccines studies have identified cell-mediated and humoral involvement, with some instances of neutralizing antibody production ^{121,152,198,201,213}. In looking at what is known for human CCHF, survivors mount a humoral response whereas those who succumb, typically lack an IgG response ⁷. Other studies have examined antibody and neutralizing responses from the various vaccine platforms. DNA vaccines following a three round vaccination regimen have induced detectable antibodies with neutralizing capacity observed up to 1:160 in PRNT dilutions and achieved 100% protection, depending on the antigens encoded on the DNA plasmids ^{121,213}. A cell culture based inactivated virus vaccine achieved high IgG titers (1:102,400) and a high neutralizing response of 1:1,024, however, this also required three vaccination rounds, an alum adjuvant, and conferred 80% protection against the clinical isolate Turkey-Kelkit06 in IFNAR mice ¹⁹⁸. Antibody titers, neutralization capacity, and challenge virus presented here were similar, though through the VSV platform, we achieved greater protection with a single dose. These studies, along with the current study, suggest other facets of the immune system are likely involved in conferring complete protection.

A limitation of our study is that T cell responses were not evaluated and could be contributory as other groups have shown ^{121,200,202}. Future studies serially examining the antibody and T cell repertoire after prime and boosting doses following Δ GrVSV- Δ CCHFV-GPC, but before CCHFV challenge, would be informative for the STAT-1-/- mouse model. Ideally, an immunocompetent, larger animal model is much needed in the CCHF field to further test the array of CCHFV experimental vaccines which have shown promise in these mouse models. A promising step forward appears to be the non-human primate (NHP) disease model that has been recently developed ²¹⁴. However, CCHF diseases in this model appear dependent on limited strain and challenge route.

In conclusion, this study offers not only a tool to study the biology of CCHFV as it relates to structural G_C, but also serves to develop and characterize a replication-competent pseudotype, in relation to CCHF vaccine development. The replication-competent construct provides up to 100% protection with an observed humoral response, with a single-injection from a human isolate challenge strain. This information is valuable in designing future studies in CCHFV animal models and establishes characterized tools to examine the biology of structural CCHFV-G_C in a pseudotyped rVSV system.

CHAPTER 8: Methodology⁶

CELL CULTURE, CHALLENGE VIRUS, AND ANTIBODIES

Baby hamster kidney cells (BHK) (kindly provided by M. Whitt, University of Tennessee Health Science Center, Memphis, TN), African green monkey kidney E6 clone cells (Vero E6) (American Type Culture Collection [ATCC], Manassas, VA), a clone from the SW-13 human adrenocortical carcinoma cell line (SW-13-CDC) (kindly provided by É. Bergeron of Centers for Disease Control and Prevention, Atlanta, GA), and human hepatocarcinoma cells (HuH-7, obtained from Fischer Scientific, Waltham, MA) were maintained in Dulbecco's modified Eagle's medium (DMEM) supplemented with 10% fetal bovine serum (FBS; Invitrogen, Carlsbad, CA), 2mM L-glutamine (Invitrogen), and 1% penicillin-streptomycin (P/S; Invitrogen), cumulatively called D10. CCHFV challenge stocks, strains IbAr10200 and Turkey-200406546 [referred as Turkey2004, throughout] (kindly provided by T. Ksiazek, UTMB – World Reference Center for Emerging Viruses and Arboviruses, Galveston, TX), were propagated in Vero E6 cells once, plus previous passages in suckling mice and Vero cells since isolation. All *in vitro* and *in vivo* work with CCHFV was performed in a biosafety level 4 (BSL-4) facility at the Galveston National Laboratory, University of Texas Medical Branch, Galveston, Texas, USA. All cell and viral stocks were tested and free of mycoplasma, by PCR kit (IntronBio, Gyungg-Do, South Korea). Monoclonal antibodies (MAb) mouse- α -CCHFV-G_C 11E7 and 8A1, and mouse- α -CCHFV-G_N antibody 13G8 were generated and characterized as described previously^{111,113}. Described antibodies are available at BEI Resources (ATCC) except for 8A1, which was kindly provided by United States Armed Forces Research Institute for Infectious Diseases, Frederick, MD.

⁶ These methods have been previously published or are *in prep.* for publication from the references: Kuhn *et al.*, 2016; Cajimat *et al.*, 2017; Rodriguez *et al.*, 2018a; Rodriguez *et al.*, 2018b (*in prep.*)

GENERATION OF Δ GrVSV-CCHFV-GPC VECTORS

The rVSV vector was cloned and recovered from cDNA as previously described²¹⁵. Briefly, a BlueScript backbone plasmid under T7 polymerase promoter control encoding a Δ G, VSV Indiana backbone expressing a chimeric Zaire ebolavirus (ChEBOV) glycoprotein (GP), was used as the vector (designated pVSV Δ G-ChEBOV-GP-3). This plasmid was modified by cutting out an existing ChEBOV-GP coding sequence via *MluI* and *NheI* restriction sites, yielding a pVSV Δ G vector. An insert, coding for the codon optimized open reading frame of the complete CCHFV glycoprotein precursor (GPC), was digested and ligated into the pVSV Δ G vector. The CCHFV-GPC insert was created by overhang PCR mutagenesis; flanking a 3' *MluI* restriction site plus Kozak sequence, and a 5' *XbaI* restriction site, from a PCR amplified, codon optimized, pCAGG-CCHFV-GPC (kindly provided by J. Kortekaas, Central Veterinary Institute, Lelystad, Netherlands). This ligated and cloned plasmid, designated pVSV Δ G-CCHFV-GPC, was transfected into BHK cells that were also co-transfected with VSV protein N, P, G, and, L 'helper' plasmids under T7 promoter control and driven by infection (MOI 5) with recombinant vaccinia virus expressing T7 polymerase (rVV-TF7-3; kindly provided by M. Whitt). Recovered virus, designated VSV-G*- Δ GrVSV-CCHFV-GPC, was collected 24-48 hr post infection/transfection, filtered twice through a 0.2 μ m filter to remove vaccinia virus, plaque purified onto VSV-G* complemented BHK cells, and stored at -80°C for further use. All plasmid maps and cloning primer sequences are available upon request.

INFECTIONS, ENUMERATION, GROWTH KINETICS, AND PREPARATION OF VIRAL MATERIAL

For infections of replication deficient vector, semi-confluent (~60-80%) monolayers of BHK cells were transfected with 1 μ g/1x10⁶ cells using pCAGG-VSV-G (Indiana). Once

monolayers displayed cell rounding and syncytia, they were infected at a MOI of 0.1 with VSV-G*- Δ GrVSV-CCHFV-GPC. Supernatants were harvested at 24 hrs post infection (hpi) and clarified at 2,000 rpm for 10 min at 4°C. Confluent monolayers of BHK cells were infected with replication competent Δ GrVSV- Δ CCHFV-GPC at MOI 0.1 for 1 hr at 37°C with 5% CO₂ with rocking at 15 min intervals and harvested/clarified at 48 hpi. Plaque assays for viral titrations were carried out in an analogous manner, with an overlay media final concentration of 1.25% Avicel RC-581 (FMC BioPolymer, Philadelphia, PA) in 1X Eagles minimum essentials medium (MEM) with 5% FBS and 1% P/S on BHK cells for 24-48 hpi. After incubations, overlays were aspirated and a 10% buffered formalin fix with a 1X crystal violet stain was incubated onto monolayers for one hr. Plaques were enumerated and plaque forming units (pfu) were determined by averaging technical replicates per sample. Single-cycle growth curves at MOI 0.1 were performed by absorbing rVSV-GFP, Δ GrVSV- Δ CCHFV-GPC, or CCHFV onto duplicate monolayers of BHK cells in six-well plates as described above. Inoculum was aspirated, cells were washed three times with PBS, and D5 was added to monolayers and incubated at various time points indicated in Figure 2A. At designated time points, samples were collected, clarified, and stored at -80°C until titrations were performed described above.

CCHFV-G_C PROTEIN ANALYSIS

Immunofluorescence analysis was carried out by infecting Huh-7 monolayers at a MOI of 0.1 for 24 hpi. Cells were fixed with 4% (w/v) paraformaldehyde, permeabilized with 1% Triton X-100 and stained with 1:500 diluted MAb 8A1 or 13G8. Cells were washed, blocked with 5% BSA, and incubated with a dilution of 1:1,000 secondary goat- α -mouse MAb conjugated to fluorescein isothiocyanate (FITC)(Invitrogen). Cells were mounted and counterstained with the nuclear stain of 4',6-diamidino-2-phenylindole (DAPI) (Invitrogen). Stained cells were examined on a Nikon Eclipse Ti-S fluorescence

microscope. Whole virions were analyzed by infecting BHK cell monolayers, semi-purifying clarified supernatants over a 20% sucrose cushion at 37,000 rpm for 45 min at 4°C using a Beckman SW 41 Ti rotor. Viral pellets were lysed using NP-40 with 1x Protease Inhibitor Cocktail (Invitrogen). Recombinant VSV lysates were incubated at 56°C for 10 min and protein subsequently quantified using BCA Protein Assay per manufacturers' instructions (Thermo Fisher Scientific, Waltham, MA). Per institutional inactivation protocols, CCHFV lysates had a modified inactivation protocol using instead 2X Laemmli Sample Buffer (LSB) (Thermo Fisher Scientific) at 95°C for 15 min boiling and transfer to a fresh tube. Approximately 200 ng of purified and semi-purified virion associated total protein was mixed 1:1 with 1x LSB (without β -mercaptoethanol) and run on 4-20% gradient Mini-PROTEAN TGX electrophoresis gels (Bio-Rad, Hercules, California). Coomassie staining was accomplished via incubating TGX gels in Coomassie Fluor Orange protein gel stain (Thermo Fisher Scientific) per manufacturers' instructions and imaged at 300 nm on a Gel Doc XR+ gel documentation system (BioRad). Western blots were run on TGX gels using wet tank transfer to Hybond-P polyvinylidene difluoride (PVDF) membranes (GE Healthcare, Little Chalfont, UK). Membranes were blocked with 5% BSA overnight at 4°C in Tris/0.1% Tween 20 (Sigma-Aldrich) followed by incubation with primary MAb 11E7 diluted at 1:1,000, overnight at 4°C. Secondary horse radish peroxidase (HRP) conjugated goat- α -mouse antibody (Thermo Fisher Scientific) was diluted 1:10,000 and incubated on the membrane for 1 h at room temperature. Detection of HRP was accomplished via Pierce ECL western blotting substrate (Thermo Fisher Scientific), Hyperfilm ECL (GE Healthcare), and Kodak Carestream film with X-OMAT 2000 Processor (Eastman Kodak Company, Rochester, NY).

RNA PURIFICATION, cDNA CREATION, AND SANGER SEQUENCING ANALYSIS

Clarified viral supernatants were placed in TRIzol LS (Thermo Fisher Scientific) at a ratio of 1:5, mixed, incubated for 10 min at room temperature, and transferred to fresh tubes. RNA was isolated from sample mixtures using Zymo Research Direct-zol RNA min-prep (Zymo Research Corp, Irvine, CA), per manufacturers' instructions. RNA was quantified using a NanoDrop 8000 (Thermo Fisher Scientific) and approximately 500 ng total RNA was used to create cDNA using the SuperScript III First-Strand Synthesis System (Invitrogen) and a VSV-M, matrix protein gene 3' forward primer. Sanger sequencing on the cDNA was performed using VSV-M, VSV-L, and CCHFV-GPC (codon optimized) open reading frame primer sets and accomplished by the UTMB Molecular Genomics Core using an ABI Prism 3130XL DNA Sequencer (Applied Biosystems, Foster City, CA). Sequence analysis was performed using Geneious R9 (Biomatters, Auckland, New Zealand) based on consensus and plasmid maps. All cDNA/sequencing primers and consensus/plasmid maps are available upon request.

DEEP SEQUENCE ANALYSIS OF VIRAL RNA GENOMES

To analyze the stocks of CCHFV or rVSV vaccine vectors used in this study we performed deep sequencing analysis of RNA isolated from these virus stocks. Briefly, viral RNA was isolated from a Trizol LS (Invitrogen)/sample mixture using a Direct-zol RNA mini-prep (Zymo Research), per manufacturer's instructions. Approximately 150 ng of purified RNA was used to make cDNA using the Ovation RNA-seq 2.0 kit (NuGen) and this in turn was used for the preparation of the double-stranded DNA library, using Encore Ion Torrent library prep kit. Sequencing was performed by the UTMB Molecular Core on the Ion Torrent using 318-v2 deep sequencing chips. Sequence analysis was performed using DNA Star Seqman NGen software (DNA Star) based on unpaired analysis of 125 base pair overlaps.

ULTRASTRUCTURAL ANALYSIS

Viruses were propagated in multiple T-150 flasks of confluent BHK cells. Viral supernatants were harvested and clarified as described above. Clarified supernatants were concentrated by mixing with buffered 4x polyethylene glycol with incubation for 4 hrs at 4°C, followed by centrifugation at 6,800xg for 30 mins at 4°C. Concentrated pellets were re-suspended in PBS with protease inhibitor and overlaid atop Optiprep (Sigma-Aldrich) continuous gradients of 6-48% buffered iodixanol. Viruses were banded by ultracentrifugation at 25,000xg for 15 hrs at 4°C using a SW 41 Ti rotor. Bands were harvested, washed in PBS, and pelleted at 27,000xg for 1 h at 4°C using a SW 41 Ti rotor to remove residual iodixanol. Purified viral pellets were re-suspended in PBS and absorbed onto Formvar-carbon coated nickel grids (Electron Microscopy Sciences [EMS], Hatfield, PA) for 10-30 mins, incubated with MAb 11E7 at 1:10 dilutions. Antibodies were absorbed for 30 mins in wet chamber and washed with PBS containing 1% BSA, and incubated with the secondary antibody, goat- α -mouse conjugated to 15 nm colloidal gold particles (EMS), at a dilution of 1:20 for 30 mins. Grids were washed with PBS and 1% BSA, fixed using 2% (w/v) aqueous glutaraldehyde for 10 mins, and finally stained with 2% (w/v) aqueous uranyl acetate. Grids were examined at 60 kV using a Philips CM-100 transmission electron microscope.

ETHICS OF CARE, VACCINATION, AND ANIMAL CHALLENGE

Animal studies were approved by the UTMB Institutional Animal Care and Use Committee (IACUC). Animal research was carried out in compliance with the Animal Welfare Act and other federally regulated stipulations regarding animals and adherences

to the Guide for the Care and Use of Laboratory Animals, National Research Council, 2013. The animal facilities where this research was conducted are accredited by the Association for Assessment and Accreditation of Laboratory Animal Care International. This study used female 4 to 8 weeks old 129S6/SvEv-Stat1tm1Rds mice (STAT-1^{-/-}) (Taconic, Germantown, NY). After an acclimatization period in barrier conditions in environmentally enriched sterile housing, mice were anesthetized by isoflurane and implanted with subdermal transponders, which provide coded identifiers and permitted body temperature measurements (Biomedic Data Solutions, Seaford, DE). Vaccine preparations were diluted in Hanks balanced salts medium with 2% FBS, along with PBS for control groups. After anesthesia by isoflurane, 500 μ l of each preparation was administered intraperitoneally (i.p.), with five STAT-1^{-/-} mice per experimental group. Clinical scoring, body temperature, and weight, were recorded daily. At 35 days post vaccination (prime), mice were challenged with 500 μ l i.p. with either 100 pfu of CCHFV-Ibar10200 or CCHFV-Turkey200406546 (referred to as Turkey2004), respectively. All challenge doses were frozen for storage and verified by back-titrations by plaque assay on SW-13-CDC cells as outlined above. After challenge, animals were observed for clinical scoring, temperature, and weight change. Upon reaching institutionally approved endpoint score criteria, or study end-point, blood samples were collected into K3EDTA containing collection tubes (Granier, USA) and plasma was separated then frozen at -80°C for storage, further analysis, and/or irradiation.

ANTI-CCHFV-GPC IgG ELISA DEVELOPMENT

Iodixanol gradient purified Δ GrVSV- Δ CCHFV-GPC and rVSV-GFP were re-suspended in NP-40 buffer and BCA protein quantified (previously described above) and were used as whole virion antigens in coating Immunosorbent 96-well plates (Thermo Fisher Scientific). Matrices of various antigen, blocking, primary antibodies

(hyperimmune mouse ascetic fluid [HMAF kindly provided by T. Ksiazek], 8A1, and 11E7) to CCHFV/CCHFV-GPC, and secondary antibody (MAb HRP-goat- α -mouse) concentrations were used to develop optimal detection conditions for the CCHFV-GPC via ELISA. Per optimizations, one microgram of purified antigen per mL was suspended in sterile filtered sodium bicarb/carbonate buffer (pH 9.6) and allowed to incubate on immunosorbent plates overnight at 4°C. Plates were washed with PBS containing a concentration 0.1% tween-20 and 0.001% thimerosal. Blocking occurred with 5% milk dissolved in wash buffer, for 2 hrs at room temperature. Sera from STAT-1-/- mice was added 1:100 and diluted 2-fold by pipetting across plates and allowed to incubate for one hr at 37°C. Plates were washed, and a secondary anti-mouse antibody conjugated to HRP was added at 1:5,000 dilution for one hr at 37°C. ABTS Peroxidase substrate (KPL, SeraCare Life Sciences, Milford, MA) was incubated for 15 mins at room temperature prior to the addition of a 1% SDS stop solution. Plates were read with nine reads per well at 405 nm with a plastic correction factor accounted for from a 490nm reading per well. Test sera was evaluated using both purified Δ GrVSV- Δ CCHFV-GPC and rVSV-GFP antigen.

PLAQUE REDUCTION NEUTRALIZATION ASSAY

Serial dilutions of sera from four mice per treatment group, were aliquoted into cluster tubes with D10 and allowed to incubate with 100 pfu of CCHFV, isolate Turkey 2004, for approximately 2 hrs on ice. Resulting sera plus virus mixture was then overlaid onto 6-well plates of confluent SW-13-CDC cells and absorbed for 1 hr at 37°C with 5% CO₂ with rocking at 15 min intervals. Plaque assays were carried out in a manner described above in previous methods section. Resulting plaques were enumerated and compared to sera plus media only wells run for each sample, and a percent neutralization was calculated and reported for each dilution. Hyper-immune mouse ascetic fluid [HMAF] raised against CCHFV was additionally serially diluted and run as a positive control.

IMMUNOHISTOCHEMISTRY OF TISSUES

Tissue sections were deparaffinized and rehydrated through xylene and graded ethanols. Slides went through heat antigen retrieval in a steamer at 95°C for 20 mins in Sigma Citrate Buffer, pH6.0, 10X (Sigma Aldrich, St. Louis, MO). To block endogenous peroxidase activity, slides were treated with a 3% hydrogen peroxide and rinsed in distilled water. The tissue sections were processed for IHC using the Thermo Autostainer 360 (ThermoFisher, Kalamazoo, MI). Sequential 15 min incubations with avidin D and biotin solutions (Vector, Burlingame, CA) were performed to block endogenous biotin reactivity. Specific anti-CCHFV immunoreactivity was detected using a primary polyclonal rabbit- α -CCHFV-NP antibody (IBT BioServices, Rockville, MD) at a 1:3200 dilution for 60 mins. A secondary biotinylated goat- α -rabbit-IgG (Vector Laboratories, Burlingame, CA) at 1:200 dilution for 30 mins followed by Vector Horseradish Peroxidase Streptavidin, R.T.U (Vector) for 30 mins. Slides were developed with Dako DAB chromagen (Dako, Carpinteria, CA) for 5 mins and counterstained with Harris hematoxylin for 30 seconds. Tissue sections from uninfected mice were used as negative controls.

GENERATION OF HUMAN DERMAL DENDRITIC CELLS AND LANGERHANS CELLS

Langerhans and dermal dendritic cells were generated based on the protocol by Rozis et al.⁹¹. Briefly, umbilical cord blood samples were obtained from consented mothers in full term labor at the obstetrics and gynecology department at the University of Texas Medical Branch (UTMB) after approval was obtained from the Internal Review Board. CD34+ cells were isolated using immunomagnetic beads (STEMCELL Technologies, Vancouver, BC,

Canada) and cultured in complete RPMI1640 (100 IU/mL of penicillin, 0.1 mg/mL of streptomycin, 2 mM l-glutamine; Sigma-Aldrich) with 10% fetal bovine serum (Invitrogen, Carlsbad, CA, USA) supplemented with 100 ng/mL of granulocyte-macrophage colony stimulating factor (GM-CSF), and 100 ng/mL of TNF- α (Miltenyi Biotec, Auburn, CA, USA). After 5 days, two distinct populations were present: CD14⁺ CD1a⁻ and CD14⁻CD1a⁺ (Figure 1A). CD14⁺ cells were separated with immunomagnetic beads (STEMCELL Technologies, Vancouver, BC, Canada) and cultured separately for a further 5–7 days in GM-CSF (100 ng/mL) and IL-4 (1000 units/mL) (Miltenyi Biotec, Auburn, CA, USA). The remaining cells were cultured for the same period in medium supplemented with GM-CSF (100 ng/mL), TNF- α (100 ng/mL) and transforming growth factor- β (1 ng/mL) (Miltenyi Biotec, Auburn, CA, USA). Purity of generated cell populations was assessed by flow cytometry (Guava easyCyte, MerckMillipore, Burlington, MA, USA) using CD11b and CD207 (STEMCELL Technologies, Vancouver, BC, Canada) antibodies.

TICK SALIVARY GLAND EXTRACT PREPARATION

Hyalomma marginatum used in this study were collected in Yozgat state of Turkey in 2012. The strain has been maintained by standard rearing practices at the University Texas Medical Branch, Galveston, TX as previously described¹³. The ticks were tested negative for CCHFV, Tick-Borne Encephalitis Virus (TBEV), and *Rickettsia spp.* Unfed adults were placed into an ear bag on a New Zealand white rabbit (*Oryctolagus cuniculus*) and allowed to feed following protocols approved (#1209055, 31 August 2013) by the Institutional Animal Care and Use Committee of UTMB. The ticks were removed on the second day after commencement of feeding, separated by sex, surface cleaned with 70% ethanol and dissected. Salivary glands were removed and placed into sterile-filtered 0.15 M, Dulbecco's phosphate buffered saline (Sigma, St. Louis, MO, USA), pH 7.2 held on

ice. Salivary glands were sonicated at 55 kHz for 1 min on ice in a water bath. Salivary glands were pelleted by centrifugation at $10,000 \times g$ for 10 min and clarified salivary gland extract (SGE) was sterile filtered through a 0.22 μm Durapore-PVDF syringe filter apparatus (MerckMillipore, Burlington, MA, USA). Protein concentration was determined by Pierce BCA protein assay (Thermo, Rockford, IL, USA) and protein sizes were analyzed by BioAnalyzer (Agilent Technologies, Austin, TX, USA; see supplemental Figure S1) using an Agilent Protein 80 Kit, separated into 20 μL aliquots, subsequently frozen at $-70^{\circ}C$ and thawed not more than twice.

LC AND dDC STUDIES

For all of the experiments ca. 500,000 LCs or dDCs were used and either incubated with cell culture medium (mock), 10 μg of *H. marginatum* SGE in cell culture medium (SGE), CCHFV IbAr10200 at a multiplicity of infection (MOI) of 0.1 (=virus), or both 0.1 MOI CCHFV and 10 μg of *H. marginatum* SGE (=virus + SGE). For virus replication studies, cells were infected with either CCHFV strain IbAr10200 or AP92/P7 at a MOI of 0.1 and incubated for 48 h at $37^{\circ}C$ after which supernatant was collected. Viral titers in supernatant were measured by plaque assay as previously described¹⁰⁰. For the other studies, cells were infected with CCHFV strain IbAr10200 at a MOI of 1, and incubated at $37^{\circ}C$. For the gene array studies, cells were harvested 12 h post infection to determine gene expression levels. For the cytokine studies, supernatant was collected 24 h after infection.

GENE ARRAY ASSAY

LCs and dDCs were harvested 12 h post infection and total RNA was isolated from cells by phenol/chloroform extraction based on approved BSL4 protocols. RNA quality was determined using the BioAnalyzer (Agilent Technologies, Austin, TX, USA) using an

Agilent RNA 6000 Nano Kit. RNA from all samples were reverse transcribed to cDNA using the QuantiTect Rev. Transcription Kit (Qiagen, Valencia, CA, USA). The RT² Profiler™ PCR Array Human Dendritic & Antigen Presenting Cell (Qiagen, Valencia, CA, USA) was used and the samples were run on a Roche Lightcycler real-time detection system (Roche, Basel, Switzerland). RT² Profiler™ PCR Array profiles 84 related genes simultaneously and enable gene expression analysis of 170+ pathways. Data analysis was conducted using Ingenuity® Pathway Analysis (Qiagen, Valencia, CA, USA).

CYTOKINE DETECTION

To determine secreted cytokine levels from the dDCs and LCs, supernatant was collected 24 h after infection and clarified by briefly centrifuging for 3 min at 10,000 ×g. Twenty-microliter amounts of clarified supernatant were run in duplicates with a multiplex Milliplex MAP Human Cytokine/Chemokine kit (MerckMillipore, Burlington, MA, USA) according to the manufacturer's instructions. The kit simultaneously quantifies granulocyte-macrophage colony-stimulating factor (GM-CSF), IFN- α , interleukin-1 α (IL-1 α) and -1 β (IL-1 β), IL-6, IL-7, IL-8, IL-10, IL-12 (p40), IL-12 (p70), IL-15, MCP-1, and tumor necrosis factor (TNF). The samples were run on a Luminex Platform (Qiagen, Valencia, CA, USA) and analyzed using Luminex 100 IS software (Luminex).

MIGRATION ASSAY

A migration assay was performed based on the protocol by Skallova et al.⁹⁴. Deidentified buffy coats were obtained from adult healthy donors from the UTMB Blood Bank by centrifugation enrichment with clinical approval from the UTMB Institutional Review Board. Monocytes were isolated from peripheral blood mononuclear cell (PBMC) pools using positive selection anti-CD14 monoclonal antibody coated magnetic beads according

to manufacturer's instructions (Miltenyi Biotec, Auburn, CA, USA). Monocytes were supplemented with Advanced RPMI 1640 media, 10% FBS, 2 mM l-glutamine (Invitrogen, Carlsbad, CA, USA), 1% penicillin/streptomycin (Invitrogen, Carlsbad, CA, USA), and monocytes were differentiated to monocyte derived dendritic cell (moDC) phenotype by the addition of 0.05 mM β -mercaptoethanol, 50 ng/mL granulocyte-macrophage colony-stimulating factor (GM-CSF), and 16 ng/mL interleukin-4 (IL-4) (R&D Systems, Minneapolis, MN, USA). The moDC were incubated for one week at 37 °C, 5% CO₂, harvested with Accutase cell detachment solution (STEMCELL Technologies, Vancouver, BC, Canada), and were incubated with 1 μ g/mL lipopolysaccharide (LPS) from *Escherichia coli* O55:B5 (Sigma, St. Louis, MO, USA) was added to each well to induce moDC maturation. The moDC were pelleted by centrifugation and suspended in Roswell Park Memorial Institute (RMPI) medium with 20 μ g/mL of tick SGE and placed into a polycarbonate membrane insert within a 24-well Fluorimetric QCM Cell Migration Assay (MerckMillipore, Burlington, MA, USA) migration chamber at a density of 5×10^5 cell per chamber. Cells were incubated above wells containing serum-free RMPI with or without 1 μ g/mL of the chemoattractant, recombinant human CCL-19 (MIP-3 β) (BioLegend, San Diego, CA, USA) for 24 h prior to staining, lysing, and quantifying cell migration according to kit instructions. Within the Cell Migration Assay, cells must migrate through an 8 μ m pore membrane to a bottom chamber. Invaded cells on the bottom of the insert membrane are dissociated from the membrane when incubated with Cell Detachment Buffer. These cells are subsequently lysed and detected by the patented CyQUANT GR dye (Molecular Probes, Invitrogen, Carlsbad, CA, USA). This green-fluorescent dye exhibits strong fluorescence enhancement when bound to cellular nucleic acids Quantification (i.e., cell migration) was assessed by fluorescence readings using a Tecan Infinite M200 Pro (Tecan Group, Männedorf, Switzerland) plate reader. Samples were run in biological triplicate with multiple reads per well.

FUSION ASSAY

BioCoat™ 8-well Culture Slides (Corning) were coated with 2.5µg/well of mouse laminin I and seeded with HuH7 or BHK cells at 80-90% confluency. Cells were infected with a MOI of 3 with ΔGrVSV-ΔCCHFV-GPC, Hazara virus, Dugbe virus or Crimean-Congo hemorrhagic fever virus, respectively. pH-calibrated and sterile filtered DMEM (pH 5.2 – 7.4, in 0.2 increments) was incubated for 30 minutes and then replaced by 1µM CellTracker™ Green CMFDA Dye (ThermoFisher) in serum-free DMEM for additional 2 hours. At 18 hpi cells were fixed in 4% PFA, mounted with ProLong™ Diamond Antifade Mountant with DAPI (ThermoFisher) and imaged at a magnification of 20X. Fusion index was calculated according to:

$$\text{fusion index} = 1 - \frac{\text{number of cells}}{\text{number of nuclei}} \text{ from three fields of view.}$$

IN SILICO SEQUENCE ANALYSIS

Geneious 4.8.3 (Biomatters Inc., Newark, NJ, USA) was used for sequence assembly and analysis. Topology, sizes, and targeting predictions were generated by employing open source, web based programs from the Technical University of Denmark, DTU Bioinformatics (found at <http://www.cbs.dtu.dk/index.html>), such as SignalP 4.1, NetOGlyc 4.0, NetNGlyc 1.0, Prop 1.0, tied mixture hidden Markov model (TMHMM) 2.0. SnapGene Viewer 2.82 was also utilized (http://www.snapgene.com/products/snapgene_viewer/).

STATISTICAL ANALYSIS

A one-way ANOVA test with Bonferroni's multiple comparison analysis was used to compare the mock and treatment groups for the viral titers, cytokines and cell migration. All tests were conducted in Prism (GraphPad, La Jolla, CA, USA) v5. Significance of gene

expression from the RT-qPCR arrays was determined by paired t-test performed in Microsoft Excel 2013 (Microsoft, Redmond, WA, USA). Hierarchical clustering and heatmap generation were performed using Mathematica v11 (Wolfram, Champaign, IL, USA). Statistical analysis of viral titers was performed using unpaired t-test with a 95% confidence level ($P < 0.05$) and for survival, a Kaplan-Meier survival curve with GraphPad Prism software (Graphpad Software, Inc., San Diego, CA). A power analysis utilizing parameters that included survival, neutralization capacity, and ELISA antibody titers from previous pilot studies was performed to assess adequate animal numbers for the current study to differentiate between surviving groups versus control groups to obtain a statistical significance of $p < 0.05$ with at least a 90% probability.

CHAPTER 9: All Things Considered

UNDERSTANDING THE ECOLOGY OF CRIMEAN-CONGO

As outlined in Chapters 1 and 2, CCHFV has a fascinating ecology. Its existence throughout both a diverse array of animals and the many life-stages of the *Hyalomma* tick vector, coupled with the threat of a deadly spillover event into humans, beckon for numerous studies to understand the impacts of the environment on the virus, and the virus impacts on humanity. Perturbations in nature that effect any one of these facets, such as in the case of climate change, animal migrations, or socio/geopolitical changes that favor the spread of CCHFV from endemic to naïve regions, ensure that the virus will remain both an ecological presence in nature, and a continued global public health threat. As the data supported in Chapter 1, the detection and comparisons of CCHFV genomes from *Hyalomma lusitanicum* ticks isolated in Spain, suggest migratory birds likely seed CCHFV up the Iberian Peninsula, from Northern Africa into Spain ⁵⁹. It is not a far stretch to imagine both the tick vector and potentially CCHFV, being able to take root not only in Spain, but to continue spreading throughout undeveloped areas of Southern Europe, where evidence suggests the *Hyalomma* tick vector is establishing a regional foothold in countries such as Portugal, Spain, Italy, and Germany ^{15,56,61,216}.

What remains unclear with this predicted spread of the vector, is whether the virus will be able to expand alongside the tick, and whether this means actual CCHF cases will occur or increase in frequency within human populations. As its name provides, CCHFV has had a foot hold within the Crimean Peninsula since at least the 1950s ¹. It is curious, why the virus has not expanded from its discovery point of Crimea, into the rest of Southern Europe. It is also interesting that CCHF incidence declined in areas surrounding Crimea, such as the Balkans following the 1970s, which might be attributed to the crude Bulgarian CCHFV vaccine used, as mentioned in Chapter 1 ^{20,217–220}. Nevertheless, part of the interest

in the spillover effect of CCHFV into humans, specifically for Southern Europe, is whether there are different pathologies attributed to the various CCHFV clades or even individual strains^{7,211,212,221,222}. While the Western portion of Southern Europe is currently influenced from North African strains of CCHFV, the Balkans strains have either emerged distinctly or are related to circulating strains in Turkey^{7,58,59,211,212,221–224}. The questions of whether some strains of CCHFV will be more pathogenic and others less, is one that requires both an understanding of the ecological influences of the virus transmission during spillover events, and routine epidemiological surveying for both the *Hyalomma spp.* vector and for CCHFV. Chapter 1 added to this body of knowledge directly, by providing evidence of CCHFV establishing itself in Spain. Chapter 2, also added to the ecological story of CCHFV, by being the first documented study to examine the effects of *Hyalomma* tick saliva and to a certain degree, transmission, of CCHFV to primary human skin APC. This study confirmed that the tick vector does play a role in the early pathogenesis of CCHFV. The results supported a scenario where local replication of CCHFV in host tissues likely occurs with a decrease in APC migration to draining lymph nodes. While this avenue may buy CCHFV sometime before an immune response is generated—our other findings did not completely coincide with primary literature regarding tick saliva associated transmission of pathogens^{74,86–88,225,226}. There were mild influences on the transcriptional, chemokine, or cytokine profiles of infected and SGE treated cells, and no statistical differences in replication of the virus⁹². Much of what has been published, with other ticks such as *Ixodes spp.*, describes the opposite, with a higher impact on the maturation, effector functions, or transcriptional profiles of APC^{74,86–88,225,226}. Though, a potential difference between the study in Chapter 2 and other published work is that most APC tested were moDC derived and were not HPSC produced skin APC. The differences between these two methods of generating specific APC, plus donor-to-donor variability mean that further studies should be performed to add onto the ecological roles the tick vector may play in transmission of CCHFV. It is also important to follow up from this work with

understanding the downstream effects in the ability to induce antigen presentation to T- and B-cells from infected and infected with SGE treated skin antigen presenting cells to determine if these cells have downstream consequences that have largely been unexamined at by the field.

LESSONS LEARNED: FROM PSEUDOTYPED VESICULAR STOMATITIS VIRUS, WITH LOVE

As outlined in Chapter 3 and 4, there are a number of means which lend to both studying the biology of and developing countermeasures for CCHFV. The focus for the majority of this dissertation was on expanding the utility of one of these means, known as rVSV pseudotyping. The success of the studies outlined in Chapters 4 through 7, were largely contingent on a serendipitous event from passaging the initial replication deficient pseudotype (VSV-G*-ΔGrVSV-CCHFV-GPC) until enough evolutionary pressure, forced the virus to adapt either itself, or the CCHFV-GPC ORF, to permit incorporation of a form of CCHFV-G_C that would more efficiently enable subsequent infection. This event, which enabled the adaptation(s) for the replication competent pseudotype (ΔGrVSV-ΔCCHFV-GPC) to occur, is still unclear as to what exact mutations are responsible for the outcome. It is possible that the VSV matrix protein (VSV-M), had altered residues that permitted incorporation the C-terminal truncated CCHFV-G_C onto the VSV virion. The opposite might also be true, where the truncation of the C-terminus of the CCHFV-G_C, is what enabled the uptake in the first place. The C-terminus of the CCHFV-G_C has been speculated to contain a motif for intracellular retention (likely needed for CCHFV-G_N heterodimer formations and maturations)^{44,114,158,159,227}, and removing or altering this motif, might facilitate CCHFV-G_C localization to other areas within/on the cell where assembling or budding VSV cores or immature virions, could acquire it. It could also be a combination of both. The evidence provided in this dissertation support this notion of both being involved. While the C-terminal truncation enabled a higher foci forming number of *in trans* ΔGrVSV-GFP (Figure 8e) compared to the other *in trans* constructs, this ‘titer’

was still several logs off from the titers generated by $\Delta\text{GrVSV-}\Delta\text{CCHFV-GPC}$ (Figure 6A). As the backbone of the $\Delta\text{GrVSV-}\Delta\text{CCHFV-GPC}$ also contains the numerous mutations outlined in Table 4, this would suggest that a synergy of both likely enable the replication competence of the $\Delta\text{GrVSV-}\Delta\text{CCHFV-GPC}$. While additional mutagenesis studies would be beneficial in elucidating what specific residue changes enable the replication competence, the end utility might be outweighed by other existing low containment CCHFV platforms such as VLP systems, which likely provide a closer approximation to the exterior phenotype of wt CCHFV. This is not to say that either the replication deficient ($\text{VSV-G}^*\text{-}\Delta\text{GrVSV-CCHFV-GPC}$) and replication competent ($\Delta\text{GrVSV-}\Delta\text{CCHFV-GPC}$) pseudotypes have little utility. On the contrary, this dissertation demonstrates they can be used to successfully study elements of the CCHFV-GPC expression and to develop countermeasures against CCHFV.

The central utility of the replication deficient pseudotype ($\text{VSV-G}^*\text{-}\Delta\text{GrVSV-CCHFV-GPC}$), is in its ability to serve as single-round infectious vector for CCHFV-GPC expression either *in vitro* or *in vivo*. This system can be used at higher MOIs, without the potential biosafety risks associated with using a replicative virus, to generate CCHFV-GPC antigens *en mass*. These antigens could be used for downstream applications such as ELISA's or antibody generation for hybridomas. And, while pilot studies outlined in Chapter 7, did not demonstrate protection from the replication deficient pseudotype ($\text{VSV-G}^*\text{-}\Delta\text{GrVSV-CCHFV-GPC}$), the replication competent pseudotype ($\Delta\text{GrVSV-}\Delta\text{CCHFV-GPC}$) also demonstrated limited efficacy in preventing vaccinated mice from succumbing to CCHFV infection when using the CCHFV challenge strain of IbAr10200 (Figure 31). When the challenge strain was switched with the clinical isolate of Turkey2004, efficacy of the replication competent pseudotype was increased to 100%. It could be of benefit, not to discredit the replication deficient pseudotype in future *in vivo* studies, as vaccinated STAT-1-/- mice outcome appears associated to the CCHFV challenge strain. It would be prudent to investigate the outcome(s) of a replication deficient vaccination strategy with

the Turkey2004 challenge strain in the future. Single-round infectious or replication deficient viral vaccine vectors are likely to be licensed over un-attenuated live-viral vectors in human trials, and future work into VSV-G*- Δ GrVSV-CCHFV-GPC should not be discounted for this reason.

As for the replication competent pseudotype (Δ GrVSV- Δ CCHFV-GPC), it showed strong utility as a pre-screening tool for both small molecule antagonists and entry inhibitors to wt CCHFV. Many of these experimental countermeasures that antagonized the replication competent pseudotype outlined in Chapters 5 and 6, also antagonized wt CCHFV *in vitro*. On top of these findings, the replication competent pseudotype was proven safe in the STAT-1-/- mouse model, Which has not been the case with several other replication competent pseudotyped rVSV (within the STAT-1-/- mouse model) ²⁰⁴. Additionally, with two stains of CCHFV, the replication competent pseudotype was also able to afford protection, with up to 100% protection following a lethal challenge dose of CCHFV within the STAT-1-/- mouse model. This protection could be afforded with a single prime dose of the replication competent pseudotype. This single-dose vaccination strategy is the first in the field to be able to provide a CCHFV animal model, 100% protection. Taken together, this supports the notion that this replication competent pseudotype, can serve as an experimental vaccine which is both attenuated and able to afford a degree of protection to CCHFV with just a single-injection.

THE MORAL OF THE STORY: PREVENTING AND TREATING CRIMEAN-CONGO

Given the prevalence of CCHFV, the broad distribution and expansion of the tick vector, and the numerous reservoir animals which can host the virus—eradication is an untenable option. Therefore, limiting or preventing the spillover events of human disease are likely to be the most effective options at mitigating human cases of CCHF. Environmental prevention efforts that either limit or prevent transmission in competent hosts and vectors, are likely to be the most effective strategies; while vaccination efforts

aimed at preventing human cases will likely face numerous challenges in clinical development. However, there have been promising clinical uses for the rVSV platform in terms of limiting localized outbreaks, and in vaccination of higher-risk populations ²²⁸. Additionally, antivirals which would work throughout the various stages of CCHF, could also be used for therapeutic benefit in targeted populations. The inhibitory compounds outlined in Chapter 5, which have been, or are currently being, clinically developed as treatment options for HIV ¹⁶⁸ and RSV ²²⁹, could be an effective measure at controlling acute CCHFV infections, which should be experimentally evaluated *in vivo*. As further shown in Chapter 6, the repurposing of clinically approved compounds, such as the anti-tuberculosis drug rifampicin and the high blood pressure medication, isradipine, could provide some benefit, if proven useful in CCHFV *in vivo* models by expediting the antiviral drug development process for CCHF. In closing, this dissertation has investigated the biology of CCHFV and its tick vector and has developed and evaluated a number of relevant prevention and therapeutic options, both *in vitro* and *in vivo*, which should be further evaluated as countermeasure options for mitigation of this threat to global public health.

References

1. Hoogstraal, H. The epidemiology of tick-borne Crimean-Congo hemorrhagic fever in Asia, Europe, and Africa. *J. Med. Entomol.* **15**, 307–417 (1979).
2. Casals, J., Henderson, B. E., Hoogstraal, H., Johnson, K. M. & Shelokov, A. *A Review of Soviet Viral Hemorrhagic Fevers, 1969.* **122**, 437–453 (Oxford University Press, 1970).
3. Chumakov, M. P. A short review of investigation of the virus of Crimean hemorrhagic fever. *Endem. viral Infect. (hemorrhagic fever with Ren. Syndr. Crime. hemorrhagic fever, Omsk hemorrhagic fever, Astrakhan virus from Hyalomma pl. Plumb. tick)* 193–196 (1965).
4. Chumakov, M. P. A new tick-borne virus disease--Crimean hemorrhagic fever. *Izd Otd Primorsk. Armii, Simferopol Crimean* **he**, 13–43 (1945).
5. Simpson, D. I. H. ; Knight, E. M. ; Courtois, G. ; Williams, M. C. ; Weinbren, M. P. ; Kibukamusoke, J. W. *Congo virus: a hitherto undescribed virus occurring in Africa. Part 1. Human isolations-clinical notes.* *East African Medical Journal* **44**, (Medical Association of East Africa, 1967).
6. Woodall, J. P. ; Williams, M. C. ; Simpson, D. I. H. *Congo virus: a hitherto undescribed virus occurring in Africa. Part 2. Identification studies.* *East African Medical Journal* **44**, (Medical Association of East Africa, 1967).
7. Bente, D. A. *et al.* Crimean-Congo hemorrhagic fever: History, epidemiology, pathogenesis, clinical syndrome and genetic diversity. *Antiviral Res.* **100**, 159–189 (2013).
8. Ergönül, Ö. Crimean-Congo haemorrhagic fever. *Lancet Infect. Dis.* **6**, 203–214 (2006).
9. WHO | Crimean-Congo haemorrhagic fever (CCHF). *WHO* (2018). Available at: <http://www.who.int/emergencies/diseases/crimean-congo-haemorrhagic-fever/en/>. (Accessed: 19th August 2018)
10. Creative Commons — Attribution 4.0 International — CC BY 4.0. Available at: <https://creativecommons.org/licenses/by/4.0/>. (Accessed: 21st August 2018)
11. Gargili, A. *et al.* The role of ticks in the maintenance and transmission of Crimean-Congo hemorrhagic fever virus: A review of published field and laboratory studies. *Antiviral Res.* **144**, 93–119 (2017).
12. Spengler, J. R. *et al.* A chronological review of experimental infection studies of the role of wild animals and livestock in the maintenance and transmission of Crimean-Congo hemorrhagic fever virus. *Antiviral Res.* (2016). doi:10.1016/j.antiviral.2016.09.013
13. Gargili, A., Thangamani, S. & Bente, D. Influence of laboratory animal hosts on the life cycle of *Hyalomma marginatum* and implications for an in vivo transmission model for Crimean-Congo hemorrhagic fever virus. *Front. Cell.*

Infect. Microbiol. **3**, 39 (2013).

14. Xia, H. *et al.* Transstadial Transmission and Long-term Association of Crimean-Congo Hemorrhagic Fever Virus in Ticks Shapes Genome Plasticity. *Sci. Rep.* **6**, 35819 (2016).
15. Estrada-Peña, A. *et al.* Crimean-Congo hemorrhagic fever virus in ticks, Southwestern Europe, 2010. *Emerg. Infect. Dis.* **18**, 179–80 (2012).
16. Espy, N. *et al.* Ribavirin Had Demonstrable Effects on the Crimean-Congo Hemorrhagic Fever Virus (CCHFV) Population and Load in a Patient With CCHF Infection. *J. Infect. Dis.* (2018). doi:10.1093/infdis/jiy163
17. Roth, C. & Formenty, P. Application for Inclusion of Ribavirin in the WHO Model List of Essential Medicines. *World Heal. Organ. Appl. Inclusion, Sel. Use Essent. Med. Policy, Access Ration. Use* (2006).
18. Bodur, H. *et al.* Effect of oral ribavirin treatment on the viral load and disease progression in Crimean-Congo hemorrhagic fever. *Int. J. Infect. Dis.* **15**, e44–e47 (2011).
19. Papa, A., Papadimitriou, E. & Christova, I. The Bulgarian vaccine Crimean-Congo haemorrhagic fever virus strain. *Scand. J. Infect. Dis.* **43**, 225–229 (2011).
20. Mousavi-Jazi, M., Karlberg, H., Papa, A., Christova, I. & Mirazimi, A. Healthy individuals' immune response to the Bulgarian Crimean-Congo hemorrhagic fever virus vaccine. *Vaccine* **30**, 6225–6229 (2012).
21. Christova, I., Kovacheva, O., Georgieva, G., Ivanova, S., & Argirov, D. Vaccine against Congo-Crimean haemorrhagic fever virus-Bulgarian input in fighting the disease. *Probl Infect Parasit Dis* **37**, 7–8 (2010).
22. Adams, M. J. *et al.* Changes to taxonomy and the International Code of Virus Classification and Nomenclature ratified by the International Committee on Taxonomy of Viruses (2017). *Arch. Virol.* **162**, (2017).
23. Kuhn, J. *et al.* Genomic Characterization of the Genus Nairovirus (Family Bunyaviridae). *Viruses* **8**, 164 (2016).
24. Lasecka, L. & Baron, M. D. The molecular biology of nairoviruses, an emerging group of tick-borne arboviruses. *Arch. Virol.* **159**, 1249–1265 (2014).
25. Clerx, J. P. M., Casals, J. & Bishop, D. H. L. Structural characteristics of Nairoviruses (Genus Nairovirus, Bunyaviridae). *J. Gen. Virol.* **55**, 165–178 (1981).
26. Elliott, R. M., Schmaljohn, C. S. & Collett, M. S. in 91–141 (Springer, Berlin, Heidelberg, 1991). doi:10.1007/978-3-642-76018-1_4
27. Clerx, J. P. M. & Bishop, D. H. L. Qalyub virus, a member of the newly proposed Nairovirus genus (bunyaviridae). *Virology* **108**, 361–372 (1981).
28. Barnwal, B., Karlberg, H., Mirazimi, A. & Tan, Y.-J. The Non-structural Protein of Crimean-Congo Hemorrhagic Fever Virus Disrupts the Mitochondrial Membrane Potential and Induces Apoptosis. *J. Biol. Chem.* **291**, 582–92 (2016).
29. Wang, X. *et al.* Molecular basis for the formation of ribonucleoprotein complex of

- Crimean-Congo hemorrhagic fever virus. *J. Struct. Biol.* **196**, 455–465 (2016).
30. Sanchez, A. J., Vincent, M. J. & Nichol, S. T. Characterization of the glycoproteins of Crimean-Congo hemorrhagic fever virus. *J. Virol.* **76**, 7263–75 (2002).
 31. Erickson, B. R., Deyde, V., Sanchez, A. J., Vincent, M. J. & Nichol, S. T. N-linked glycosylation of Gn (but not Gc) is important for Crimean Congo hemorrhagic fever virus glycoprotein localization and transport. *Virology* **361**, 348–355 (2007).
 32. Altamura, L. A. *et al.* Identification of a novel C-terminal cleavage of Crimean-Congo hemorrhagic fever virus PreGN that leads to generation of an NSM protein. *J. Virol.* **81**, 6632–42 (2007).
 33. Bergeron, E., Vincent, M. J. & Nichol, S. T. Crimean-Congo hemorrhagic fever virus glycoprotein processing by the endoprotease SKI-1/S1P is critical for virus infectivity. *J. Virol.* **81**, 13271–6 (2007).
 34. Devignot, S., Bergeron, E., Nichol, S., Mirazimi, A. & Weber, F. A virus-like particle system identifies the endonuclease domain of Crimean-Congo hemorrhagic fever virus. *J. Virol.* **89**, 5957–67 (2015).
 35. Xiao, X., Feng, Y., Zhu, Z. & Dimitrov, D. S. Identification of a putative Crimean-Congo hemorrhagic fever virus entry factor. *Biochem. Biophys. Res. Commun.* **411**, 253–258 (2011).
 36. Garrison, A. R. *et al.* Crimean–Congo hemorrhagic fever virus utilizes a clathrin- and early endosome-dependent entry pathway. *Virology* **444**, 45–54 (2013).
 37. Simon, M., Johansson, C. & Mirazimi, A. Crimean-Congo hemorrhagic fever virus entry and replication is clathrin-, pH- and cholesterol-dependent. *J. Gen. Virol.* **90**, 210–215 (2009).
 38. Podbilewicz, B. Virus and cell fusion mechanisms. *Annu Rev Cell Dev Biol* **30**, 111–139 (2014).
 39. Garry, C. E. & Garry, R. F. Proteomics computational analyses suggest that the carboxyl terminal glycoproteins of Bunyaviruses are class II viral fusion protein (beta-penetrenes). *Theor. Biol. Med. Model.* **1**, 10 (2004).
 40. Walter, C. T. & Barr, J. N. Recent advances in the molecular and cellular biology of bunyaviruses. *J. Gen. Virol.* **92**, 2467–2484 (2011).
 41. Wichgers Schreur, P. J., Kormelink, R. & Kortekaas, J. Genome packaging of the Bunyavirales. *Curr. Opin. Virol.* **33**, 151–155 (2018).
 42. Vincent, M. J. *et al.* Crimean-Congo hemorrhagic fever virus glycoprotein proteolytic processing by subtilase SKI-1. *J. Virol.* **77**, 8640–9 (2003).
 43. Elliott, R. M. & Weber, F. Bunyaviruses and the type I interferon system. *Viruses* **1**, 1003–1021 (2009).
 44. Overby, A. K., Popov, V. L., Pettersson, R. F. & Neve, E. P. A. The cytoplasmic tails of Uukuniemi Virus (Bunyaviridae) G(N) and G(C) glycoproteins are important for intracellular targeting and the budding of virus-like particles. *J.*

- Virol.* **81**, 11381–91 (2007).
45. Shi, X., Lappin, D. F. & Elliott, R. M. Mapping the Golgi targeting and retention signal of Bunyamwera virus glycoproteins. *J. Virol.* **78**, 10793–802 (2004).
 46. Ergonul, O. Crimean-Congo hemorrhagic fever virus: New outbreaks, new discoveries. *Curr. Opin. Virol.* **2**, 215–220 (2012).
 47. Bodur, H., Akinci, E., Ascioğlu, S., Öngürü, P. & Uyar, Y. Subclinical infections with Crimean-Congo hemorrhagic fever virus, Turkey. *Emerg. Infect. Dis.* **18**, 640–2 (2012).
 48. Leblebicioglu, H., Ozaras, R., Irmak, H. & Sencan, I. Crimean-Congo hemorrhagic fever in Turkey: Current status and future challenges. *Antiviral Res.* **126**, 21–34 (2016).
 49. Papa, A. *et al.* Crimean-Congo hemorrhagic fever virus, Greece. *Emerg. Infect. Dis.* **20**, 288–90 (2014).
 50. Vasilenko S, Chumakov M, Butenko A, Smirnova S, T. & M, P. V. Contribution to the question of Crimean-hemorrhagic fever (CHF) in Bulgaria (in Russian). (*In English, NAMRU3-T857.*) *Mater 15 Nauchn Sess Inst Polio Virus Entsefalitov (October 1968)* **3**, 90–2 (1968).
 51. Papa, A; Velo, E. Ecology of the CCHF endemic area in Albania. *Vector-borne and zoonotic diseases* **9**, 713–716 (2009).
 52. Estrada-Peña, A. & de la Fuente, J. The ecology of ticks and epidemiology of tick-borne viral diseases. *Antiviral Res.* **108**, 104–28 (2014).
 53. Estrada-Peña, A., Ayllón, N. & de la Fuente, J. Impact of Climate Trends on Tick-Borne Pathogen Transmission. *Front. Physiol.* **3**, 64 (2012).
 54. Estrada-Peña, A., Sánchez, N. & Estrada-Sánchez, A. An assessment of the distribution and spread of the tick *Hyalomma marginatum* in the western Palearctic under different climate scenarios. *Vector Borne Zoonotic Dis.* **12**, 758–68 (2012).
 55. Estrada-Peña, A., Ruiz-Fons, F., Acevedo, P., Gortazar, C. & de la Fuente, J. Factors driving the circulation and possible expansion of Crimean-Congo haemorrhagic fever virus in the western Palearctic. *J. Appl. Microbiol.* **114**, 278–86 (2013).
 56. Kampen, H., Poltz, W., Hartelt, K., Wölfel, R. & Faulde, M. Detection of a questing *Hyalomma marginatum marginatum* adult female (Acari, Ixodidae) in southern Germany. **43**, (2007).
 57. Gale, P. *et al.* Impact of climate change on risk of incursion of Crimean-Congo haemorrhagic fever virus in livestock in Europe through migratory birds. *J. Appl. Microbiol.* **112**, 246–57 (2012).
 58. Negredo, A. *et al.* Autochthonous Crimean–Congo Hemorrhagic Fever in Spain. *N. Engl. J. Med.* **377**, 154–161 (2017).
 59. Cajimat, M. N. B. *et al.* Genomic Characterization of Crimean–Congo Hemorrhagic Fever Virus in *Hyalomma* Tick from Spain, 2014. *Vector-Borne*

- Zoonotic Dis.* **17**, 714–719 (2017).
60. Deyde, V. M., Khristova, M. L., Rollin, P. E., Ksiazek, T. G. & Nichol, S. T. Crimean-Congo hemorrhagic fever virus genomics and global diversity. *J. Virol.* **80**, 8834–42 (2006).
 61. Palomar, A. M. *et al.* Crimean-Congo Hemorrhagic Fever Virus in Ticks from Migratory Birds, Morocco 1. *Emerg. Infect. Dis.* **19**, 260–263 (2013).
 62. Zivcec, M. *et al.* Unique strain of Crimean-Congo hemorrhagic fever virus, Mali. *Emerg. Infect. Dis.* **20**, 911–3 (2014).
 63. NIAID Emerging Infectious Diseases/Pathogens | NIH: National Institute of Allergy and Infectious Diseases. Available at: <https://www.niaid.nih.gov/research/emerging-infectious-diseases-pathogens>. (Accessed: 14th August 2018)
 64. WHO | List of Blueprint priority diseases. *WHO* (2018). Available at: <http://www.who.int/blueprint/priority-diseases/en/>. (Accessed: 14th August 2018)
 65. Wikel, S. K. in *Biology of ticks*, vol. 2 (ed. Daniel E. Sonenshine, R. M. R.) 88–128 (Oxford University Press, 2014).
 66. JONGEJAN, F. & UILENBERG, G. The global importance of ticks. *Parasitology* **129**, S3 (2005).
 67. Mason, L. M. K., Veerman, C. C., Geijtenbeek, T. B. H. & Hovius, J. W. R. Ménage à trois: Borrelia, dendritic cells, and tick saliva interactions. *Trends Parasitol.* **30**, 95–103 (2014).
 68. Hovius, J. W. R. Spitting Image: Tick Saliva Assists the Causative Agent of Lyme Disease in Evading Host Skin's Innate Immune Response. *J. Invest. Dermatol.* **129**, 2337–2339 (2009).
 69. Labuda, M. & Nuttall, P. A. Tick-borne viruses. *Parasitology* **129 Suppl**, S221–45 (2004).
 70. Nuttall, P. A. in *Biology of ticks*, vol. 2 (ed. Daniel E. Sonenshine, R. M. R.) 180–210 (Oxford University Press, 2014).
 71. Nestle, F. O., Di Meglio, P., Qin, J.-Z. & Nickoloff, B. J. Skin immune sentinels in health and disease. *Nat. Rev. Immunol.* **9**, 679–91 (2009).
 72. Connolly-Andersen, A.-M., Douagi, I., Kraus, A. a & Mirazimi, A. Crimean Congo hemorrhagic fever virus infects human monocyte-derived dendritic cells. *Virology* **390**, 157–162 (2009).
 73. Peyrefitte, C. N. *et al.* Differential activation profiles of Crimean-Congo hemorrhagic fever virus- and Dugbe virus-infected antigen-presenting cells. *J. Gen. Virol.* **91**, 189–198 (2010).
 74. Cavassani, K. A., Aliberti, J. C. J. C., Dias, A. R. V., Silva, J. S. J. S. & Ferreira, B. R. Tick saliva inhibits differentiation, maturation and function of murine bone-marrow-derived dendritic cells. *Immunology* **114**, 235–245 (2005).
 75. Preston, S. G. *et al.* Novel Immunomodulators from Hard Ticks Selectively

- Reprogramme Human Dendritic Cell Responses. *PLoS Pathog.* **9**, e1003450 (2013).
76. Arasli, M. Pathogenesis of Crimean–Congo Hemorrhagic Fever From an Immunological Perspective. *Curr. Trop. Med. Reports* **3**, 14–19 (2016).
 77. de la Fuente, J. *et al.* Tick-Pathogen Interactions and Vector Competence: Identification of Molecular Drivers for Tick-Borne Diseases. *Front. Cell. Infect. Microbiol.* **7**, 114 (2017).
 78. Bray, M. Pathogenesis of viral hemorrhagic fever. *Curr. Opin. Immunol.* **17**, 399–403 (2005).
 79. West, H. C. & Bennett, C. L. Redefining the Role of Langerhans Cells As Immune Regulators within the Skin. *Front. Immunol.* **8**, 1941 (2018).
 80. Tay, S. S., Roediger, B., Tong, P. L., Tikoo, S. & Weninger, W. The Skin-Resident Immune Network. *Curr. Dermatol. Rep.* **3**, 13–22 (2014).
 81. Boltjes, A. & van Wijk, F. Human Dendritic Cell Functional Specialization in Steady-State and Inflammation. *Front. Immunol.* **5**, 131 (2014).
 82. van den Berg, L. M. *et al.* Caveolin-1 mediated uptake via langerin restricts HIV-1 infection in human Langerhans cells. *Retrovirology* **11**, 123 (2014).
 83. Cerny, D. *et al.* Selective Susceptibility of Human Skin Antigen Presenting Cells to Productive Dengue Virus Infection. *PLoS Pathog.* **10**, e1004548 (2014).
 84. Yan, L., Woodham, A. W., Da Silva, D. M. & Kast, W. M. in 333–350 (Humana Press, New York, NY, 2015). doi:10.1007/978-1-4939-2013-6_25
 85. Šimo, L., Kazimirova, M., Richardson, J. & Bonnet, S. I. The Essential Role of Tick Salivary Glands and Saliva in Tick Feeding and Pathogen Transmission. *Front. Cell. Infect. Microbiol.* **7**, 281 (2017).
 86. Nuttall, P. A. & Labuda, M. Tick-host interactions: saliva-activated transmission. *Parasitology* **129 Suppl**, S177-89 (2004).
 87. Wu, J. *et al.* Two immunoregulatory peptides with antioxidant activity from tick salivary glands. *J. Biol. Chem.* **285**, 16606–13 (2010).
 88. Yu, D. *et al.* A tick B-cell inhibitory protein from salivary glands of the hard tick, *Hyalomma asiaticum asiaticum*. *Biochem. Biophys. Res. Commun.* **343**, 585–590 (2006).
 89. Jablonka, W. *et al.* Identification and Mechanistic Analysis of a Novel Tick-Derived Inhibitor of Thrombin. *PLoS One* **10**, e0133991 (2015).
 90. Moulton, J. R., Gordon, S. W., Linthicum, K. J. & Moulton, J. R. Transmission of Crimean-Congo hemorrhagic fever virus in two species of *Hyalomma* ticks from infected adults to cofeeding immature forms. *Am. J. Trop. Med. Hyg.* **48**, 576–580 (1993).
 91. Rozis, G., Benlahrech, A., Duraisingham, S., Gotch, F. & Patterson, S. Human Langerhans' cells and dermal-type dendritic cells generated from CD34 stem cells express different toll-like receptors and secrete different cytokines in response to

- toll-like receptor ligands. *Immunology* **124**, 329–338 (2008).
92. Rodriguez, S. *et al.* Interactions of Human Dermal Dendritic Cells and Langerhans Cells Treated with Hyalomma Tick Saliva with Crimean-Congo Hemorrhagic Fever Virus. *Viruses* **10**, 381 (2018).
 93. Fukunaga, A., Khaskhely, N. M., Sreevidya, C. S., Byrne, S. N. & Ullrich, S. E. Dermal dendritic cells, and not Langerhans cells, play an essential role in inducing an immune response. *J. Immunol.* **180**, 3057–64 (2008).
 94. Skallová, A., Iezzi, G., Ampenberger, F., Kopf, M. & Kopecky, J. Tick saliva inhibits dendritic cell migration, maturation, and function while promoting development of Th2 responses. *J. Immunol.* **180**, 6186–6192 (2008).
 95. Yoshida, R. *et al.* Molecular cloning of a novel human CC chemokine EB11-ligand chemokine that is a specific functional ligand for EB11, CCR7. *J. Biol. Chem.* **272**, 13803–9 (1997).
 96. Bromley, S. K., Thomas, S. Y. & Luster, A. D. Chemokine receptor CCR7 guides T cell exit from peripheral tissues and entry into afferent lymphatics. *Nat. Immunol.* **6**, 895–901 (2005).
 97. Veldkamp, C. T. *et al.* Solution Structure of CCL19 and Identification of Overlapping CCR7 and PSGL-1 Binding Sites. *Biochemistry* **54**, 4163–6 (2015).
 98. Bunyaviridae Chap 42 - Fields Virology 6th.pdf.
 99. Gowen, B. B. & Hickerson, B. T. Hemorrhagic fever of bunyavirus etiology: disease models and progress towards new therapies. *J. Microbiol.* **55**, 183–195 (2017).
 100. Bente, D. A. *et al.* Pathogenesis and immune response of Crimean-Congo hemorrhagic fever virus in a STAT-1 knockout mouse model. *J. Virol.* **84**, 11089–100 (2010).
 101. Oestereich, L. *et al.* Evaluation of Antiviral Efficacy of Ribavirin, Arbidol, and T-705 (Favipiravir) in a Mouse Model for Crimean-Congo Hemorrhagic Fever. *PLoS Negl. Trop. Dis.* **8**, (2014).
 102. Devendra, K. Effects of exposure to high concentrations of ribavirin in d... : The Pediatric Infectious Disease Journal. *Pediatr. Infect. Dis. J.* **9**, S88–S90 (1990).
 103. Dokuzoguz, B. *et al.* Severity scoring index for crimean-congo hemorrhagic fever and the impact of ribavirin and corticosteroids on fatality. *Clin. Infect. Dis.* **57**, (2013).
 104. Bausch, D. G., Hadi, C. M., Khan, S. H. & Lertora, J. J. L. Review of the Literature and Proposed Guidelines for the Use of Oral Ribavirin as Postexposure Prophylaxis for Lassa Fever. *Clin. Infect. Dis.* **51**, 1435–1441 (2010).
 105. Johnson, S. *et al.* in *Cochrane Database of Systematic Reviews* (ed. Johnson, S.) (John Wiley & Sons, Ltd, 2017). doi:10.1002/14651858.CD012713
 106. Yilmaz, G. *et al.* Ribavirin in Treatment of Crimean-Congo Hemorrhagic Fever (CCHF): An International Multicenter Retrospective Analysis. *Open Forum Infect.*

Dis. **3**, (2016).

107. Conger, N. G. *et al.* Health care response to CCHF in US soldier and nosocomial transmission to health care providers, Germany, 2009. *Emerg. Infect. Dis.* **21**, 23–31 (2015).
108. Phase 3 Efficacy and Safety Study of Favipiravir for Treatment of Uncomplicated Influenza in Adults - Full Text View - ClinicalTrials.gov. Available at: <https://clinicaltrials.gov/ct2/show/NCT02008344>. (Accessed: 1st November 2018)
109. Marriott, A. C., El-Ghorr, A. A. & Nuttall, P. A. Dugbe nairovirus M RNA: Nucleotide sequence and coding strategy. *Virology* **190**, 606–615 (1992).
110. Honig, J. E., Osborne, J. C. & Nichol, S. T. The high genetic variation of viruses of the genus Nairovirus reflects the diversity of their predominant tick hosts. *Virology* **318**, 10–16 (2004).
111. Ahmed, A. A. *et al.* Presence of broadly reactive and group-specific neutralizing epitopes on newly described isolates of Crimean-Congo hemorrhagic fever virus. *J. Gen. Virol.* **86**, 3327–3336 (2005).
112. Zivcec, M. *et al.* Identification of broadly neutralizing monoclonal antibodies against Crimean-Congo hemorrhagic fever virus. (2017). doi:10.1016/j.antiviral.2017.08.014
113. Bertolotti-ciarlet, A. *et al.* Cellular Localization and Antigenic Characterization of Crimean-Congo Hemorrhagic Fever Virus Glycoproteins. *Society* **79**, 6152–6161 (2005).
114. Suda, Y. *et al.* Analysis of the entry mechanism of Crimean-Congo hemorrhagic fever virus, using a vesicular stomatitis virus pseudotyping system. *Arch. Virol.* **161**, 1447–1454 (2016).
115. Suda, Y. *et al.* The Development of a Novel Diagnostic Assay That Utilizes a Pseudotyped Vesicular Stomatitis Virus for the Detection of Neutralizing Activity against Crimean-Congo Hemorrhagic Fever Virus. *Jpn. J. Infect. Dis.* **71**, 205–208 (2018).
116. Bergeron, É. *et al.* Recovery of Recombinant Crimean Congo Hemorrhagic Fever Virus Reveals a Function for Non-structural Glycoproteins Cleavage by Furin. *PLoS Pathog.* **11**, e1004879 (2015).
117. Welch, S. R. *et al.* Identification of 2'-deoxy-2'-fluorocytidine as a potent inhibitor of Crimean-Congo hemorrhagic fever virus replication using a recombinant fluorescent reporter virus. *Antiviral Res.* **147**, 91–99 (2017).
118. Scholte, F. E. M. *et al.* Crimean-Congo Hemorrhagic Fever Virus Suppresses Innate Immune Responses via a Ubiquitin and ISG15 Specific Protease. *Cell Rep.* **20**, 2396–2407 (2017).
119. Zivcec, M. *et al.* Assessment of Inhibitors of Pathogenic Crimean-Congo Hemorrhagic Fever Virus Strains Using Virus-Like Particles. *PLoS Negl. Trop. Dis.* **9**, 1–23 (2015).

120. Bergeron, E., Albariño, C. G., Khristova, M. L. & Nichol, S. T. Crimean-Congo hemorrhagic fever virus-encoded ovarian tumor protease activity is dispensable for virus RNA polymerase function. *J. Virol.* **84**, 216–26 (2010).
121. Hinkula, J. *et al.* Immunization with DNA Plasmids Coding for Crimean-Congo Hemorrhagic Fever Virus Capsid and Envelope Proteins and/or Virus-Like Particles Induces Protection and Survival in Challenged Mice. *J. Virol.* **91**, (2017).
122. Shtanko, O., Nikitina, R. A., Altuntas, C. Z., Chepurnov, A. A. & Davey, R. A. Crimean-Congo Hemorrhagic Fever Virus Entry into Host Cells Occurs through the Multivesicular Body and Requires ESCRT Regulators. *PLoS Pathog.* **10**, (2014).
123. Letchworth, G. J. J., Rodriguez, L. L. L., Del C Barrera, J. & DEL CBARRERA, J. Vesicular stomatitis. *Vet. J.* **157**, 239–260 (1999).
124. Lawson, N. D., Stillman, E. A., Whitt, M. A. & Rose, J. K. Recombinant vesicular stomatitis viruses from DNA. *Proc. Natl. Acad. Sci.* **92**, 4477–4481 (1995).
125. Haglund, K., Forman, J., Kräusslich, H.-G. & Rose, J. K. Expression of Human Immunodeficiency Virus Type 1 Gag Protein Precursor and Envelope Proteins from a Vesicular Stomatitis Virus Recombinant: High-Level Production of Virus-like Particles Containing HIV Envelope. (2000). doi:10.1006/viro.1999.0120
126. Kretzschmar, E. *et al.* High-efficiency incorporation of functional influenza virus glycoproteins into recombinant vesicular stomatitis viruses. *J. Virol.* **71**, 5982–9 (1997).
127. Schnell, M. J., Buonocore, L., Kretzschmar, E., Johnson, E. & Rose, J. K. Foreign glycoproteins expressed from recombinant vesicular stomatitis viruses are incorporated efficiently into virus particles. *Proc. Natl. Acad. Sci. U. S. A.* **93**, 11359–11365 (1996).
128. Ito, H. *et al.* Mutational analysis of the putative fusion domain of Ebola virus glycoprotein. *J. Virol.* **73**, 8907–12 (1999).
129. Takada, A. *et al.* A system for functional analysis of Ebola virus glycoprotein. *Proc. Natl. Acad. Sci. U. S. A.* **94**, 14764–9 (1997).
130. Lichty, B. D., Power, A. T., Stojdl, D. F. & Bell, J. C. Vesicular stomatitis virus: Re-inventing the bullet. *Trends Mol. Med.* **10**, 210–216 (2004).
131. Rose, N. F. *et al.* An Effective AIDS Vaccine Based on Live Attenuated Vesicular Stomatitis Virus Recombinants. *Cell* **106**, 539–549 (2001).
132. Garbutt, M. *et al.* Properties of Replication-Competent Vesicular Stomatitis Virus Vectors Expressing Glycoproteins of Filoviruses and Arenaviruses Properties of Replication-Competent Vesicular Stomatitis Virus Vectors Expressing Glycoproteins of Filoviruses and Arenaviruses. *J. Virol.* **78**, 5458–5465 (2004).
133. Zinkernagel, R. M., Adler, B. & Holland, J. J. Cell-Mediated Immunity to Vesicular Stomatitis Virus Infections in Mice. *Pathobiology* **46**, 53–70 (1978).
134. Zinkernagel, R. M., Althage, A. & Holland, J. Target antigens for H-2-restricted

- vesicular stomatitis virus-specific cytotoxic T cells. *J. Immunol.* **121**, 744–8 (1978).
135. Fehr, T. *et al.* T-Independent Activation of B Cells by Vesicular Stomatitis Virus: No Evidence for the Need of a Second Signal. *Cell. Immunol.* **168**, 184–192 (1996).
 136. Johnson, J. E. *et al.* Neurovirulence properties of recombinant vesicular stomatitis virus vectors in non-human primates. *Virology* **360**, 36–49 (2007).
 137. Suder, E. *et al.* Human Vaccines & Immunotherapeutics The vesicular stomatitis virus-based Ebola virus vaccine: From concept to clinical trials The vesicular stomatitis virus-based Ebola virus vaccine: From concept to clinical trials. (2018). doi:10.1080/21645515.2018.1473698
 138. ElSherif, M. S. *et al.* Assessing the safety and immunogenicity of recombinant vesicular stomatitis virus Ebola vaccine in healthy adults: a randomized clinical trial. *CMAJ* **189**, E819–E827 (2017).
 139. Geisbert, T. W. *et al.* Vesicular stomatitis virus-based Ebola vaccine is well-tolerated and protects immunocompromised nonhuman primates. *PLoS Pathog.* **4**, e1000225 (2008).
 140. Halperin, S. A. *et al.* Six-Month Safety Data of Recombinant Vesicular Stomatitis Virus–Zaire Ebola Virus Envelope Glycoprotein Vaccine in a Phase 3 Double-Blind, Placebo-Controlled Randomized Study in Healthy Adults. *J. Infect. Dis.* **215**, 1789–1798 (2017).
 141. Brown, K. S., Safronetz, D., Marzi, A., Ebihara, H. & Feldmann, H. Vesicular Stomatitis Virus-Based Vaccine Protects Hamsters against Lethal Challenge with Andes Virus. *J. Virol.* **85**, 12781–12791 (2011).
 142. Higa, M. M., Petersen, J., Hooper, J. & Doms, R. W. Efficient production of Hantaan and Puumala pseudovirions for viral tropism and neutralization studies. *Virology* **423**, 134–142 (2012).
 143. Ogino, M. *et al.* Use of vesicular stomatitis virus pseudotypes bearing hantaan or seoul virus envelope proteins in a rapid and safe neutralization test. *Clin. Diagn. Lab. Immunol.* **10**, 154–60 (2003).
 144. Jones, S. M. *et al.* Live attenuated recombinant vaccine protects nonhuman primates against Ebola and Marburg viruses. *Nat. Med.* **11**, 786–790 (2005).
 145. Mire, C. E. *et al.* Vesicular Stomatitis Virus-Based Vaccines Protect Nonhuman Primates against Bundibugyo ebolavirus. *PLoS Negl. Trop. Dis.* **7**, (2013).
 146. Geisbert, T. W. *et al.* Development of a New Vaccine for the Prevention of Lassa Fever. *PLoS Med.* **2**, e183 (2005).
 147. Roberts, A. *et al.* Vaccination with a recombinant vesicular stomatitis virus expressing an influenza virus hemagglutinin provides complete protection from influenza virus challenge. *J. Virol.* **72**, 4704–11 (1998).
 148. Schlereth, B., Rose, J. K., Buonocore, L., ter Meulen, V. & Niewiesk, S.

- Successful vaccine-induced seroconversion by single-dose immunization in the presence of measles virus-specific maternal antibodies. *J. Virol.* **74**, 4652–7 (2000).
149. Kahn, J. S., Roberts, A., Weibel, C., Buonocore, L. & Rose, J. K. Replication-competent or attenuated, nonpropagating vesicular stomatitis viruses expressing respiratory syncytial virus (RSV) antigens protect mice against RSV challenge. *J. Virol.* **75**, 11079–87 (2001).
 150. Ezelle, H. J., Markovic, D. & Barber, G. N. Generation of hepatitis C virus-like particles by use of a recombinant vesicular stomatitis virus vector. *J. Virol.* **76**, 12325–34 (2002).
 151. Palin, A. *et al.* An optimized vaccine vector based on recombinant vesicular stomatitis virus gives high-level, long-term protection against *Yersinia pestis* challenge. *Vaccine* **25**, 741–750 (2007).
 152. Garrison, A. R. *et al.* A DNA vaccine for Crimean-Congo hemorrhagic fever protects against disease and death in two lethal mouse models. *PLoS Negl. Trop. Dis.* **11**, E0005908 (2017).
 153. Simon, M., Johansson, C., Lundkvist, Å. & Mirazimi, A. Microtubule-dependent and microtubule-independent steps in Crimean-Congo hemorrhagic fever virus replication cycle. *Virology* **385**, 313–322 (2009).
 154. Bergmann, J. E., Tokuyasu, K. T. & Singer, S. J. Passage of an integral membrane protein, the vesicular stomatitis virus glycoprotein, through the Golgi apparatus en route to the plasma membrane. *Proc. from Natl. Acad. Sci.* **78**, 1746–1750 (1981).
 155. Whitt, M. A. Generation of VSV pseudotypes using recombinant ΔG-VSV for studies on virus entry, identification of entry inhibitors, and immune responses to vaccines. *J. Virol. Methods* **169**, 365–374 (2010).
 156. Sanchez, A. J., Vincent, M. J., Erickson, B. R. & Nichol, S. T. Crimean-congo hemorrhagic fever virus glycoprotein precursor is cleaved by Furin-like and SKI-1 proteases to generate a novel 38-kilodalton glycoprotein. *J. Virol.* **80**, 514–25 (2006).
 157. Jayakar, H. R. & Whitt, M. A. Identification of Two Additional Translation Products from the Matrix (M) Gene That Contribute to Vesicular Stomatitis Virus Cytopathology. *J. Virol.* **76**, 8011–8018 (2002).
 158. Shi, X., Kohl, A., Li, P. & Elliott, R. M. Role of the cytoplasmic tail domains of Bunyamwera orthobunyavirus glycoproteins Gn and Gc in virus assembly and morphogenesis. *J. Virol.* **81**, 10151–60 (2007).
 159. Fukushi, S. *et al.* Vesicular stomatitis virus pseudotyped with severe acute respiratory syndrome coronavirus spike protein. *J. Gen. Virol.* **86**, 2269–2274 (2005).
 160. Doms, R. W. What Came First—the Virus or the Egg? *Cell* **168**, 755–757 (2017).
 161. Kielian, M. & Rey, F. A. Virus membrane-fusion proteins: more than one way to make a hairpin. *Nat. Rev. Microbiol.* **4**, 67–76 (2006).

162. Blumenthal, R., Schoch, C., Puri, A. & Clague, M. J. A Dissection of Steps Leading to Viral Envelope Protein-Mediated Membrane Fusion. *Ann. N. Y. Acad. Sci.* **635**, 285–296 (1991).
163. Liao, M. & Kielian, M. Domain III from class II fusion proteins functions as a dominant-negative inhibitor of virus membrane fusion. *J. Cell Biol.* **171**, 111–120 (2005).
164. Cifuentes-Munoz, N., Salazar-Quiroz, N. & Tischler, N. D. Hantavirus Gn and Gc envelope glycoproteins: Key structural units for virus cell entry and virus assembly. *Viruses* **6**, 1801–1822 (2014).
165. Tischler, N. D., Gonzalez, A., Perez-Acle, T., Roseblatt, M. & Valenzuela, P. D. T. Hantavirus Gc glycoprotein: evidence for a class II fusion protein. *J. Gen. Virol.* **86**, 2937–2947 (2005).
166. Koehler, J. W. *et al.* A Fusion-Inhibiting Peptide against Rift Valley Fever Virus Inhibits Multiple, Diverse Viruses. *PLoS Negl. Trop. Dis.* **7**, e2430 (2013).
167. Filone, C. M., Heise, M., Doms, R. W. & Bertolotti-Ciarlet, A. Development and characterization of a Rift Valley fever virus cell–cell fusion assay using alphavirus replicon vectors. *Virology* **356**, 155–164 (2006).
168. Hardy, H. & Skolnik, P. R. Enfuvirtide, a New Fusion Inhibitor for Therapy of Human Immunodeficiency Virus Infection. *Pharmacotherapy* **24**, 198–211 (2004).
169. Schmidt, A. G., Yang, P. L. & Harrison, S. C. Peptide inhibitors of flavivirus entry derived from the E protein stem. *J. Virol.* **84**, 12549–54 (2010).
170. Hrobowski, Y. M., Garry, R. F. & Michael, S. F. Peptide inhibitors of dengue virus and West Nile virus infectivity. *Virol. J.* **2**, 49 (2005).
171. Bosch, B. J. *et al.* Severe acute respiratory syndrome coronavirus (SARS-CoV) infection inhibition using spike protein heptad repeat-derived peptides. *Proc. Natl. Acad. Sci. U. S. A.* **101**, 8455–60 (2004).
172. Cianci, C. *et al.* Orally active fusion inhibitor of respiratory syncytial virus. *Antimicrob. Agents Chemother.* **48**, 413–22 (2004).
173. Douglas, J. L. *et al.* Inhibition of respiratory syncytial virus fusion by the small molecule VP-14637 via specific interactions with F protein. *J. Virol.* **77**, 5054–64 (2003).
174. Bossart, K. N. *et al.* Inhibition of Henipavirus fusion and infection by heptad-derived peptides of the Nipah virus fusion glycoprotein. *Virol. J.* **2**, 57 (2005).
175. Barriga, G. P. *et al.* Inhibition of the Hantavirus Fusion Process by Predicted Domain III and Stem Peptides from Glycoprotein Gc. *PLoS Negl. Trop. Dis.* **10**, e0004799 (2016).
176. Cifuentes-Munoz, N., Barriga, G. P., Valenzuela, P. D. T. & Tischler, N. D. Aromatic and polar residues spanning the candidate fusion peptide of the Andes virus Gc protein are essential for membrane fusion and infection. *J. Gen. Virol.* **92**, 552–563 (2011).

177. Lee, K. K. *et al.* Capturing a fusion intermediate of influenza hemagglutinin with a cholesterol-conjugated peptide, a new antiviral strategy for influenza virus. *J. Biol. Chem.* **286**, 42141–9 (2011).
178. Porotto, M. *et al.* Viral entry inhibitors targeted to the membrane site of action. *J. Virol.* **84**, 6760–8 (2010).
179. Moscona, A. *et al.* Fusion properties of cells persistently infected with human parainfluenza virus type 3: participation of hemagglutinin-neuraminidase in membrane fusion. *J. Virol.* **65**, 2773–7 (1991).
180. Casey, J. R., Grinstein, S. & Orłowski, J. Sensors and regulators of intracellular pH. *Nat. Rev. Mol. Cell Biol.* **11**, 50–61 (2010).
181. Surtees, R. *et al.* Heat Shock Protein 70 Family Members Interact with Crimean-Congo Hemorrhagic Fever Virus and Hazara Virus Nucleocapsid Proteins and Perform a Functional Role in the Nairovirus Replication Cycle. *J. Virol.* **90**, 9305–16 (2016).
182. Punch, E. K. *et al.* Potassium is a trigger for conformational change in the fusion spike of an enveloped RNA virus. *J. Biol. Chem.* **293**, 9937–9944 (2018).
183. Adams, C. P. & Brantner, V. V. Estimating The Cost Of New Drug Development: Is It Really \$802 Million? *Health Aff.* **25**, 420–428 (2006).
184. The Pathogen Box | Catalysing neglected disease drug discovery. Available at: <https://www.pathogenbox.org/>. (Accessed: 1st November 2018)
185. Vila, T. & Lopez-Ribot, J. L. Screening the Pathogen Box for Identification of *Candida albicans* Biofilm Inhibitors. *Antimicrob. Agents Chemother.* **61**, e02006-16 (2017).
186. Preston, S. *et al.* Screening of the ‘Pathogen Box’ identifies an approved pesticide with major anthelmintic activity against the barber’s pole worm. *Int. J. Parasitol. Drugs Drug Resist.* **6**, 329–334 (2016).
187. Ross, B. N., Myers, J. N., Muruato, L. A., Tapia, D. & Torres, A. G. Evaluating New Compounds to Treat *Burkholderia pseudomallei* Infections. *Front. Cell. Infect. Microbiol.* **8**, 210 (2018).
188. Mukherjee, S. *et al.* Enhancing dengue virus maturation using a stable furin over-expressing cell line. *Virology* **497**, 33–40 (2016).
189. Yi, L. *et al.* Small molecules blocking the entry of severe acute respiratory syndrome coronavirus into host cells. *J. Virol.* **78**, 11334–9 (2004).
190. Chaipan, C. *et al.* Proteolytic activation of the 1918 influenza virus hemagglutinin. *J. Virol.* **83**, 3200–11 (2009).
191. Ao, Z. *et al.* Characterization of a trypsin-dependent avian influenza H5N1-pseudotyped HIV vector system for high throughput screening of inhibitory molecules. *Antiviral Res.* **79**, 12–18 (2008).
192. Garcia, J.-M. & Lai, J. C. Production of influenza pseudotyped lentiviral particles and their use in influenza research and diagnosis: an update. *Expert Rev. Anti.*

Infect. Ther. **9**, 443–455 (2011).

193. Borhani, N. O. *et al.* Final Outcome Results of the Multicenter Isradipine Diuretic Atherosclerosis Study (MIDAS). *JAMA* **276**, 785 (1996).
194. Sodeik, B., Griffiths, G., Ericsson, M., Moss, B. & Doms, R. W. Assembly of vaccinia virus: effects of rifampin on the intracellular distribution of viral protein p65. *J. Virol.* **68**, 1103–14 (1994).
195. Dowall, S. D., Carroll, M. W. & Hewson, R. Development of vaccines against Crimean-Congo haemorrhagic fever virus. (2017). doi:10.1016/j.vaccine.2017.05.031
196. Bereczky, S. *et al.* Crimean-Congo hemorrhagic fever virus infection is lethal for adult type I interferon receptor-knockout mice. *J. Gen. Virol.* **91**, 1473–1477 (2010).
197. Zivcec, M. *et al.* Lethal Crimean-Congo hemorrhagic fever virus infection in interferon α/β receptor knockout mice is associated with high viral loads, proinflammatory responses, and coagulopathy. *J. Infect. Dis.* **207**, 1909–1921 (2013).
198. Canakoglu, N. *et al.* Immunization of Knock-Out α/β Interferon Receptor Mice against High Lethal Dose of Crimean-Congo Hemorrhagic Fever Virus with a Cell Culture Based Vaccine. *PLoS Negl. Trop. Dis.* **9**, 1–14 (2015).
199. Ghiasi, S. M., Salmanian, A. H., Chinikar, S. & Zakeri, S. Mice orally immunized with a transgenic plant expressing the glycoprotein of Crimean-Congo hemorrhagic fever virus. *Clin. Vaccine Immunol.* **18**, 2031–2037 (2011).
200. Buttigieg, K. R. *et al.* A novel vaccine against Crimean-Congo haemorrhagic fever protects 100% of animals against lethal challenge in a mouse model. *PLoS One* **9**, e91516 (2014).
201. Kortekaas, J. *et al.* Crimean-Congo Hemorrhagic Fever Virus Subunit Vaccines Induce High Levels of Neutralizing Antibodies But No Protection in STAT1 Knockout Mice. *Vector-Borne Zoonotic Dis.* **15**, 759–764 (2015).
202. Dowall, S. *et al.* A Crimean-Congo hemorrhagic fever (CCHF) viral vaccine expressing nucleoprotein is immunogenic but fails to confer protection against lethal disease. *Hum. Vaccin. Immunother.* **12**, 519–527 (2016).
203. Zivcec, M., Safronetz, D., Scott, D. P., Robertson, S. & Feldmann, H. Nucleocapsid protein-based vaccine provides protection in mice against lethal Crimean-Congo hemorrhagic fever virus challenge. *PLoS Negl. Trop. Dis.* **12**, e0006628 (2018).
204. Marzi, A. *et al.* Stat1-Deficient Mice Are Not an Appropriate Model for Efficacy Testing of Recombinant Vesicular Stomatitis Virus–Based Filovirus Vaccines. *J. Infect. Dis.* **212**, S404–S409 (2015).
205. Martinez, I. *et al.* Recombinant vesicular stomatitis (Indiana) virus expressing New Jersey and Indiana glycoproteins induces neutralizing antibodies to each serotype in swine, a natural host. *Vaccine* **22**, 4035–4043 (2004).

206. Spengler, J. R. *et al.* Crimean-Congo Hemorrhagic Fever in Humanized Mice Reveals Glial Cells as Primary Targets of Neurological Infection. *J. Infect. Dis.* (2017). doi:10.1093/infdis/jix215
207. Forger, J. M., Bronson, R. T., Huang, A. S. & Reiss, C. S. Murine infection by vesicular stomatitis virus: initial characterization of the H-2d system. *J. Virol.* **65**, 4950–8 (1991).
208. Preble, O. T., Costello, L. E., Huang, D. D. & Barmada, M. A. Neurovirulence mutant of vesicular stomatitis virus with an altered target cell tropism in vivo. *Infect. Immun.* **29**, 744–57 (1980).
209. Causey, O. R., Kemp, G. E., Madbouly, M. H. & David-West, T. S. Congo virus from domestic livestock, African hedgehog, and arthropods in Nigeria. *Am. J. Trop. Med. Hyg.* **19**, 846–50 (1970).
210. Ergonul, O. & Whitehouse, C. A. in *Crimean-Congo Hemorrhagic Fever* 3–11 (Springer Netherlands, 2007). doi:10.1007/978-1-4020-6106-6_1
211. Midilli, K. *et al.* The first clinical case due to AP92 like strain of Crimean-Congo Hemorrhagic Fever virus and a field survey. *BMC Infect. Dis.* **9**, 90 (2009).
212. Papa, A. *et al.* A novel AP92-like Crimean-Congo hemorrhagic fever virus strain, Greece. *Ticks Tick. Borne. Dis.* **5**, 590–593 (2014).
213. Spik, K. *et al.* Immunogenicity of combination DNA vaccines for Rift Valley fever virus, tick-borne encephalitis virus, Hantaan virus, and Crimean Congo hemorrhagic fever virus. *Vaccine* **24**, 4657–4666 (2006).
214. Haddock, E. *et al.* A cynomolgus macaque model for Crimean–Congo haemorrhagic fever. *Nat. Microbiol.* **3**, 556–562 (2018).
215. Mire, C. E. *et al.* Single-dose attenuated Vesiculovax vaccines protect primates against Ebola Makona virus. *Nature* **520**, 688–691 (2015).
216. Maltezou, H. C. *et al.* Crimean-Congo hemorrhagic fever in Europe: current situation calls for preparedness. *Euro Surveill. Bull. Eur. sur les Mal. Transm. = Eur. Commun. Dis. Bull.* **15**, 19504 (2010).
217. Yashina, L. Genetic variability of Crimean-Congo haemorrhagic fever virus in Russia and Central Asia. *J. Gen. Virol.* **84**, 1199–1206 (2003).
218. Drosten, C., Minnak, D., Emmerich, P., Schmitz, H. & Reinicke, T. Crimean-Congo Hemorrhagic Fever in Kosovo. *J. Clin. Microbiol.* **40**, 1122–1123 (2002).
219. Papa, A. *et al.* Crimean-Congo Hemorrhagic Fever in Albania, 2001. *Eur. J. Clin. Microbiol. Infect. Dis.* **21**, 603–606 (2002).
220. Papa, A., Christova, I., Papadimitriou, E. & Antoniadis, A. Crimean-Congo hemorrhagic fever in Bulgaria. *Emerg. Infect. Dis.* **10**, 1465–7 (2004).
221. Salehi-Vaziri, M. *et al.* The First Fatal Case of Crimean-Congo Hemorrhagic Fever Caused by the AP92-Like Strain of the Crimean-Congo Hemorrhagic Fever Virus. *Jpn. J. Infect. Dis.* **69**, 344–346 (2016).
222. Panayotova, E., Papa, A., Trifonova, I. & Christova, I. Crimean-Congo

- hemorrhagic fever virus lineages Europe 1 and Europe 2 in Bulgarian ticks. *Ticks Tick. Borne. Dis.* **7**, 1024–8 (2016).
223. England, M. E. *et al.* *Hyalomma* ticks on northward migrating birds in southern Spain: Implications for the risk of entry of Crimean-Congo haemorrhagic fever virus to Great Britain. *J. Vector Ecol.* **41**, 128–134 (2016).
 224. Burt, F. J. & Swanepoel, R. Molecular epidemiology of African and Asian Crimean-Congo haemorrhagic fever isolates. *Epidemiol. Infect.* **133**, 659–66 (2005).
 225. Jaworski, D. C., Rosell, R., Coons, L. B. & Needham, G. R. Tick (Acari: Ixodidae) attachment cement and salivary gland cells contain similar immunoreactive polypeptides. *J. Med. Entomol.* **29**, 305–309 (1992).
 226. Kazimírová, M. *et al.* Tick-Borne Viruses and Biological Processes at the Tick-Host-Virus Interface. *Front. Cell. Infect. Microbiol.* **7**, 339 (2017).
 227. Thomas, D. C. & Roth, M. G. The basolateral targeting signal in the cytoplasmic domain of glycoprotein G from vesicular stomatitis virus resembles a variety of intracellular targeting motifs related by primary sequence but having diverse targeting activities. *J. Biol. Chem.* **269**, 15732–15739 (1994).
 228. Henao-Restrepo, A. M. *et al.* Efficacy and effectiveness of an rVSV-vectored vaccine in preventing Ebola virus disease: final results from the Guinea ring vaccination, open-label, cluster-randomised trial (Ebola Ça Suffi t!). *Lancet* **389**, 505–518 (2017).
 229. Perron, M. *et al.* GS-5806 Inhibits a Broad Range of Respiratory Syncytial Virus Clinical Isolates by Blocking the Virus-Cell Fusion Process. *Antimicrob. Agents Chemother.* **60**, 1264–73 (2015).

Vita

Sergio Enrique Rodriguez drew his first breath on September 10th, 1985 at 6:22pm in his home town of McAllen, Texas. When first handed to his loving parents, Sarah and Henry Rodriguez, the physician proclaimed: ‘This handsome little fellow has the knack!’ Sergio would not discover as to what, however, for nearly twenty years. His knack came in the form of a garnering his first (but not last) C+ whilst completing a microbiology course for his baccalaureate degree in science at Baylor University in Waco, Texas. With wounded pride, he swore revenge on the microbial world and delved into graduate studies pertaining to environmental microbiology at Texas A&M University – Corpus Christi. He did this for some time until misplacing his graduate advisor and ultimately absconding with a Master of Science. Like many members belonging to the viral family *Herpesviridae*, graduate school would continue to cling to him and reemerge for an additional six and a half years. During this time, the locale and beach were slightly different, and he spent his days researching and teaching about the virological universe with and to a number of *Homo sapiens* at the University of Texas Medical Branch in Galveston, Texas. In his spare time, he learned about the mysteries of the universe, how to knit, how to crochet (yes, they’re different), and how to build large Lego replicas. After being a sufficient pain in enough people’s assignments, he was shooed away from Galveston’s sandy shores and handed two pieces of paper bearing ‘Doctor of Philosophy’ and ‘Master of Public Health’. He is survived by his wife Brittany Ross, two Boston terriers named Watson and Crick, and his four publications on the facets of learning high containment virology. He can probably no longer be reached at the following ‘permanent’ address.

Permanent address: 713 Church St., Galveston, Texas, USA 77550

This dissertation was typed by: Sergio’s fingers

Figures used with ‘permission’ as denoted in legends or are ‘original’ works by Sergio.